Controlling crystal size in microfluidic solvent exchange processes

R. R. van Nes

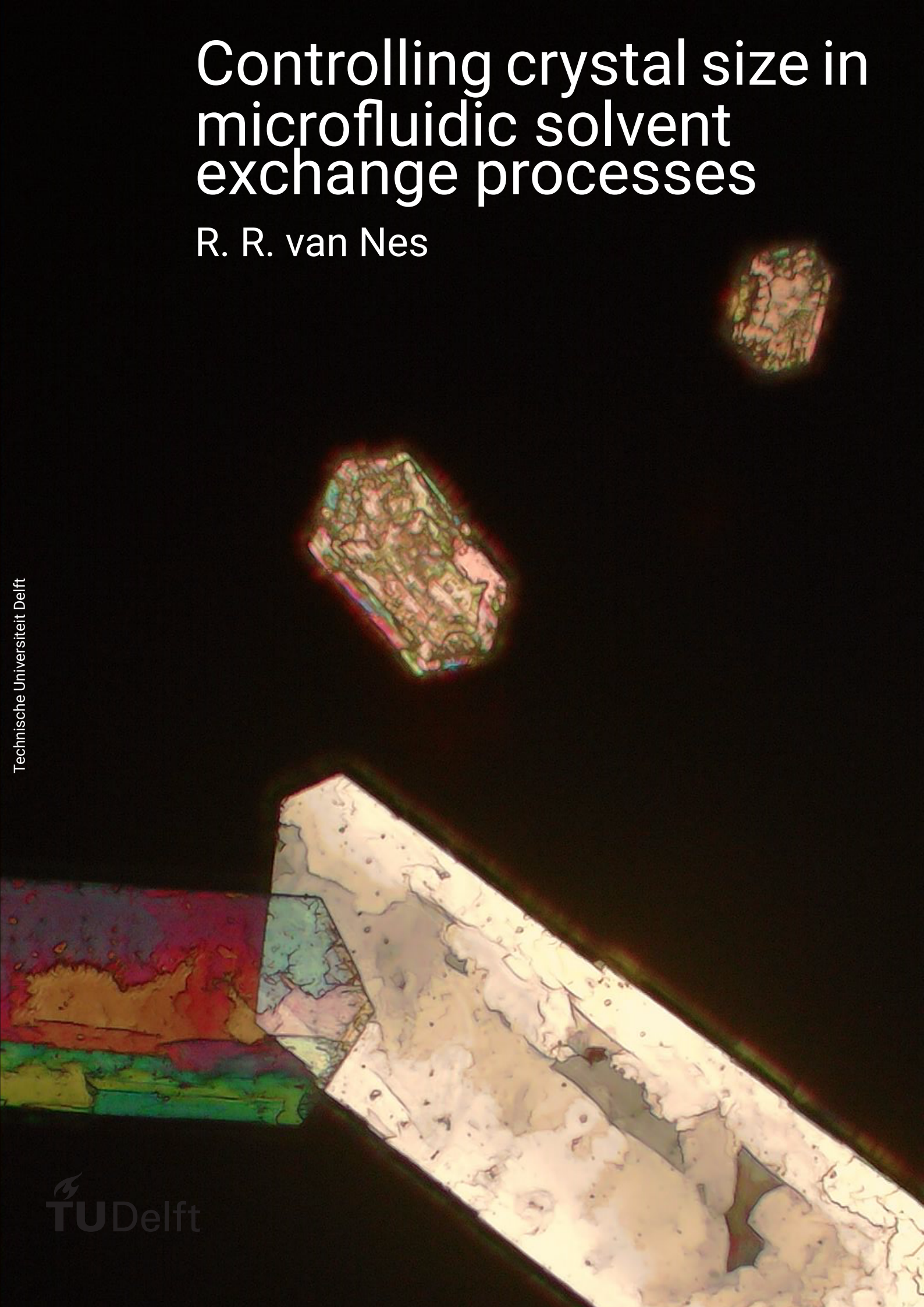

Technische Universiteit Delft

TU Delft

Controlling crystal size in microfluidic solvent exchange processes

by

R. R. van Nes

in partial fulfillment to obtain the degree of Master of Science
at the Delft University of Technology,
to be defended publicly on Thursday May 27^{th}, 2021 at 10:00 AM.

Student number:	4388364	
Project duration:	August 17^{th}, 2020 – April 23^{rd}, 2021	
Thesis committee:	Dr. ir. H. B. Eral,	TU Delft, supervisor
	Prof. dr. ir. J. R. Padding,	TU Delft
	Dr. P. J. Hamersma,	TU Delft

This thesis is confidential and cannot be made public until December 31, 2022.

TU Delft

Abstract

Controlling Particle Size Distribution (PSD) in crystals is paramount, as it directly influences their rate of dissolution, filterability, processability, ease of formulation and even solubility. This is, for example key, in organ specific drug delivery. Most common crystallization methods fail in directly delivering narrow PSDs, which results in further processing steps such as grinding and sieving, which can cause polymorphic transitions and unstable crystal forms due to the generated heat. In traditional antisolvent crystallization, a good and poor solvent are mixed turbulently, leading to uncontrollable true mixing and supersaturation on the Kolmogorov length scale. This causes non-uniform PSDs. This work aims to directly produce crystals with a narrow PSD through controlled antisolvent crystallization in a microfluidic environment, by convectively replacing a good solution in a microfluidic channel with a poor solution that generates a supersaturation pulse through the channel because of diffusion at the solutions interface. Crystallization should occur at this interface. This process is in a laminar flow environment and has solely diffusive mixing of the solutions, which eliminates the control problems that traditional antisolvent crystallization has. It gives convection-diffusion behavior around particles (crystals) in the flow, which causes the boundary layer (BL) to be Péclet (Pe) dependent. This process is known to work in a liquid-liquid-liquid solvent exchange process, with a relation for the final volume V_f of $V_f \sim Pe^{3/4}$ for droplets formed at the solution interface. This relation is theoretically believed to be $V \sim Pe^{1/2}$ for crystals formed at the solution interface. This work shows that a second process, being the sedimentation of crystals, is happening simultaneously. V_f measurements include both crystals that have formed at the interface, as well as crystals that have sedimented. As the current theoretical model does not take sedimentation into account, V_f is no longer a representative measure of the experiment. In seeded linear growth rate measurements, it is easy to distinguish between sedimenting crystals and seeds. The same process, but seeded, is therefore investigated to find out if the linear growth rate G, which is believed to follow $G \sim Pe^{1/3}$, does fit the model. The existence of the supersaturation pulse in liquid-liquid-solid solvent exchange is confirmed experimentally, as the (supersaturation dependent) linear growth rate follows the supersaturation pulse shape. Those experiments also show that the linear growth rate is positively correlated to Pe. More experiments are needed to validate the theoretical relation $G \sim Pe^{1/3}$.

Key words: Antisolvent Crystallization, Solvent Exchange, Convection-diffusion problems, Péclet, Particle Size Distribution, Crystal Size Distribution, Boundary Layer behavior.

Preface

Dear reader,

I think every thesis is like being dropped in the ocean. First, it feels like swimming. You are dropped in an ocean of information and have no clue what to do with it. Once you've gotten the hang of it, it feels like you climbed in a little rowing boat and start rowing. Every stroke feels a bit useless, as you see no land approaching on the horizon, but as you also don't have any option than to keep rowing, you just do it. You just keep getting to know more about the subject and keep doing your experiments. And then, suddenly, there is a breakthrough. Everything comes together. There is a line of land on the horizon, and the rowing doesn't feel as tough anymore. The final strokes with the paddle are easy, as you know you've almost made it. The eight months of my thesis were just like the outline above, and this document is the summary that proves it.

This project would not have been possible without many people. First of all, my supervisor Burak Eral. From the very beginning of the project, Burak had guided excellently. Our relationship developed from a mentor-mentee role, to the degree of co-scientists. We have had many fruitful discussions about the project, and his creativity never ceases to amaze me. I have learnt a big deal about research from him: how frustrating it can be, but also how euphoric you can feel when it works. A big thank you is in place. I also owe a lot to Vikram Korede, my daily supervisor. He helped me out big time with the experimental setup, discussion on the topic and all the other daily stuff that comes with doing a master thesis. Then logically, my direct predecessor Lale Yildiz. She helped me out with a lot of questions, and kindly allowed me to recycle some of her very clear images. Furthermore, I want to thank Johan Padding and Peter Hamersma for taking place in my thesis committee.

In the lab, I of course also recieved a lot of help. From Michel van den Brink and Jaap van Raamt, with all the daily lab stuff. Fred Marquez Penha, for lab help and proof reading. Meng Meng with the spin coater. Ankur Gupta, from Colorado, on part of the derivation. My fellow students with whom I held breaks and shared lab frustrations: Emma, Egem, Max, Rene, Jochem. Friends that have read parts of the report, Anne, Jelle, Michelle, Tjebbe, Marijke, Gijs. Thank you all for the help.

Last but not least: my parents. Thank you for your support throughout my whole study time, and also through the course of this thesis. The road to becoming an official engineer is almost finished now. I guess you are happy too.

Thank you all, and thank you a lot.

Riemer
Delft, April 2021

Contents

List of Figures

List of Tables

Nomenclature

Symbol	Unit	Description
A	m^2	Surface area
c	mol/m^3 or kg/m^3	Concentration
Δc	mol/m^3	Degree of supersaturation
d	m	Characteristic length
D	m^2/s	Diffusion coefficient
E_{kin}	$[J]$	Kinetic energy
E_{pot}	$[J]$	Potential energy
g	m/s^2	Gravitational acceleration
G	m/s	Growth rate
H	m	Characteristic height
h	m	Channel height
i	$[-]$	Order of reaction
k_b	$(m^2\,kg)/(s^2K)$	Boltzmann constant
k_d	m/s	Rate factor
k_r	m/s	Rate constant
K_G	m/s	Growth rate factor
L	m	Characteristic length
L	m	Lateral extension
m	kg	Mass
Q	m^3/s	Flow rate
r_c	m	Critical nucleus radius
R	m	Radius of curvature
R	m	Radius
R_G	m/s	Change in mass per unit of area
S	$[-]$	Relative supersaturation
t	s	Time
T	K or °C	Temperature
U	m/s	Maximum flow velocity
$\overline{U}$	m/s	Mean flow velocity
v	m/s	Velocity
V	m^3	Volume
V_f	m^3	Final volume
w	m	Channel width
α	$[-]$	Shape factor
β	$[-]$	Shape factor
ϵ	$[-]$	Error
ζ	$[-]$	Supersaturation
ϑ	$degree$	Contact angle
Θ	$[-]$	Dimensionless concentration
λ	m	Boundary layer thickness
ν	m^2/s	Kinematic viscosity
ξ	$[-]$	Dimensionless length
ρ	kg/m^3	Density
τ	s	Temporal width of supersaturation pulse
ψ	m^3/s	Stream function

Abbreviation	**Justification**
API	Active Pharmaceutical Ingredient
BC	Boundary Condition
BCF	Burton-Carbrera-Frank model
BL	Boundary layer
CSD	Crystal Size Distribution
MSDS	Material Safety Data Sheet
PBP	Prandtl-Blasius-Pohlhausen
PDF	Probability Density Function
PDMS	Polydimethylsiloxane
PSD	Particle Size Distribution
RDP	Ramer-Douglas-Peucker
Pe	Péclet number
Re	Reynolds number

1

Introduction

Crystals are beautiful, and crystallization is even more so. Crystals are everywhere. They are a vital part of everyday life, and they are also used in high tech applications. From the salt and sugar that you eat, to the pain killer that you take, up until the spark from a lighter. The chips in your computer, high end drugs, maybe a fancy diamond on your ring. Without crystals, our life would be radically different, Our wealth would not be where it is today.

All crystals are formed in the process of crystallization. Crystallization results in a solid phase product from a dissolved phase solute. The formed products are stable, and have very high purities. The beauty and elegance of crystallization is in its integration of processes. It both separates and purifies. Once a crystal has formed, it is basically ready to use. Only some drying is usually needed. This makes crystals and crystallization chemically interesting, as high purities are required in many applications.

The most obvious of those applications is in pharmaceutical use. Drugs, or rather active pharmaceutical ingredients (APIs), that enter the body must be very pure, otherwise they may do more harm than good. Where in the body the APIs dissolve is of great importance. Think of the exact same hypothetical, orally taken, crystalline API that treats both stomach- and colon cancer. For stomach cancer, it should dissolve quite quickly, in a matter of minutes. For colon cancer however, it should dissolve very slowly. Another example are the blue or green specks in your laundry powder (although they are mostly present for marketing reasons). If those are not uniformly sized, they will not distribute evenly throughout the laundry powder and sink to the bottom or float to the top.

The goal here is clear, the solution however is rather complicated. Crystals with a very narrow Particle Size Distribution (PSD, or Crystal Size Distribution (CSD)) are desired, but current crystallization methods are not good at achieving this directly [1]. After crystallization, the product is pure, but still has to be separated on size, for example by grinding and sieving. This takes away the elegance of crystallization. The purification and separation is no longer a one-step process as further work-up steps are required. The heat generated by the grinding is also problematic: it can cause deterioration of heat sensitive crystals, leading to unstable products or even to a morphological (shape) shift. This is where this thesis comes in: the goal is to find out if very narrow PSDs can be reached directly with microfluidic antisolvent crystallization.

Crystallization can be performed through various methods, but the principle is the same in all: try to get so much of the solute (the compound that you dissolve) in the solvent (the liquid in which the solute gets dissolved), that it is no longer energetically favourable to be in solution and the solution start crystallizing. Right before the crystallization starts, the solution is supersaturated: it has too much solute in it. The goal of crystallization is to create this supersaturation [1–4].

One of the methods of crystallization is to reduce the solubility of solute in the solvent, by mixing in another solvent. That second solvent should have a very low solubility, such that it strongly reduces the solubility of a mixture of the two solvents to create the supersaturation and induce crystallization. The result is a three-phase liquid-liquid-solid system with two liquid solvents and a solid phase solute (or product). The first solvent is called the good solvent (as it dissolves a lot of solute), and the second solvent is the poor solvent (as it dissolves very little solute). The system that is used in this thesis consists of aqueous ethanol (liquid, good solvent), water (liquid, poor solvent), and aspirin (solid). This type of crystallization is called a solvent exchange process, or antisolvent crystallization [1–4]. The exact same theory also holds for liquid-liquid-liquid systems, where again two liquid solvents are present, and where the solute is also a liquid. For

example, a system with again the solvents aqueous ethanol and water, but now with oil as a solute. In a liquid-liquid-liquid system, very small droplets instead of crystals are produced.

Performing this process randomly, that is, just throwing the poor solvent into the good solvent (which has enough solute in it), gives a very wide PSD, just like all random crystallization processes. The good news here is that it is possible to do this in a more controlled way. In 2015, Zhang et al. found out that in a controlled liquid-liquid-liquid solvent exchange system, very narrow PSDs can be achieved. Also, it is possible to dictate where the peak of the PSD is, that is, to control the size of the product [5].

The general idea behind Zhangs method of solvent exchange is to limit the location where the exchange of solvents can take place. This is done by filling a microfluidic channel (thickness ~ 0.3 mm) with good solvent, and then slowly replacing that good solvent with the poor solvent by pumping it in from one side of the channel. This creates an interface between the good and poor solvent. That interface is the only place where mixing of the good and poor solvent happens. The mixing happens through forward diffusion of the poor solvent, and through back diffusion of the good solvent. At the interface, a supersaturated region forms. That creates good conditions for droplet formation at the interface, but the rest of the channel has unfavourable conditions for crystallization. This interface is pulsed through the channel, creating a system with very location- and time specific conditions for droplet formation. This pulse is also referred to as the supersaturation pulse. Zhang found that increasing the flow rate of the poor solvent also increased droplet size while retaining the narrow PSD. Zhangs experimental setup is shown in Figure 1.1a, his results in Figure 1.1b.

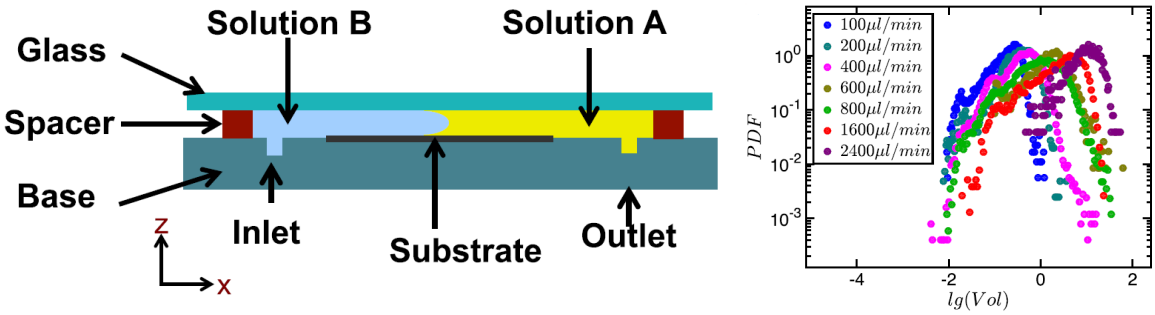

(a) Experimental setup.

(b) Results from Zhang.

Figure 1.1: Experimental setup and results from Zhang. On the left: a solvent exchange process is performed in a microfluidic channel. Good solution (solution A) is replaced by poor solution (solution B). This creates a supersaturation pulse through the channel, at the interface of the solutions. Droplet formation occurs at the interface, and onto the substrate. On the right: PSDs resulting from the solvent exchange experiments. On the x-axis, logarithmic volume is shown. On the y-axis, the probability density function (PDF), which is a normalized PSD is shown. All PDFs are very narrow and have a sharp peak. Increasing flow rate also gives an increase in final droplet volume. Adopted from Zhang [5].

Trying to reproduce such a system in a liquid-liquid-solid environment is challenging. Previous researchers (Korede [6], Yildiz [7]) have laid the groundwork for this thesis. They found that antisolvent crystallization can occur in such a channel, but a relation between poor solvent flow rate and PSD does not seem to be present [7]. The goal of this thesis is to find out if the basic principles of the solvent exchange process that works in a liquid-liquid-liquid environment, also are present in a liquid-liquid-solid environment. That leads to three research questions:

1. Does the supersaturation pulse also exist in a liquid-liquid-solid environment?
2. Do crystals with a uniform PSD form at the interface during the solvent exchange process?
3. Does a relation between the poor solvent flow rate and the final crystal volume exist?

2

Theoretical background

2.1. Crystallization theory

Crystals are solid highly ordered lattice structures of atoms, ions or molecules that are very stable. They are generally very pure (≤ 99%), which makes them suitable for applications where contamination are highly unwanted. They can be identified through various properties. Firstly, its morphology. Crystals can only take a set number of shapes, dependent on how they are formed. Aspirin formed from aqueous solutions, for example, can take on both a hexagonal and a needle shape. Being able to take on multiple shapes is called polymorphology. Secondly, crystals can be identified by their characteristic lattice distance. Every crystal type has a unique length between the lattice layers. This length can be measure, for example with X-Ray Diffraction experiments. An example of a crystal lattice is shown in Figure 2.1 [1–4, 8].

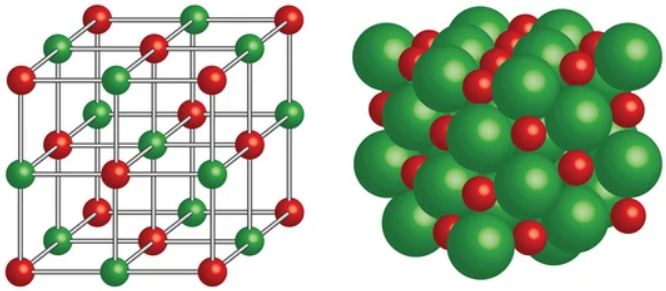

Figure 2.1: Example of a crystal lattice. This lattice consists of two types of molecules (red and green). Crystals can also exist with a single type of molecule. Crystal lattices follow a set pattern, resulting in the final crystal shape. Lattice layers have a unique, set length for every crystal type. Adopted from [9].

The formation of crystals is called crystallization. Crystallization follows a set pattern. Firstly, enough solute has to be present in the solution such that it is energetically more favorable to be in the solid phase than in the dissolved phase. Secondly, nuclei have to form or have to be introduced that serve as the starting point for a crystal. Lastly, these nuclei have to grow to the final crystal size. These steps will be discussed in detail below.

2.1.1. (Super)saturation

All liquids can dissolve a certain amount of solute in them. The theoretical maximum concentration of solute a solvent can dissolve is the saturation concentration c_{sat}. The saturation concentration is dependent on, among others, the solute, the solvent, and temperature. Three different types of solutions can be distinguished: undersaturated, saturated and supersaturated solutions, where $c < c_{sat}$, $c = c_{sat}$ and $c > c_{sat}$ respectively. The supersaturated region consists of two zones: the meta-stable zone and the labile zone. In the meta-stable zone, nucleation, which is the formation of very small crystal nuclei, can occur. In the labile zone, the solution starts crystallizing. A solution cannot stay in the labile zone, as the equilibrium drives it

back to the stable zone. The saturation can be plotted in a temperature-concentration phase diagram. An example of a saturation concentration graph is given in Figure 2.2.

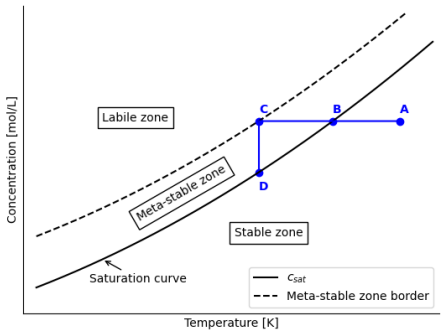

Figure 2.2: Various regimes of saturation in a temperature versus concentration plot. The solid black line is the saturation concentration. The undersaturated, saturated and supersaturated regimes are below, at and above the black line respectively. The meta-stable zone is between the solid black and the dotted black line. Crystallization occurs when the supersaturation exceeds the meta-stable zone. The solution crystallizes until the saturation concentration is reached. An example of such a trajectory is the blue line path from A (undersaturated) to B (saturated) to C (supersaturated) to D (saturated), where the crystallization occurs once the meta-stable zone is exceeded at point C. Saturation curves are not necessarily as temperature dependent as in this example, and can even be practically temperature independent.

The amount of supersaturation can be expressed in the relative supersaturation ratio S [−], or in the degree of supersaturation difference compared to c_{sat} $[mol/m^3]$, which would be Δc $[mol/m^3]$. Both are used frequently in literature, and are expressed as

$$S = \frac{c - c_{sat}}{c_{sat}} \tag{2.1}$$

and

$$\Delta c = c - c_s. \tag{2.2}$$

The relative supersaturation S can also be converted to a percentage of saturation, where for example $S = 0.4$ and $S = 1.1$ correspond to saturations of 40% and 110% respectively. Supersaturation is important, as it is the driving force behind crystallization.

2.1.2. Nucleation

Nucleation is the formation of nuclei in a solution. In a solution, the solute tends to organize itself in clusters, driven by supersaturation. These clusters continually form and fall apart, until they reach a critical radius r_c $[m]$. Then, they no longer fall apart, as it is energetically more favourable to stay together. This is visualized in Figure 2.3. Nucleation is a complex and not fully understood phenomenon, mainly because the moment of nucleation is very difficult to observe due to its small time- and length scales. The theory posed in the beginning of this paragraph is just that: a theory. It is not known if this is really happening, but it is the best explanation science can give [3]. Nucleation can occur in two ways: primary nucleation, where the crystal nucleus is formed directly from the liquid phase to the solid phase, and secondary nucleation, where an existing crystal is the origin of a new nucleus. These two forms are explained further under the next headers.

Primary nucleation

Primary nucleation is the direct formation of a solid phase crystal from a liquid phase solution. It is the formation of an entirely new nucleus. Primary nucleation can happen both homogeneously and heterogeneously. In homogeneous primary nucleation, the nucleus is formed purely from the solute. Homogeneous nucleation only occurs in meticulously cleaned systems with very smooth walls. In heterogeneous primary nucleation, the nucleation is triggered by something external. This could be a spec of dust, some impurity or the system walls. Heterogeneous nucleation is more likely to happen, as the impurities in the system get wetted by the system, which decreases the surface tension, making crystallization easier. Therefore, in lower supersaturation systems, heterogeneous primary nucleation is more likely than homogeneous primary nucleation [2, 4].

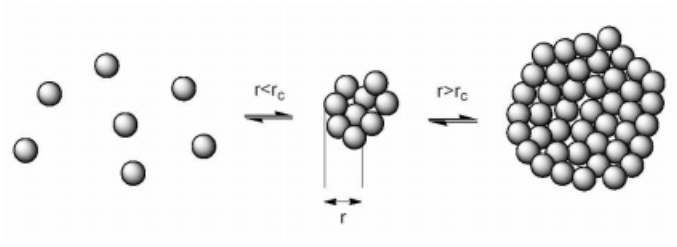

Figure 2.3: Nucleus formation in a two-step process. Equilibrium between individual solute molecules and a nucleus. Once the nucleus reaches the critical radius r_c, the nucleus no longer dissolves but it can grow. This is again an equilibrium, between larger and Adopted from Dalmolen [10].

Secondary nucleation

In secondary nucleation, the new nucleus forms from an already existing crystal, for example when an existing nucleus collides with a wall, impeller or baffle and breaks into two. This results in two new, individual nuclei. The main methods of secondary nucleation are i) seeding (or initial breeding or dust breeding), ii) contact nucleation, iii) shear breeding, and iv) attrition (or collision breeding) [2, 4]. The idea behind all forms is the same: a new nucleus forms due to the presence of an already existing nucleus or nuclei. The way it is formed however is different. In seeding, external crystals are purposely added to the supersaturation to act as nucleation sites [11, 12]. Contact nucleation is the type of nucleation as described in the example above: a crystal collides with either another crystal or some part of the system (like a wall, baffle, impeller or shaft) and breaks into two or more separate, new nuclei. Shear breeding is a form of nucleation due to a strong shear flow along the crystal that breaks away part of the crystal, resulting in a new nucleus. Attrition is the phenomenon where existing crystals are 'polished', and thus lose their sharp edges which in turn become new nuclei. It is comparable to erosion of a sharp mountain peak that dulls overtime. The rate and method of secondary nucleation is one of the factors that determine the mean crystal size and the crystal size distribution [2, 4, 13]

2.1.3. Crystal growth

Once the nucleus has spawned (either through primary or secondary nucleation), the nucleus starts growing, as long as the solution is still supersaturated. The easiest way to think of crystal growth is through the linear growth rate

$$G = \frac{dL}{dt} \tag{2.3}$$

which is the change in the characteristic length scale L with respect to the change in time t in units of $[m/s]$ [4]. The linear growth rate is always defined for a specific face of the crystal, as different faces grow at different rates. A more rigid way of defining the growth of a crystal is therefore through its change in mass, $\frac{dm}{dt}$. This is linked to the linear growth rate through

$$R_G = \frac{1}{A}\frac{dm}{dt} = 3\frac{\alpha}{\beta}\rho G = 3\frac{\alpha}{\beta}\rho\frac{dL}{dt}, \tag{2.4}$$

where R_G $[kg/(m^2 s)]$ is the change in mass per unit of area per unit of time, A $[m^2]$ is the surface area, α $[-]$ and β $[-]$ are volume and area shape features to correct for the specific shape of the crystal and ρ $[kg/m^3]$ is the density of the crystal. The change in mass however is very difficult to measure during experiments, and furthermore the shape and area factors must be knowns in order to transform linear growth rates into mass growth rates and vice versa [4].

Simple molecular growth model

The growth rate models give some insight in what happens on macro scale with the crystals, but lacks in giving insight into what happens on a molecular level. The easiest way to look at the events on a molecular level, is to consider what the most favourable places are for new molecules to join the crystal structure. If molecules are represented as cubes, three possible locations of joining the crystal exist: at the surface, with one neighbouring molecule, at the step between two lattice layers, with two neighbouring molecules, or at a kink, with three neighbouring molecules. These sites are energetically increasingly favourable, and therefore

molecules tend to migrate towards the sites with more neighbours through surface diffusion. A visualisation of these sites can be found in Figure 2.4.

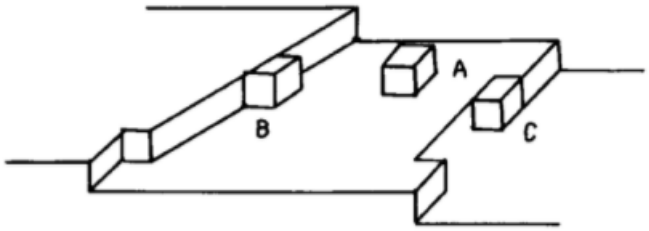

Figure 2.4: Crystal growth sites: A) surface site (terrace site), B) step site and C) kink site. The more contact area a new part of the crystal has, the more energetically favourable, and thus the more likely that site is. Newly joined molecules can also move over the crystal surface, for example from location A to B, when it is energetically more favourable. Adopted from Reid and Ohara [14].

Although the model described above is elegant in its simplicity, it fails to address two important questions: i) how do steps in crystals occurs, and ii) what is the phenomenon that dictates and controls the growth rate? These fundamental questions call for more detailed models. The Burton-Cabrera-Frank model (BCF model) aims at answering these questions.

Burton-Cabrera-Frank surface diffusion model

In 1949, Frank put forward the idea that crystal growth tends to occur from imperfections that previously formed in the crystal [15]. The most common imperfection is a screw dislocation, where two layers of molecules that should be in the same lattice layer, are not in the same lattice layer. This causes an imperfection in the lattice that can act as a step site. If then the crystal starts growing in accordance with the theory above, a rotating growth starts. Hence the name screw dislocation. Screw dislocations allow for continuous crystal growth through surface diffusion of absorbed molecules, as the dislocation spirals and thus does not disappear. The growth of screw dislocations is visualised in Figure 2.5.

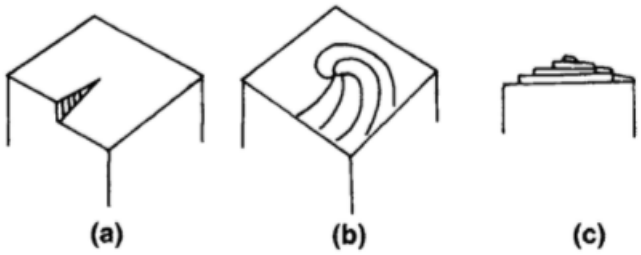

Figure 2.5: Screw dislocation. Screw dislocations allow for continuous crystal growth through surface diffusion of absorbed molecules, as the dislocation spirals and thus does not disappear. Adopted from Mullin [3].

In 1951, Burton and Cabrera refined this model and formularized it [16]. The main takeaways from their derivations are that the model works at low supersaturations and that growth rates are supersaturation dependent. The model also assumes that surface diffusion is the rate limiting step in the growth process. Therefore, the concept above is the BCF surface diffusion model. This assumption is unlikely to hold in liquid-solid systems, where diffusion in the boundary layer tends to be the rate limiting step [4]. The Chernov bulk diffusion model takes that assumption into account.

Chernov bulk diffusion model

In 1961, Chernov introduced the Chernov bulk diffusion model. The Chernov bulk diffusion model has its rate limiting step in the boundary layer limitations [17]. The main takeaways from this model are discussed. This model also works at low supersaturations, and shows a positive correlation between the supersaturation and the growth rate. More importantly, it shows that with an increasing boundary layer (BL) thickness λ $[m]$, comes a decreasing growth rate. From a reaction-diffusion perspective, this is expected, as further explained in subsection 2.1.4. The importance of this conclusion is that it relates agitation of solutions and

hydrodynamic conditions such as flow to crystal growth, as those factors all influence BL thickness. Due to the above mentioned correlations between hydrodynamics and crystal growth, this model was used in the present work.

2.1.4. Diffusion-reaction theory

The slowest process in any system determines the rate of the whole system. The step in the system that is the slowest, is called the rate limiting step. In a diffusion-reaction problem, there are two steps: diffusion and reaction. The reaction takes place at a surface, and the reactants have to diffuse (through a BL) to that surface. The slowest of these two steps is the rate limiting step. A parallel to crystallization is easy: just replace the reaction step with surface absorption and incorporation into the lattice, and the exact same theory holds.

For a one-dimensional case, the diffusive limitation in the growth rate can be described as

$$\frac{dm}{dt} = DA\left(\frac{dc}{dx}\right) \tag{2.5}$$

where m $[kg]$ is the mass of the crystal, t $[s]$ is the time, D $[m^2/s]$ is the diffusion coefficient, A $[m^2]$ is the area of the crystal surface and $\frac{dc}{dx}$ $[kg/m^4]$ is the concentration gradient in the BL. That concentration gradient can be approximated, on the assumption of linearity in the concentration profile, to be

$$\frac{dc}{dx} = \frac{c - c_s}{\lambda} \tag{2.6}$$

where c $[kg/m^3]$ and c_i $[kg/m^3]$ are the bulk and surface solute concentrations respectively. Here, the link between BL thickness and growth rate becomes apparent. Combining Equation 2.5 and Equation 2.6 results in

$$\frac{dm}{dt} = \frac{D}{\lambda}A(c - c_s) = k_d A(c - c_s), \tag{2.7}$$

with the rate factor $k_d = \frac{D}{\lambda}$ $[m/s]$. This inversely couples BL thickness and growth rate. Physically, this also makes sense: having a thicker BL results in a longer travel time for solute molecules to reach the surface, and thus in a slower process.

The reactive step (incorporation of molecules into the lattice) can be described analogously. The reaction rate $k_r \Delta c$ now dominates the process. That results in

$$\frac{dm}{dt} = k_r A(c - c_s)^i \tag{2.8}$$

where k_r $[m/s]$ is the rate constant, and i $[-]$ determines the order of the reaction. The reaction and diffusion effects can be combined into one rate factor, being

$$\frac{1}{K_G} = \frac{1}{k_d} + \frac{1}{k_r} \tag{2.9}$$

where K_G $[m/s]$ is the growth rate factor. This then yields a combined reaction-diffusion equation of

$$\frac{dm}{dt} = K_G A \Delta c. \tag{2.10}$$

When $k_d << k_r$, $K_G \approx k_d$ and thus the system is diffusion dominated. As $k_d = \frac{D}{\lambda}$, thicker BLs lead to a more diffusively dominated and slower system.

2.1.5. Methods of crystallization

Inducing crystallization is caused by moving a solution from the stable zone, through the meta-stable zone to the labile zone, as shown in Figure 2.2. Bringing a solution from the stable zone to the labile zone can be done in various ways, three of which are described below.

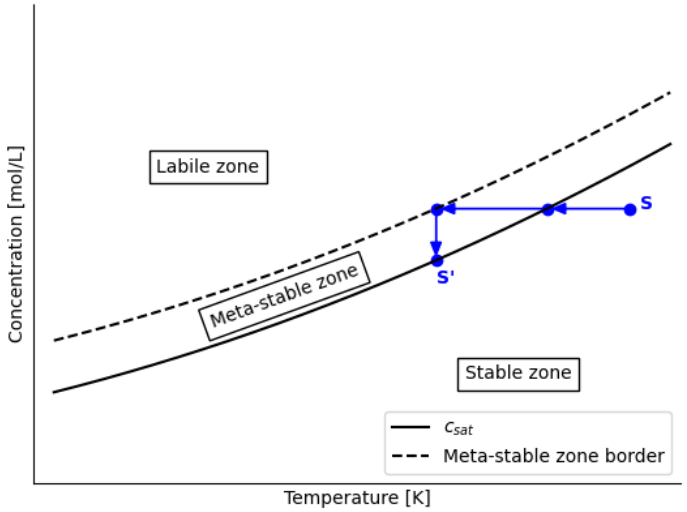

Figure 2.6: Saturation regimes in cooling crystallization. As c_{sat} is temperature dependent, the solubility decreases when the solution S is cooled. This moves the solution from the stable, through the meta-stable to the labile regime, where crystallization occurs. The solution then falls back to the solubility curve to become solution S'.

Cooling crystallization

Cooling crystallization makes use of the often occurring property that the saturation concentration is strongly temperature (T [K *or* °C]) dependent. As T increases, c_{sat} also increases and vice versa. That means that by lowering the temperature, a higher supersaturation is realised, and thus nucleation and crystallization are induced. This can be visualised as moving horizontally through the temperature-concentration plot in Figure 2.2. The main benefit of this crystallization method is that it is conceptually easy, the main downside is that heat exchange operations are usually very energy intensive.

Evaporative crystallization

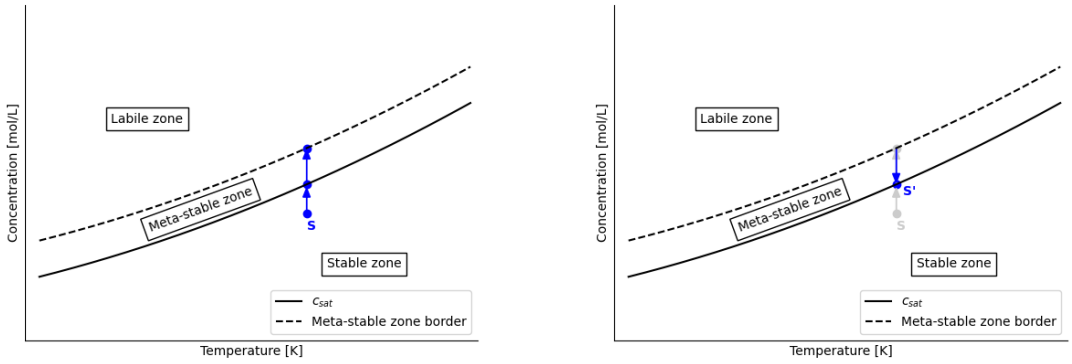

(a) (b)

Figure 2.7: Saturation regimes in evaporative crystallization. In evaporative crystallization, the removal of solvent through evaporation leads to an increase of solute concentration. The temperature is constant and high, as the solution is at the boiling point. The solution S travels from the stable, through the meta-stable zone to the labile zone, where crystallization occurs. The solution then falls back to the solubility curve, as the crystallization decreases the concentration of solute.

Evaporative crystallisation increases the concentration of the solute in the solution by removing the solvent from the solution through evaporation. This can be visualized by moving vertically through the zones

in Figure 2.7, as the concentration increases, which induces nucleation and crystallization. The benefits and downsides are the same as in cooling crystallization: it is conceptually easy but very energy intensive.

Antisolvent crystallization

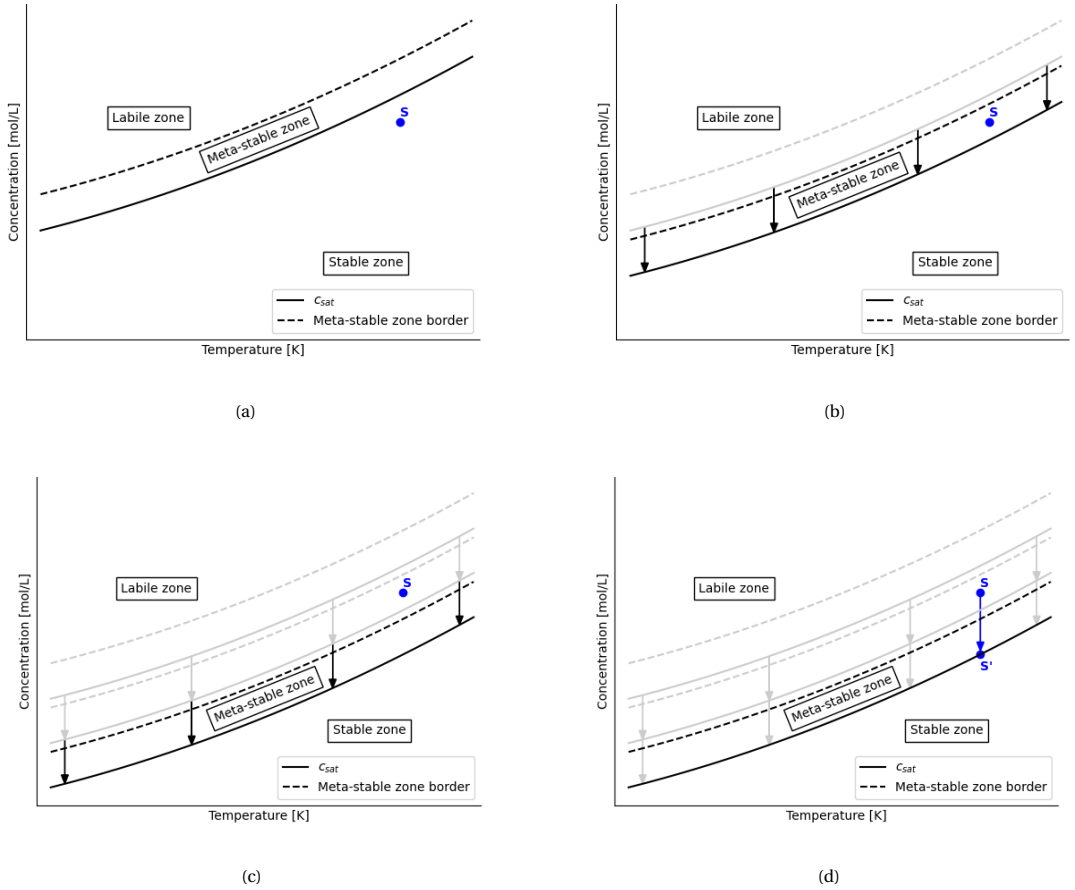

Figure 2.8: In antisolvent crystallization, crystallization is induced by the same principle as cooling- and evaporative crystallization: move the solution from the stable zone, through the meta-stable zone, to the labile zone where nucleation and crystallization occur. In antisolvent crystallization however, the intention is not to change the concentration of the solution (point S), rather to lower the solubility curve of the solute in the solvent. That is, the solubility moves in the negative vertical direction. Once the solution S reaches the labile zone, crystallization occurs, and the solution falls back to the solution S' on the saturation curve.

Antisolvent crystallization (also referred to as solvent exchange or drowning out) is a method of crystallization where a second solution (the poor solution or antisolvent) is added to a solution where the solute is already present (the good solution). The concept is the same as with all crystallization: move from the stable, through the meta-stable to the labile zone to induce crystallization. In antisolvent crystallization however, the goal is not to move the location of the solution in the temperature-concentration plot, rather the goal is to move the solubility line. The effect is the same: the solution moves through the zones, until it enters the labile zone and starts crystallizing. This phenomenon is visualized in Figure 2.8. In reality, keeping the solution at a constant concentration is not realistic, as the antisolvent dilutes the full solution. The fundamental aspect to antisolvent crystallization is the reduction of the solubility, which is why this visualisation is chosen.

In industry, most antisolvent crystallization happens through turbulent mixing of the two solutions. This creates big variations in the particle size distribution. The working principle is the following. To induce antisolvent crystallization, mixing on the molecular level is needed. Mixing on the macro scale is not enough. From a fluid dynamics point of view, that means that all liquid needs to mix diffusively. This is achieved best by mixing the whole system turbulently, until the filament layer thickness in eddies and vortexes generated by the turbulence is in the order of the Kolmogorov length scale. Once the Kolmogorov length scale is reached, diffusive mixing becomes dominant over convective mixing and the molecular scale mixing takes

place. Controlling where and where eddies occur, and thus where and when, and at what rate, the supersaturation occurs, is nearly impossible. That causes the wide, unwanted PSDs.

Advantages of antisolvent crystallization include its possibilities to be used at moderate and low temperatures, making it suitable for temperature sensitive solutes. A big disadvantage is that as the good and bad solution get mixed, they need to be separated before recycling of the solution is possible.

2.2. Theoretical model of antisolvent crystallization in confined channels

The experimental setup in this research comprises of a very small ($14x52x0.3\ mm$) channel. Therefore, gaining fundamental insight in hydrodynamic conditions, mass transfer and BL behaviour in such an environment is imperative.

2.2.1. Relevant dimensionless numbers

In chemical engineering, processes often compete with one-another. For example a slow flow in which both convection and diffusion play a role. These competitions are bundled in dimensionless numbers, which are the ratio between the two processes. The most important ones for this research are elaborated upon below.

Reynolds number

The Reynolds number (Re) is the ratio between inertial and viscous forces in a flowing medium and is defined as

$$Re = \frac{\rho v d}{\nu}, \tag{2.11}$$

where ρ $[kg/m^3]$ is the density of the fluid, v $[m/s]$ is the fluid velocity, d $[m]$ is the characteristic length and ν $[m^2/s]$ is the fluids dynamic viscosity. The Reynolds number gives an indication of the turbulence of a flow. The higher Re, the more turbulent a flow is.

Péclet number

The Péclet number is the ratio between convective and diffusive mass transfer (the example in the introduction of this section). It is defined as

$$Pe = \frac{vd}{D}, \tag{2.12}$$

where v $[m/s]$ is the fluid velocity, d $[m]$ is the characteristic length and D $[m^2/s]$ is the fluids diffusion coefficient. The higher the Péclet number, the more dominant the convective element is.

Intermezzo - Background on experimental setup

To understand why the next sections are discussed, it is important to understand the experimental setup and the experiment properly, and to understand some of the implicit assumption made in the derivations below. The experiment consists of a microfluidic channel ($WxLxH = 14x52x0.3\ mm$) in which a poor solution replaces a good solution (see Figure 2.9). The used solutions are aspirin saturated water (poor solution), and aspirins saturated aqueous ethanol (50%/50%vol, good solution). The channel is first fully filled with good solution. The poor solution then replaces the good solution, creating a mixing front, which is depicted with the red dotted line in the figure. At the mixing front, also called the solution interface, the poor solution diffuses into the good solution and vice versa. At the front, the antisolvent crystallization should take place, and due to the local supersaturation, crystals should nucleate and grow. These crystals are now particles in a flow. To understand how they grow, you need to understand how solute is transported to the crystal. How the solute is transported to the crystal is boundary layer dependent, and how the boundary layer forms depends on the flow around the particle. As non-spherical particles are very hard to model, the crystal is assumed to be a sphere from now on.

Figure 2.9: Schematic view of the channel. The good solution is depicted in pink, the poor solution in light blue. Adapted from Yildiz [7].

2.2.2. Mass transfer in confined channels

For a channel of heigth h $[m]$ and width w $[m]$ where a fluid flows with maximum velocity U $[m/s]$ and mean velocity $\overline{U}$ $[m/s]$, the flow rate Q $[m^3/s]$ is defined as $Q = hw\overline{U}$. For a kinematic viscosity ν of the fluid, the Reynolds number Re is defined as $Re = \overline{U}h/\nu = Q/(w\nu)$. Introducing a diffusion coefficient D, the Péclet number is $Pe = \overline{U}h/D = Q/(wD)$. The relevant length scale in both numbers is h, as the channel height is orders of magnitude smaller than its length and width.

2.2.3. Boundary layer behavior

The following section is based on the book *'Analysis of Transport Phenomena'* by W. M. Deen [18]. Boundary layers (BLs) are thin layers that form around particles and behave differently from the bulk of the fluid. Three types of BLs are distinguished: momentum BLs, thermal BLs and concentration BLs. The last one is of interest for this project, as heat is neglected and species transport is of interest for crystal formation and growth. To determine the BL behavior, first, the flow field around a particle must be defined. The stream function ψ $[m^3/s]$ is helpful here, as it visualizes the flow of the fluid around objects. A detailed derivation of the problem below can be found in Appendix A.1. This derivation follows the following structure:

1. Determination and definition of the stream function ψ.
2. Determination of boundary conditions to solve for ψ.
3. Lots of algebra with a substitution for ψ to be able to solve the flow profile.
4. Determination of the 2-D flow profile in v_r and v_ϑ.
5. Nondimensionalization of v_r and v_ϑ.

The stream function for a bidirectional flow in spherical coordinates is defined as

$$v_r \equiv \frac{1}{r^2 \sin(\vartheta)} \frac{\partial \psi}{\partial \vartheta}, \; v_\vartheta \equiv -\frac{1}{r \sin(\vartheta)} \frac{\partial \psi}{\partial r}, \tag{2.13}$$

where v_r and v_ϑ are the fluid velocity in the respective directions. These stream functions have a corresponding Stokes' equation [18]. A Stokes' equation is a stationary and linearized version of the Navier-Stokes equation. It is reversible, and much easier to solve than the Navier-Stokes equation. It is defined as

$$E^4 \psi = 0, \tag{2.14}$$

where E^2 is an operator that is comparable with the Laplacian operator $\nabla^2 = \frac{1}{r^2}\frac{\partial}{\partial r}\left(\frac{1}{r^2}\frac{\partial}{\partial r}\right) + \frac{1}{r^2 \sin\vartheta}\frac{\partial}{\partial \vartheta}\left(\sin\vartheta \frac{\partial}{\partial \vartheta}\right)$, but is not exactly the same, as

$$E^4 = E^2(E^2), \; E^2 = \frac{\partial^2}{\partial r^2} + \frac{\sin\vartheta}{r^2}\frac{\partial}{\partial \vartheta}\left(\frac{1}{\sin\vartheta}\frac{\partial}{\partial \vartheta}\right). \tag{2.15}$$

This problem needs four boundary conditions to be solved. The first two are a no-penetration and a no-slip boundary condition at the sphere surface, such that

$$v_r(R, \vartheta) = 0, \; v_\vartheta(R, \vartheta) = 0, \tag{2.16}$$

and the third and fourth represent uniform flow far away (in the bulk) from the particle, being

$$v_r(\infty, \vartheta) \to U\cos\vartheta, \; v_\vartheta(\infty, \vartheta) \to -U\sin\vartheta. \tag{2.17}$$

Rewriting the boundary conditions in terms of the stream function instead of velocities using Equation 2.13 and integration of the uniform flow boundary conditions yields (for both bulk boundary conditions)

$$\psi(\infty, \vartheta) \to \frac{r^2 U \sin^2\vartheta}{2}. \tag{2.18}$$

Note that as the stream functions value are arbitrary, integration constants are set to zero. This outcome suggests to look for a solution for $\psi(r, \vartheta)$ of the form

$$\psi(r, \vartheta) = f(r)\sin^2\vartheta, \tag{2.19}$$

where $f(r)$ is some function of r. Substitution of this suggested solution into the Stokes' equation (Equation 2.14) gives

$$E^2\left[\frac{\partial^2}{\partial r^2}\left(f(r)\sin^2\vartheta\right)+\frac{\sin\vartheta}{r^2}\frac{\partial}{\partial\vartheta}\left(\frac{1}{\sin\vartheta}\frac{\partial}{\partial\vartheta}\left(f(r)\sin^2\vartheta\right)\right)\right]=0, \tag{2.20}$$

which reduces to

$$E^2\left[\sin^2\vartheta\frac{\partial f^2}{\partial r^2}-2\sin^2\vartheta\frac{f}{r^2}\right] \tag{2.21}$$

Now applying the operator $E^2=\frac{\partial^2}{\partial r^2}+\frac{\sin\vartheta}{r^2}\frac{\partial}{\partial\vartheta}\left(\frac{1}{\sin\vartheta}\frac{\partial}{\partial\vartheta}\right)$ again gives

$$\frac{\partial^2}{\partial r^2}\left(\sin^2\vartheta\frac{\partial^2 f}{\partial r^2}-2\sin^2\vartheta\frac{f}{r^2}\right)+\frac{\sin\vartheta}{r^2}\frac{\partial}{\partial\vartheta}\left(\frac{1}{\sin\vartheta}\frac{\partial}{\partial\vartheta}\left(\sin^2\vartheta\frac{\partial^2 f}{\partial r^2}-2\sin^2\vartheta\frac{f}{r^2}\right)\right)=0, \tag{2.22}$$

which in turn reduces to

$$\left(\frac{\partial^2}{\partial r^2}-\frac{2}{r^2}\right)^2 f=0. \tag{2.23}$$

Now that the stream function differential equation has been rewritten in terms of $f(r)$, this should happen to the BCs (Equation 2.16 and Equation 2.18) as well. This results in

$$f(R)=0,\ b\frac{\partial f(r)}{\partial r}\Big|_R=0,\ f(\infty)\to\frac{r^2U}{2}. \tag{2.24}$$

As Equation 2.23 is and equidimensional equation, it can be solved and has solutions of the form $f(r)=r^n$ where n is an arbitrary constant. Filling this out yields

$$\left(\frac{\partial^2}{\partial r^2}-\frac{2}{r^2}\right)^2 r^n=0, \tag{2.25}$$

which results in a fourth order polynomial in n that factors out into

$$(n-2)(n+1)(n-1)(n-4)=0. \tag{2.26}$$

This gives solutions for $n=-1,1,2,4$, which in turn implies to look for solutions of $f(r)$ of the form

$$f(r)=Ar^4+Br^2+Cr+\frac{D}{r}, \tag{2.27}$$

where A, B, C and D are arbitrary contants. The BCs as defined for $f(r)$ must also hold for this equation. Working this out yields $A=0$, $B=\frac{U}{2}$, $C=-\frac{3}{4}\frac{U}{R}$ and $D=\frac{1}{4}UR^3$. From $\psi(r,\vartheta)=f(r)\sin^2\vartheta$, this results in

$$\psi(r,\vartheta)=UR^2\sin^2\vartheta\left[\frac{1}{2}\left(\frac{r}{R}\right)^2-\frac{3}{4}\left(\frac{r}{R}\right)+\frac{1}{4}\left(\frac{R}{r}\right)\right] \tag{2.28}$$

This value for the stream function can be plugged into the definition of the stream function as in Equation 2.13, giving

$$v_r=U\cos\vartheta\left[1-\frac{3}{2}\left(\frac{R}{r}\right)+\frac{1}{2}\left(\frac{R}{r}\right)^3\right] \tag{2.29}$$

and

$$v_\vartheta=-U\sin\vartheta\left[1-\frac{3}{4}\left(\frac{R}{r}\right)-\frac{1}{4}\left(\frac{R}{r}\right)^3\right]. \tag{2.30}$$

These are the velocity components in the r and ϑ direction, defining the 2-D flow profile around a sphere. When these are nondimensionalized using $\xi=\frac{r}{h}$, where ξ is the dimensionless length and h is the channel height. The result are the dimensionless velocity components

$$\tilde{v_r}(\xi,\vartheta)=\frac{v_r}{\overline{U}}=\cos\vartheta\left[1-\frac{3}{2\xi}+\frac{1}{2\xi^3}\right], \tag{2.31}$$

$$\tilde{v_\vartheta}(\xi,\vartheta)=\frac{v_\vartheta}{\overline{U}}=-\sin\vartheta\left[1-\frac{3}{4\xi}-\frac{1}{4\xi^3}\right]. \tag{2.32}$$

These velocity components are necessary later on to be able to derive the convection-diffusion behaviour.

2.2.4. Convection-diffusion behaviour

In narrow channels, convection and diffusion compete. As explained in subsection 2.2.1, the Péclet number describes this phenomenon. This section will discuss and derive the convection-diffusion behaviour around a surface. A detailed version of the derivations below can be found in Appendix A.2. As the convection-diffusion behavior in the BL of the particle is very different from that in the bulk of the fluid, these regions have to be described separately. The solutions can then be tied together, to get a full concentration profile. This derivation follows the following structure:

1. Introduction and definition of the convection-diffusion equation for the bulk of the fluid.
2. Nondimensionalization of the convection-diffusion equation for the bulk of the fluid.
3. Determination of the boundary conditions for the bulk of the fluid.
4. Realization that the BCs define the flow profile in such a way, that no transport of reactants to the particle surface is possible, and that that is physically impossible as it would mean the particles cannot grow.
5. Introduction of the convection-diffusion equation for the BL.
6. Rescaling the convection-diffusion equation because of the thinness of the BL compared to the thickness of the bulk of the fluid.
7. Order of magnitude comparison of all terms to find the dominant terms, which leads to a dimensionless BL thickness.

The bulk concentration will turn out to be constant. The BL concentration profile is not. Matching (tying together) of these profiles is possible, but not done here as only the BL concentration profile is of interest. To understand this behaviour in channels, the general convection-diffusion equation is introduced:

$$\frac{\partial c}{\partial t} + v_r \frac{\partial c}{\partial r} + \frac{v_\vartheta}{r}\frac{\partial c}{\partial \vartheta} + \frac{v_\phi}{r\sin\phi}\frac{\partial c}{\partial \phi} = \frac{D}{r^2}\frac{\partial}{\partial r}\left(r^2\frac{\partial c}{\partial r}\right) + \frac{D}{r^2\sin\vartheta}\frac{\partial}{\partial \vartheta}\left(\sin\vartheta\frac{\partial c}{\partial \vartheta}\right) + \frac{D}{r^2\sin\phi}\frac{\partial^2 c}{\partial \phi^2}. \tag{2.33}$$

Upon realisation that this is an axisymmetric problem (the fluid keeps moving in the same two directions, no movement in the ψ direction) and thus $\Theta = \Theta(\xi, \vartheta)$ only ($\Theta \neq \Theta(\phi)$), and the assumption of steady state, this leads to the simplified convection-diffusion equation

$$v_r \frac{\partial c}{\partial r} + \frac{v_\vartheta}{r}\frac{\partial c}{\partial \vartheta} = \frac{D}{r^2}\frac{\partial}{\partial r}\left(r^2\frac{\partial c}{\partial r}\right) + \frac{D}{r^2\sin\vartheta}\frac{\partial}{\partial \vartheta}\left(\sin\vartheta\frac{\partial c}{\partial \vartheta}\right) \tag{2.34}$$

which, using

$$\xi = \frac{r}{h},\ \Theta = \frac{c - c_\infty}{c_0 - c_\infty},\ Pe = \frac{\overline{U}h}{D}\ \ (r = h\xi,\ c = \Theta(c_0 - c_\infty) + c_\infty) \tag{2.35}$$

can be nondimenzionalized. Here ξ is the dimensionless length, Θ is the dimensionless concentration and Pe is defined using the relevant scales. Those are the fluid mean velocity $\overline{U}$, the channel height h and the diffusion coefficient D. Also needed are the dimensionless velocity components $\tilde{v}_r = v_r/\overline{U}$ and $\tilde{v}_\vartheta = v_\vartheta/\overline{U}$ as derived in Equation 2.31 and Equation 2.32. The dimensionless form of the equation is

$$\begin{aligned}\tilde{v}_r\overline{U}\frac{\partial(\Theta(c_0 - c_\infty) + c_\infty)}{\partial(\xi h)} + \frac{\tilde{v}_\vartheta\overline{U}}{\xi h}\frac{\partial(\Theta(c_0 - c_\infty) + c_\infty)}{\partial \vartheta} \\ = \frac{D}{(\xi h)^2}\frac{\partial}{\partial(\xi h)}\left((\xi h)^2\frac{\partial(\Theta(c_0 - c_\infty) + c_\infty)}{\partial(\xi h)}\right) + \frac{D}{(\xi h)^2\sin\vartheta}\frac{\partial}{\partial \vartheta}\left(\sin\vartheta\frac{\partial(\Theta(c_0 - c_\infty) + c_\infty)}{\partial \vartheta}\right),\end{aligned} \tag{2.36}$$

which is simply

$$Pe\ \tilde{v}\cdot\tilde{\nabla}\Theta = \tilde{\nabla}^2\Theta. \tag{2.37}$$

This problem has the boundary conditions

$$\Theta(1,\vartheta)=1,\ \Theta(\infty,\vartheta)=0 \tag{2.38}$$

representing c_0 at the sphere surface and c_∞ far away (in the bulk) from the sphere. In Equation 2.37 $\tilde{\nabla}$ and $\tilde{\nabla}^2$ are dimensionless operators including only ξ and ϑ. Now, for $Pe \gg 1$ (which is the case in this study, see also Table 5.1), we consider the limiting behavior of $Pe \to \infty$. Physically, this means that the convective scale is much larger than the diffusive scale. The convection-diffusion equation (Equation 2.37) reduces to

$$\tilde{v}\cdot\tilde{\nabla}\Theta=0 \tag{2.39}$$

when all diffusive terms are negligible. This reduces the order of the differential equation. As $v\cdot\nabla\Theta$ is the rate of change of Θ (concentration) along a stream line, this simplification leads to not being able to transfer mass from the sphere (crystal) to the fluid and vice versa, and thus the fluid concentration is constant everywhere. As in the BL species transport takes place, a concentration gradient must be present. This raises the need for separate solutions for the BL and the bulk fluid (and the matching of these solutions through, for example, matching asymptotes). The original convection-diffusion equation (Equation 2.37) leads to $\nabla^2\Theta = O(Pe)$ for $Pe \to \infty$. In the outer region, the bulk of the fluid, the concentration is constant at c_∞. That makes $\Theta = 0$ a good initial guess, as it keeps the fluid at a constant concentration c_∞. In the inner region, the BL, the behavior is described by

$$\tilde{v}_r\frac{\partial\Theta}{\partial\xi}+\frac{\tilde{v}_\vartheta}{\xi}\frac{\partial\Theta}{\partial\vartheta}=\frac{1}{Pe}\left[\frac{\partial^2\Theta}{\partial\xi^2}+\frac{2}{\xi}\frac{\partial\Theta}{\partial\xi}+\frac{1}{\xi^2\sin\vartheta}\frac{\partial}{\partial\vartheta}\left(\sin\vartheta\frac{\partial\Theta}{\partial\vartheta}\right)\right], \tag{2.40}$$

which is the same as Equation 2.39. If we now define a new spherical coordinate $\eta = \cos\vartheta$ where $-1 \leqslant \eta \leqslant 1$ and introduce the velocity components $\tilde{v}_r$ and $\tilde{v}_\vartheta$ as defined in Equation 2.31 and Equation 2.32, we get

$$\eta\left(1-\frac{3}{2\xi}+\frac{1}{2\xi^3}\right)\frac{\partial\Theta}{\partial\xi}+\frac{\left(1-\eta^2\right)}{\xi}\left(1-\frac{3}{4\xi}-\frac{1}{4\xi^3}\right)\frac{\partial\Theta}{\partial\eta}=\frac{1}{Pe}\left[\frac{\partial^2\Theta}{\partial\xi^2}+\frac{2}{\xi}\frac{\partial\Theta}{\partial\xi}+\frac{1}{\xi^2}\frac{\partial}{\partial\eta}\left(\left(1-\eta^2\right)\frac{\partial\Theta}{\partial\eta}\right)\right]. \tag{2.41}$$

As $Pe \gg 1$, the BL is thin. This calls for rescaling of the length scale according to

$$Y=(\xi-1)\,Pe^b \ or\ \xi = Y\,Pe^{-b}+1, \tag{2.42}$$

where b is an arbitrary, to be determined constant. This rescaling is justified as the length of the BL has to be stretched (as it is thin). This also implies that $b > 0$ as Pe is large (leading to $Pe^b > 1$). Pe^b is called the stretching factor. Now, defining another variable $x = (\xi - 1)$, we can generically say that

$$\xi^{-n} = (1+(\xi-1))^{-n} = (1+x)^{-n}. \tag{2.43}$$

Applying binomial expansions to the radial and angular velocity respectively yields

$$\begin{aligned}
1-\frac{3}{2\xi}+\frac{1}{2\xi^3} &= 1-\frac{3}{2}\left[1-x+x^2\right]+\frac{1}{2}\left[1-3x+6x^2\right]+O\left(x^3\right)=\frac{3}{2}x^2+O\left(x^3\right)\\
1-\frac{3}{4\xi}-\frac{1}{4\xi^3} &= 1-\frac{3}{4}\left[1-x+x^2\right]-\frac{1}{4}\left[1-3x+6x^2\right]+O\left(x^3\right)=\frac{3}{2}x-\frac{9}{4}x^2+O\left(x^3\right)
\end{aligned} \tag{2.44}$$

Applying the expansions as in Equation 2.44, and the rescaling for ξ as in Equation 2.42, to the nondimensional equation with the new radial coordinate η, Equation 2.41, we get

$$\begin{aligned}
&\eta\left(\frac{3}{2}Y^2Pe^{-2b}+O\left(Pe^{-3b}\right)\right)Pe^b\frac{\partial\Theta}{\partial Y}+\frac{\left(1-\eta^2\right)}{\left(YPe^{-b}+1\right)}\left(\frac{3}{2}YPe^{-b}-\frac{9}{4}Y^2Pe^{-2b}+O\left(Pe^{-3b}\right)\right)\frac{\partial\Theta}{\partial\eta}\\
&\qquad=\frac{1}{Pe}\left[Pe^{2b}\frac{\partial^2\Theta}{\partial Y^2}+\frac{2}{\left(YPe^{-b}+1\right)}Pe^b\frac{\partial\Theta}{\partial Y}+\frac{1}{\left(YPe^{-b}+1\right)^2}\frac{\partial}{\partial\eta}\left(\left(1-\eta^2\right)\frac{\partial\Theta}{\partial\eta}\right)\right].
\end{aligned} \tag{2.45}$$

We now assess the order of magnitude of all five terms in this equation. This is summarized in Table 2.1.
As $Pe \gg 1$, the dominant convective and diffusive term must balance each other. That is, $Pe^{-b} \sim Pe^{2b-1}$ or $-b = 2b-1$ and thus $b = \frac{1}{3}$. This leads to a dimensionless BL thickness $\xi = YPe^{-1/3}+1$ which scales with $Pe^{-1/3}$.

Table 2.1: Comparison of the order of magnitude of the various terms in Equation 2.45.

Term	Type	Order of magnitude
$\eta\left(\frac{3}{2}Y^2Pe^{-2b}+O\left(Pe^{-3b}\right)\right)Pe^b\frac{\partial\Theta}{\partial Y}$	Convective	$O(Pe^{-b})$
$\frac{(1-\eta^2)}{(YPe^{-b}+1)}\left(\frac{3}{2}YPe^{-b}-\frac{9}{4}Y^2Pe^{-2b}+O\left(Pe^{-3b}\right)\right)\frac{\partial\Theta}{\partial\eta}$	Convective	$O(Pe^{-b})$
$\frac{1}{Pe}Pe^{2b}\frac{\partial^2\Theta}{\partial Y^2}$	Diffusive	$O(Pe^{2b-1})$
$\frac{1}{Pe}\frac{2}{(YPe^{-b}+1)}Pe^b\frac{\partial\Theta}{\partial Y}$	Diffusive	$O(Pe^{b-1})$
$\frac{1}{Pe}\frac{1}{(YPe^{-b}+1)^2}\frac{\partial}{\partial\eta}\left(\left(1-\eta^2\right)\frac{\partial\Theta}{\partial\eta}\right)$	Diffusive	$O(Pe^{-1})$

2.2.5. Crystal formation, growth and volume

The information in this section is mostly based on the master thesis of Korede [6]. The reasoning for the determination of the relation between crystal size and Péclet is similar to that of the nanodroplets as reported by Zhang [5]. The main difference is in the thickness of the boundary layer, that now scales with $\lambda \sim R/Pe^{1/3}$ instead of $\lambda \sim Pe^{1/2}$, which is derived completely analogue to Deen [18].

Aspirin crystals are formed in a solvent exchange process where a poor solution of aspirin saturated water hits a good solution of aspirin saturated aqueous ethanol (50/50 $\%vol$). The aspirin supersaturation is given by

$$\zeta(t) = \frac{c_{\infty(t)}}{c_s} - 1 \tag{2.46}$$

where $\zeta(t)$ is the (time-dependent) aspirin supersaturation, c_∞ is the aspirin concentration in the bulk and c_s is the local aspirin concentration. The maximum supersaturation is given by

$$\zeta_{max} = \frac{c_{s,eth}}{c_{s,wat}} - 1 > 0 \tag{2.47}$$

where $c_{s,eth}$ and $c_{s,wat}$ are the aspirin saturation concentration of the aqueous ethanol and water mixtures respectively. $\zeta = 0$ for both saturated initial solutions, as for those cases $c_\infty = c_{s,eth} = c_s$ and $c_\infty = c_{s,eth} = c_s$ as the solutions are saturated, and thus the bulk concentrations are equal to the solution saturation concentrations. As the poor solvent propagates through the channel, at a given point in the channel, first, no supersaturation is present ($\zeta = 0$). Then, the liquid-liquid interface (the front) passes the point during which $\zeta > 0$ due to diffusive mixing of the two liquid phases. After a while, the front has passed and only poor solvent is present, and thus the supersaturation is back to zero. This front is characterized by the maximum supersaturation ζ_{max} and some temporal width τ. This τ is independent of the fluid velocity and is only dependent on the diffusion coefficient D. Zhang suggests that $\tau \sim h^2/D$ [5]. The supersaturation pulse is visualized in Figure 2.10.

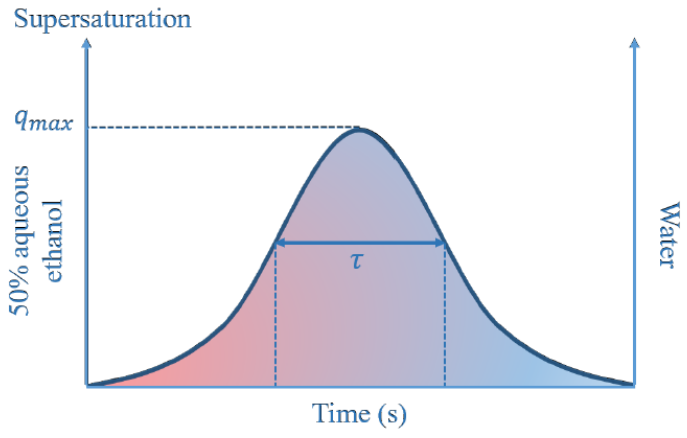

Figure 2.10: Visualisation of the supersaturation pulse. First, only saturated good solvent is present. As the mixing front passes, supersaturation increases. Once the front has passed, and the supersaturation drops back. The pulse has a temporal width τ. Adopted from Yildiz [7].

Now follows a scaling argument to find the relation between crystal size, crystal growth and Pe. The crystals are assumed to be (semi-)spheres. For a sphere with constant contact angle ϑ, lateral extension L and radius

of curvature R, the volume V scales with $V \sim R^3$. Note that the growth of the crystal is assumed to be spherically symmetrical whereas in fact it is not, due to the flow direction of the fluid. Diffusive growth behaviour implies

$$\frac{\partial m}{\partial t} = 4\pi\rho_c R^2 \frac{\partial R}{\partial t} = 4\pi D R^2 \frac{\partial c}{\partial r}\Big|_R \tag{2.48}$$

where the change of mass with respect to time is the change of volume in time ($4\pi R^2 \frac{\partial R}{\partial t}$ $[m^3/s]$) multiplied with the relevant density (ρ_c $[kg]$). This is an approach from within the droplet, where we assess the growth as a function of how much the droplet changes in size. One could also assess the growth as a function of how much solute is transported through the boundary layer to the crystal. Then, growth is characterized by the concentration gradient ($\frac{\partial c}{\partial r}|_R$ $[kg/m^4]$), how fast the solute can diffuse through the boundary layer D $[m^2/s]$, and how large the surface area is ($4\pi R^2$ $[m^2]$). Note that this analysis holds for spheres only. Addition of prefactors (α and β from subsection 2.1.3) accounts for different shapes but will not change the order-of-magnitude-argumentation.

The concentration gradient $\frac{\partial c}{\partial r}|_R$ is in the order of the boundary layer thickness and the surface and bulk concentrations according to

$$\frac{\partial c}{\partial r}\Big|_R \sim \frac{c_\infty(t) - c_{s,wat}}{\lambda}. \tag{2.49}$$

The boundary layer is assumed to follow Prandtl-Blasius-Pohlhausen-type (PBP) behavior, which means $\lambda \sim R/Pe^{1/3}$. This is also derived in subsection 2.2.4. If we remember that $\zeta(t) = \frac{c_\infty(t)}{c_s} - 1 = \frac{c_\infty(t) - c_s}{c_s}$, then logically

$$\frac{\partial c}{\partial r}\Big|_R \sim \frac{c_\infty(t) - c_{s,wat}}{\lambda} \sim \frac{c_\infty(t) - c_{s,wat}}{c_{s,wat}} \frac{c_{s,wat}}{\lambda} \sim c_{s,wat} \frac{\zeta(t)}{\lambda} \sim \frac{c_{s,wat} Pe^{1/3} \zeta(t)}{R}. \tag{2.50}$$

Plugging this final term again into Equation 2.48 gives

$$R\frac{\partial R}{\partial t} \sim \frac{D c_{s,wat}}{\rho_{asp}} Pe^{1/3} \zeta(t) \tag{2.51}$$

which can be solved to obtain

$$V_f \sim R_f^3 \sim h^3 \left(\frac{c_{s,wat}}{\rho_{asp}}\right)^{3/2} \left(\frac{c_{s,eth}}{c_{s,wat}} - 1\right)^{3/2} Pe^{1/2}. \tag{2.52}$$

We can thus conclude that under the assumptions mentioned in subsection 2.2.6 the crystal volume scales with the Péclet number according to $V_f \sim Pe^{1/2}$. The fundamental difference between Zhangs liquid-liquid-liquid (water-aqueous ethanol-oil) system and this liquid-liquid-solid (water-aqueous ethanol-aspirin) system is in the PBP behaviour that is different around solids and liquids. In liquid-liquid-liquid systems, $\lambda \sim R/Pe^{1/2}$, leading to $V_f \sim Pe^{3/4}$, whereas in liquid-liquid-solid systems $\lambda \sim Pe^{1/3}$ leading to $V_f \sim Pe^{1/2}$. This difference is due to how the fluid flows around the sphere. For a solid sphere, a no-slip boundary condition can be imposed. For a liquid sphere, the fluid in the sphere is dragged along with the fluid outside of the sphere, introducing a slip boundary condition, which automatically means that the no-slip boundary condition does not hold.

2.2.6. Assumptions

The following assumptions are taken in the derivations above:

1. Crystals are spheres.
2. Laminar flow for $Re \lesssim 1$.
3. Neglection of density difference between solutions. This is in fact a factor of about 0.9. Zhang reports this is only correct for his smallest channel [5].
4. No slip boundary condition at all walls.
5. Initial conditions: no mixing between both solvents, saturated poor solvent, saturated good solution, sharp interface at time $t = 0$.

6. The supersaturation pulse is flow rate independent.
7. No pinning and contact angle ϑ is constant. No contact angle hysteresis.
8. Symmetrical growth for droplets (true for purely diffusive growth). Does not hold here due to the flow direction, but is needed for scaling argumentation.
9. The boundary layer shows Prandtl-Blasius-Pohlhausen-type behavior.

   For the derivation of $\lambda \sim R/Pe^{1/3}$ specifically:

10. Steady state.
11. The problem is axisymetric (flow is not a function of ϕ).
12. Constant solute concentration throughout the full fluid.
13. All convection terms in the boundary layer are negligible (only diffusive behavior in the boundary layer).
14. The flow stream function for a semisphere/crystal attached to a surface is equal to the stream function of a sphere in an unconfined laminar flow.

3

Image processing

Processing large amounts of images by hand is laborious, boring, inaccurate, and not reproducible. Therefore, automatizing image processing is important. In this project, the goal of the image processing code is to identify aspirin crystals, to separate the touching and/or overlapping aspirin crystals, and to measure and document the length and width of the crystals. The full processing code used in this thesis can be found in Appendix B. Identifying and measuring the crystals are relatively straight-forward. Identifying the crystals is done using a edge detection filter, and the measuring and processing is done through fitting minimum bounding boxes to the found crystals.

The processing code written by Korede [6] and Yildiz [7] followed the philosophy of erosion and dilation to separate the touching and overlapping crystals [6, 7, 19]. First, the image is processed in such a way that it no longer consists of colors, but only of black (0) and white (1), where all background is 0 and all crystals are 1. Then, the dilation and erosion process starts. In dilation, the objects are shrunk to a certain extend by applying a mask to the image. The mask detects if a 1 is at the crystal edge, and then removes it. This causes some of the touching and overlapping crystals to no longer touch, or overlap. The computer now sees them as separate objects. This is also depicted in Figure 3.1. The crystals are then 'grown' back to the original size,

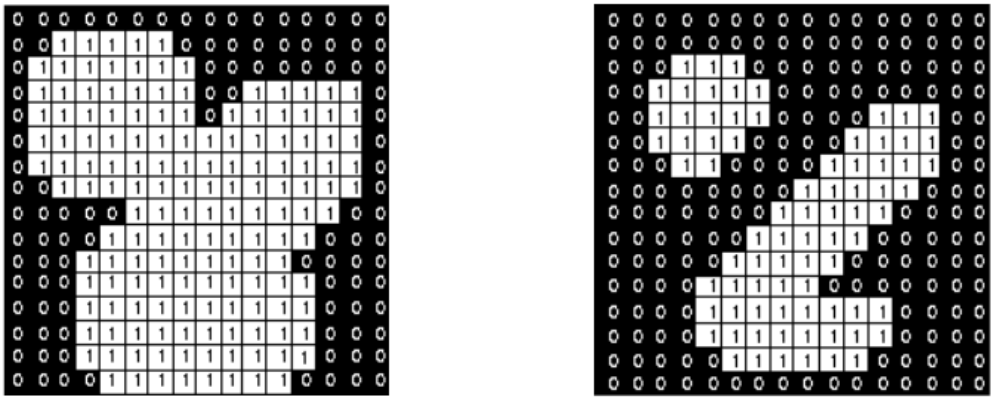

(a) Before dilation.

(b) After dilation.

Figure 3.1: Dilation of overlapping objects. Dilation shrinks objects, causing overlapping objects to be separated. The problem of dilation is also apparent here: to separate the bottom right two objects, the image should be dilated a lot further. That would cause the top left object to disappear completely. Adopted from [20].

while the computer still sees them as separate images. That is called erosion. This approach is discussed in detail by Yildiz [7]. It has a big disadvantage. For large, overlapping crystals, the dilation should be strong, as otherwise, dilation will not separate these crystals. For small crystals however, strong dilation causes them to disappear as all ones get converted to zeros. The erosion algorithm cannot detect these crystals anymore, and thus cannot grow them back. This calls for area dependent dilution and erosion, which does not work very well [7]. Therefore, a new approach to image segmentation is applied in this thesis. In 2017, Abhinav proposed an algorithm that separates overlapping rectangular objected based on the shape their contour has

[21]. The general idea is to segment the contour of a bundle of overlapping crystals into contour segments that cannot be part of overlapping crystals (that must be part of one crystal).It does this, by checking how the contour segments are orientated. Imagine walking around a square block of houses. You can only keep walking around the same block if you keep turning right. Once you take a left turn, you automatically are walking around another block of houses. The same idea is used to identify contour segments that must be part of the same crystal. The algorithm 'walks' over the full contour clockwise. When it is forced to take an anticlockwise turn, it knows that it can no longer be on the same crystal edge. A new contour segment is then started, until a next anticlockwise turn appears, or the full contour has been processed. Then, it is checked if any of the contour segments should be grouped together because they are from the same crystal, by checking if their orientation is in the same direction. The processing of images now consists of eight steps:

1. Image gathering and preprocessing (rescaling, denoising and thresholding).
2. Contour retrieval from the image (gathering all contour points).
3. Separating corner points from contour points.
4. Separating out concave corner points.
5. Defining contour segments (pieces of contour that must be of the same crystal).
6. Mapping together contour segments of the same crystal.
7. Shape fitting of the objects from the mapped contour segments (assigning minimum bounding boxes).
8. Measurement and processing of obtained data.

To find the above mentioned contour segments, it is desired to find the points where the contour makes a sharp change in direction that is opposite to the direction of the full contour. Those points are called concave points. The contour segments between those concave points are the contour segments that must be part of a single crystal. To find the concave points, first, the contour points and all corner points need to be found. Contour points can be found with edge detection algorithms. The Suzuki algorithm is used in this processing code [22]. Corner points are the points where the contour makes a significant change in direction. They are detected using the Ramer-Douglas-Peucker (RDP) algorithm [23]. From those corner points, the concave points are selected. Concave points are those corner points where the direction (clockwise or anticlockwise) of the rotation that a point has, is opposite to the average (net) rotation of the full contour. So, if a contour is analysed in the clockwise rotation, a corner that has a counterclockwise rotation is marked as a concave point. Contour-, corner- and concave points are shown for a full contour in Figure 3.2 on page 21.

Once the contour segments have been identified, the contour segments that correspond to the same crystal need to be matched. This is done by fitting an ellipse to each segment, and then checking for all segments if the orientation of the ellipses matches. When the angles of the ellipses are within a certain error ϵ, the segments are assumed to be of the same crystal. This is shown in Figure 3.3 on page 22.

Once the segments have been mapped together, they can be shape-fitted. The caliper rotation algorithm from Shamos [24] is used to fit a minimum-bounding rectangle. The rectangles are then measured and documented.

Abhinav reports a precision of his algorithm of over 80% [21]. For the analysed figure, the proposed new code has a precision of over 95%, as can be seen in Table 3.1 on page 23. A comparison between the original image, the image processed with the old code and the image processed with the new code is shown in Figure 3.4 on page 22. It has half the error in terms of length, and one tenth of the error in terms of width compared to the old code of Yildiz [7]. That is under the assumption that false measurements that the new code often has are filtered out. This is possible, because the false measurements come from unmatched segments, making them very thin in width. Filtering with a threshold of a width of 6 pixels takes out most false measurements. The code tends to work better with figures that are not too crowded with crystals.

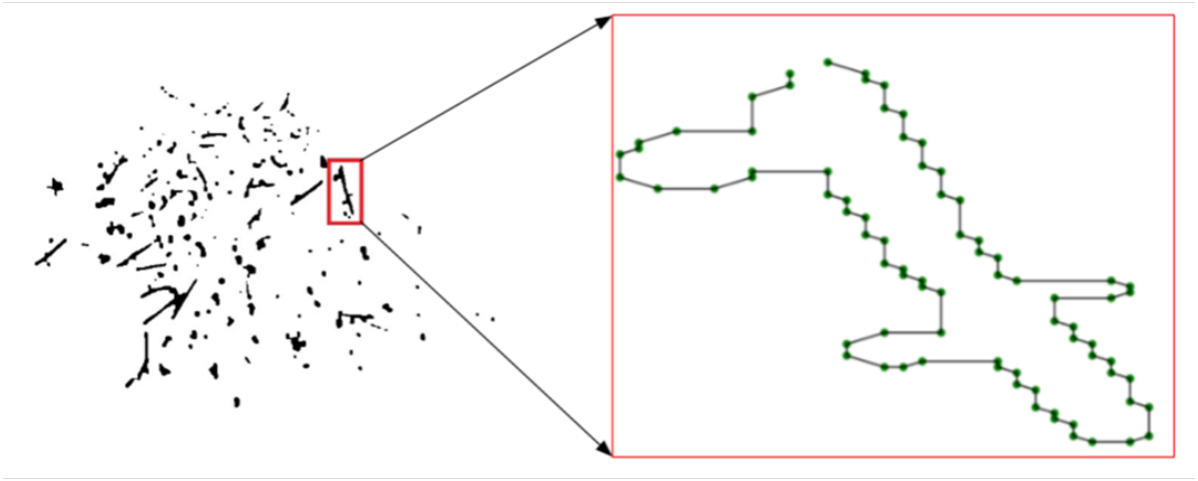

(a) Contour points.

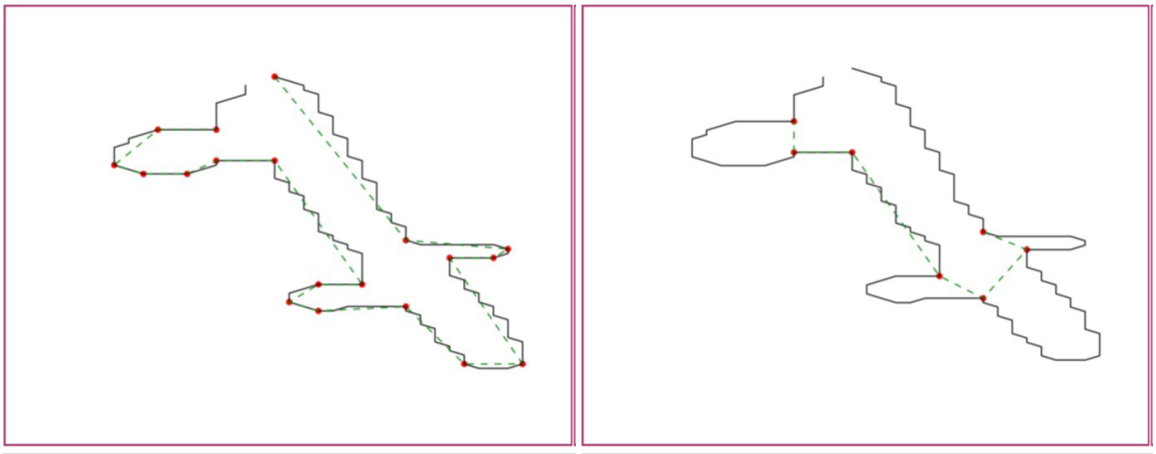

(b) Corner points.

(c) Concave points.

Figure 3.2: Contour-, corner-, and concave points from the contour of a crystal. Corner points are selected from the contour points, concave are obtained through further selection from corner points.

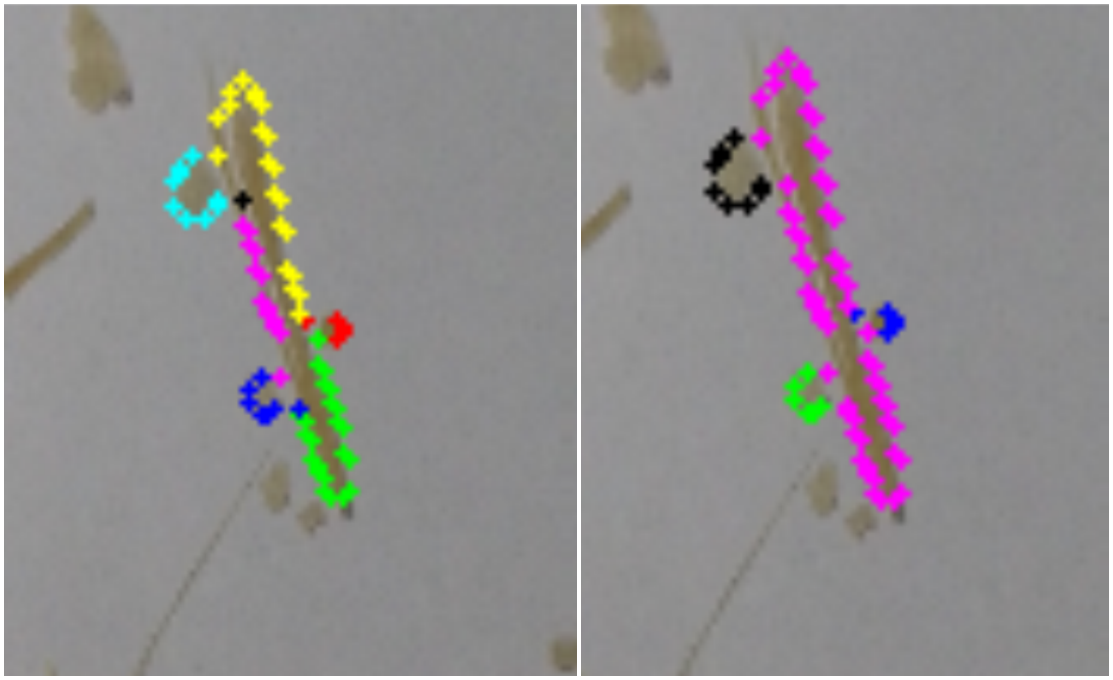

(a) Contour segments before mapping together.

(b) Contour segments after mapping together.

Figure 3.3: Contour segments before and after mapping together the corresponding ones. All contour segments are fitted with an ellipse. If the angle of two or more ellipses are within a certain error ϵ of each other, the contour segments are assumed to be in the same crystal and are mapped together.

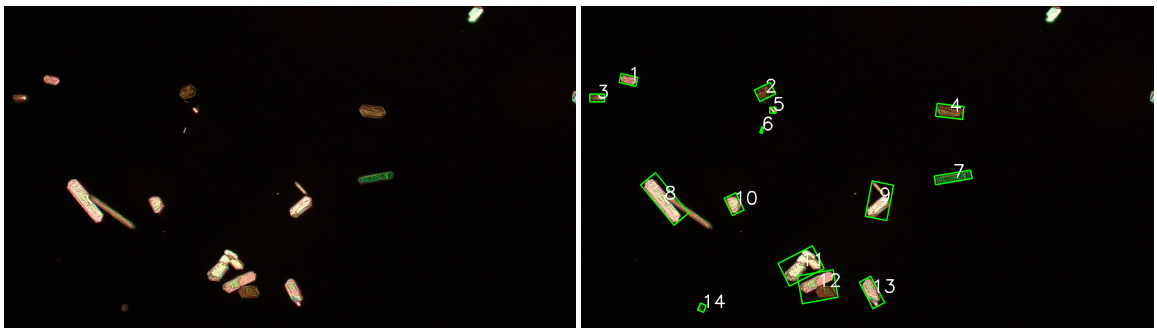

(a) Not processed.

(b) Processed with code from Yildiz.

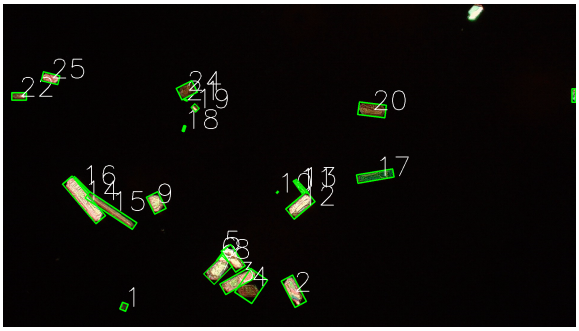

(c) Processed with code from Van Nes.

Figure 3.4: Comparison of image segmentation algorithms of Yildiz [7] and Van Nes. The code from this author separates out overlapping crystals a lot better, but does generate some more noise.

Table 3.1: Absolute errors in the old image processing code and the new image processing code. No corresponds to the crystal number in Figure 3.4c, L is the crystal length in pixels, W is the crystal width in pixels, ϵ is the absolute value of the percentual error compared to the manually measured width (L and W in the table). N/D is a not detected crystal, NO is a false detection of the software. The new code has half the error in terms of width, and on tenth of the error in terms of length compared to the old code, when the NOs are left out. NOs can be filtered out, because false measurements always have a very small width (<6 pixels).

No	L	W	L old	W new	ϵ L old	ϵ W old	L new	W new	ϵ L new	ϵ W new
1	25,378	20,792	25,080	21,541	1,043	1,027	24,326	20,241	0,988	1,036
2	101,518	41,931	100,185	42,942	1,024	0,988	99,111	42,430	0,987	1,024
3	122,823	34,7	121,824	94,541	1,102	0,864	111,463	40,177	0,992	2,725
4	75,145	41,11	N/D	N/D	0,794	0,600	94,670	68,567	N/D	N/D
5	NO	NO	N/D	N/D	NO	NO	16,553	3,383	NO	NO
6	NO	NO	N/D	N/D	NO	NO	33,601	2,143	NO	NO
7	82,03	48,352	129,252	84,971	0,951	0,977	86,267	49,497	1,576	1,757
8	83,794	34,493	N/D	N/D	0,977	0,887	85,762	38,891	N/D	N/D
9	61,602	43,218	63,506	43,382	0,984	1,017	62,610	42,485	1,031	1,004
10	8,707	3,482	N/D	N/D	1,231	0,821	7,071	4,243	N/D	N/D
11	60,105	10,796	N/D	N/D	1,105	1,859	54,406	5,808	N/D	N/D
12	92,223	41,389	121,202	73,348	1,006	0,943	91,667	43,875	1,314	1,772
13	NO	NO	N/D	N/D	NO	NO	59,464	5,583	NO	NO
14	169,012	45,393	175,411	64,661	0,975	1,081	173,347	41,992	1,038	1,424
15	187,856	20,94	N/D	N/D	0,993	0,797	189,104	26,288	N/D	N/D
16	NO	NO	N/D	N/D	NO	NO	71,421	5,517	NO	NO
17	125,522	31,136	123,628	29,428	1,025	1,114	122,494	27,939	0,985	0,945
18	20,614	6,803	19,925	7,280	1,086	1,132	18,974	6,008	0,967	1,070
19	21,225	14,674	21,000	20,000	1,001	0,830	21,213	17,678	0,989	1,363
20	90,392	43,587	91,662	43,417	0,994	1,016	90,917	42,916	1,014	0,996
21	16,372	3,962	N/D	N/D	1,472	1,472	11,119	2,692	N/D	N/D
22	50,694	27,671	49,000	26,000	1,035	1,107	49,000	25,000	0,967	0,940
23	42,626	14,001	N/D	N/D	0,947	1,077	45,000	13,000	N/D	N/D
24	57,442	43,824	59,034	42,485	0,988	1,042	58,138	42,038	1,028	0,969
25	55,845	27,907	57,489	30,806	0,984	0,927	56,749	30,105	1,029	1,104
Av. ϵ					1,034	1,028			1,065	1,295

4

Methodology

4.1. Experimental setup

Antisolvent crystallization was performed in a microfluidic setup. The setup consists of three sections: i) before the channel, ii) the channel and iii) after the channel. The specifications of the used products are given in Table 4.1. The section before the channel starts with two separate microfluidic pumps. The syringe pumps are both loaded with 20 ml syringes (internal diameter 19.9 mm) that are both connected with microfluidic tubing to bubble traps to filter out air bubbles. The bubble traps are connected to check valves with tubing. These check valves are connected directly (no tubing) with a Y-junction. The third outlet of the Y-junction is connected to the channel.

The channel is built in layers. The bottom layer is a custom made water jet cut aluminium frame, with eight M3 tapped holes for screw-thread, that fits the microscope placeholder. On top of that lays a (treated) microscopic slide face up, on which a custom cut silicon rubber channel is placed. Then, a transparent polycarbonate spacer with screw in- and outlet for the flow is place on top of the channel. This is finished with another piece of aluminium frame (without the semi-circles present at the bottom frame plate to fit the microscope support structure) with holes that match the holes of the bottom frame, but that are not threaded. The whole channel is tightened with M3 screw-thread and M3 bolts. A representative visualization of the channel can be found in Figure 4.1

After the channel, the outlet is connected with microfluidic tubing to a waste container. A representative visualisation of the experimental setup can be found in Figure 4.2. The exact products used can be found in Table 4.1.

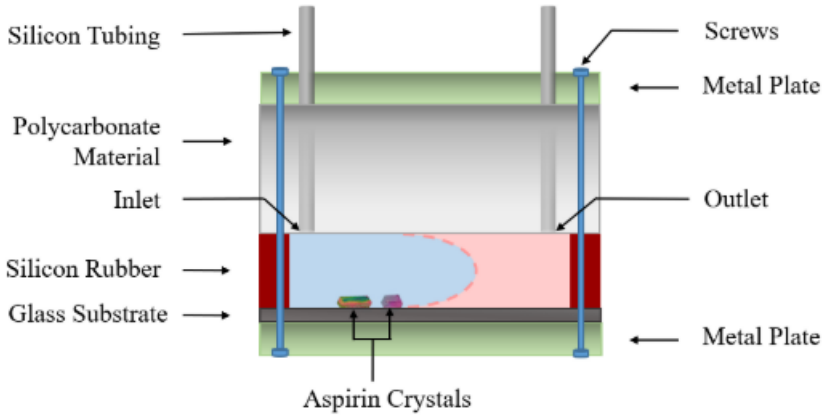

Figure 4.1: Schematic vizualisation of the microfluidic channel. The channel is made up of the glass substrate, a silicon rubber and a polycarbonate spacer that are held together with an aluminium support structure. Adopted from Yildiz [7].

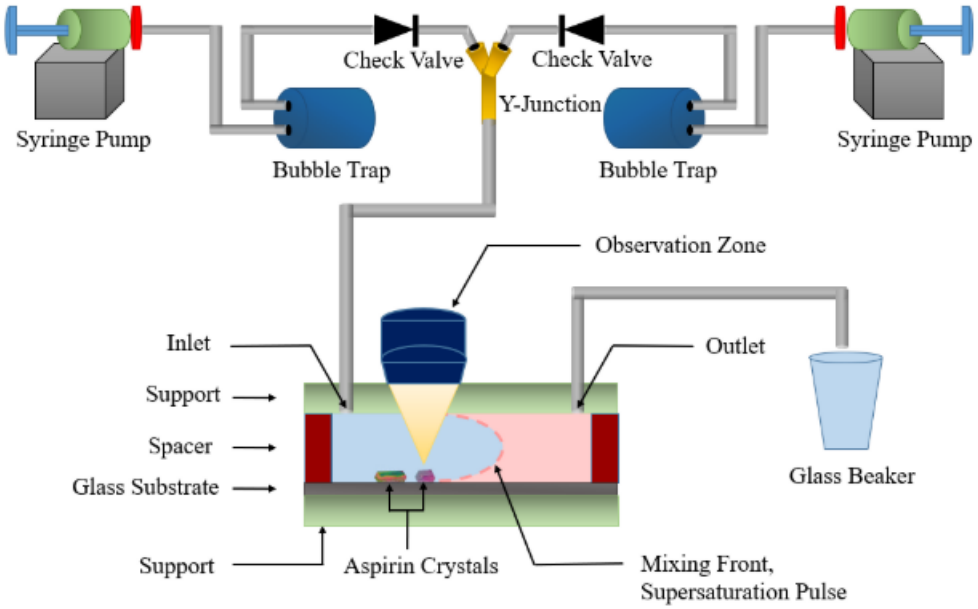

Figure 4.2: Schematic visualization of the experimental setup. The solvents are led through a microfluidic system containing bubble traps and check valves to the channel. Adopted from Yildiz [7].

Table 4.1: Chemicals, materials, and equipment for the experimental setup.

Product	**Type**
Materials	
Aluminium frame	Custom made water jet cut aluminium frame. Design can be found in Appendix C
Bolt	Aluminium bolt size M3
Bubble trap	Darwin Microfluidics inline with PTFE membrane
Check valve	Idex inline check valve
Microfluidic tubing	Darwin Microfluidics, Product SKU: SHE-TUB-SIL-1*1 (Internal Diameter 1 mm)
Microscopic slides	VWR 631-1550 Microscope Slides cut edges ($76x26$ mm)
Polycarbonate spacer	Custom made spacer. Design can be found in Appendix C
Screw-thread	Aluminium screw-thread size M3
Silicon rubber	Custom cut channel, dimensions $52x14x0.3$ mm. Design can be found in Appendix C
Syringe	Braun Omnifix 20 ml Latex Free (19.90 mm internal diameter)
Y-junction	Idex PEEK Y connector
Equipment	
Inverted microscope	Zeiss Axiovert 200 M Inverted Microscope (5x/0.25NA *or* 20x/0.40NA lens)
Syringe pump (high flow rates)	Harvard Apparatus PHD 2000 infuse/withdraw
Syringe pump (low flow rates)	NE-4002X Programmable 2 Channel Microfluidics

4.2. Antisolvent crystallization procedure

Antisolvent crystallization experiments were performed throughout this research with various variations in the substrate used. The protocol is described below. The exact products used can be found in Table 4.2.

1. Prepare a good and a poor solution of desired concentrations aspirin in glass bottles. The good solution is demineralized water with aspirin. The poor solution is a 50/50%vol ethanol/demineralized water with aspirin solution.
2. Stir the solutions vigorously with stirring beads until all crystals are dissolved.
3. Clean all of the parts of the microfluidic channel, all tubings and all connections with isopropanol, demineralized water, and isopropanol and blow them dry using pressurized N_2. Do *not* clean the glass substrate with isopropanol.
4. Assemble the microfluidic channel as shown in Figure 4.1 with a glass substrate treated as desired, but do not yet connect the tubing to the channel. Tighten the bolts well, but not so tight that the glass substrate breaks.
5. Filter both the good and the poor solution through a Whatmann pore size 0.45 μm syringe filter (white rim) to remove any solids from the solutions.
6. Fully fill 20 ml syringes with good and poor solution.
7. Connect the syringe containing poor solution to the tubing and flush the tubing with 10 ml of poor solution.
8. Connect the syringe containing good solution to the tubing and flush the tubing with 10 ml of good solution.
9. Place the channel in the microscope.
10. Connect the tubing to the channel and place the syringes in the syringe pumps. Also connect the exit tube. Make sure the syringes and channel are on the same height, to eliminate gravitational effects.
11. Set the syringe pumps to the desired volumetric flow rate.
12. Fill the channel with good solution at 100 $\mu l/min$, making sure no air bubbles are present in the channel. When air bubbles do occur, the channel can be tilted to help them out of the channel.
13. Wait for 1 min to ensure a steady flow profile.
14. Stop the flow of good solvent, and start the flow of poor solvent at the desired volumetric flow rate.
15. Run the experiment for 10 minutes.
16. Remove the glass substrate from the channel and blot the remaining liquid of the substrate to prevent evaporative crystallization.

Table 4.2: Chemicals, materials, and equipment for antisolvent crystallization experiments.

Product	**Type**
Chemicals	
Aspirin	Acetylsalicyl acid Sigma Aldrich ≥ 99.8%
Demineralized water	Elga PURELAB ULTRA 18.2 $m\Omega cm$
Ethanol	Sigma Aldrich ≥ 99.8%
Isopropanol (cleaning solvent)	VWS 2-propanol ≥ 99.8%, TECHNICAL, 20922.364
Materials	
Glass bottle	200 ml standard lab bottle with plastic screw cap
Stirring bead	Standard stirring bead
Syringe	20 ml, 19.90 mm internal diameter
Syringe filter	Whatman pore size 0.45 μm (white rim)
Equipment	
Inverted microscope	Zeiss Axiovert 200 M InvertedMicroscope (5x/0.25NA *or* 20x/0.40NA)
Syringe pump (high flow rates)	Harvard Apparatus PHD 2000 infuse/withdraw
Syringe pump (low flow rates)	NE-4002X Programmable 2 Channel Microfluidics
Microfluidic channel	
Aluminium frame	Custom made, design can be found in Appendix C
Bubble trap	Darwin Microfluidics inline with PTFE membrane
Channel	Silicon rubber with dimensions 52x14x0.3 mm
Check valve	Idex inline check valve
Hydrophobized glass substrate	According to protocol in section 4.3
Spacer	Polycarbonate spacer with two tapped tubing entrances. Design can be found in Appendix C
Microfluidic tubing	Darwin Microfluidics, Product SKU: SHE-TUB-SIL-1*1 (Internal Diameter 1 mm)
Y-junction	Idex PEEK Y connector

4.3. Hydrophobization of glass slides

Glass substrates are hydrophobiced to make them more susceptible to adhering crystals at their surface. The protocol is described below. The exact products used are given in Table 4.3.

1. Thoroughly clean a 800 ml beaker with acetone.
2. Prepare 600 ml of a 0.1 M NaOH solution in demineralized water (0.4 g NaOH per 100 ml demineralized water) in the beaker.
3. Place the designated amount of glass substrates (microscope slides) in the beaker, such that the glass substrates do not touch and the large substrate surfaces do not touch the beaker. Leave in the solution for 15 minutes.
4. Clean a desiccator with isopropanol.
5. Put a small droplet of the hydrophobizing agent trichloro(1H,1H,2H,2H-perfluorooctyl)silane in a clean glass petri dish and put in in the bottom half of the desiccator.
6. Take the glass substrates out of the NaOH solution and dry them using compressed N_2. Place them in the desiccator. Arrange the substrates such that they do not overlap.
7. Depressurize the desiccator to 100 $mbar$ and leave for 2 h.
8. Remove the slides from the desiccator and rinse with demineralized water and optionally a low fibre tissue.

Table 4.3: Chemicals, materials, and equipment for the hydrophobation of glass slides.

Product	**Type**
Chemicals	
Acetone (cleaning solvent)	VWR Acetone TECHNICAL ≥ 99%, 20063.365
Demineralized water	Elga PURELAB ULTRA 18.2 $m\Omega cm$
Hydrophobizing agent	Trichloro(1H,1H,2H,2H-perfluorooctyl)silane
Isopropanol (cleaning solvent)	VWS 2-propanol ≥ 99.8%, TECHNICAL, 20922.364
Materials	
Beaker	Standard beaker 800 ml
Glass substrates (microscopic slides)	VWR 631-1550 Microscope Slides cut edges (76x26 mm)
Petri dish	Glass petri dish that fits the desiccator
Equipment	
Desiccator	KARTELL FILTRATION & VACUUM DESICCATOR
Vacuum pump	KNF Vac control NSE 800.40

4.4. PDMS coating of glass slides

Glass slides are coated with PDMS that functions as a glue for seeding of substrates. The exact products used can be found in Table 4.4.

1. Thoroughly clean a microscopic slide with methanol.
2. Mix in a 1:10 ratio PDMS Curing Agent & PDMS in a reaction tube and mix well with a spatula until it turns opaque due to formation of small bubbles.
3. Centrifuge the mixture for 15 min at 15000 rpm to remove air and to let any dirt sink to the bottom of the tube.
4. Fix a clean microscopic slide in the spin coater using the vacuum setting.
5. Apply 0.5 ml of the PDMS and activator mixture in a line on the slide.

6. Run the spincoater on a program of 80 sec at 4500 rpm, which has a 10 sec linear rotational velocity increase in the beginning and a 10 sec linear rotational velocity decrease at the end.
7. Put the microscopic slide in a petri dish, and cure it in an oven at 65 °C for 30 min.
8. Remove the slide from the oven and sprinkle with the desired crystals.
9. Put the slide back into the oven at 65 °C for at least 3 h, until the PDMS has hardened.

Table 4.4: Chemicals, materials, and equipment for the PDMS coating of glass slides.

Product	**Type**
Chemicals	
Aspirin	Acetylsalicyl acid Sigma Aldrich ≥ 99.8% ground to desired size
Methanol (cleaning solvent)	VWR Methanol TECHNICAL ≥ 98.5%, 20903.368
PDMS	SYLGARD 184 Silicone Elastomer Base
PDMS Curing Agent	SYLGARD 184 Silicone Elastomer Curing Agent
Materials	
Microscopic slide	VWR 631-1550 Microscope Slides cut edges (76x26 mm)
Petri dish	Plastic Petri dish, internal diameter 8.6 cm
Reaction tube	Corning 50 ml
Spatula	Metal spatula
Syringe	Braun Injekt-F 1 ml
Equipment	
Centrifuge	Hettich Universal 320R
Oven	Binder 02-32825
Spincoater	POLOS Spin 150i

4.5. Safety

Lab safety is very important. During this project, proper safety measures were taken in the form of personal protective equipment and working in a safe laboratory environment. Material Safety Data Sheets (MSDS) of all used chemicals can be found in Appendix D.

5

Results and discussion

5.1. Recap previous results

In previous works [7], antisolvent crystallization experiments with various flow rates and supersaturations were performed. The main takeaways were:

1. All flow rates give similar probability density functions (PDFs) and thus crystal size distribution is not flow rate (or Péclet) dependent for that setup. This is clearly shown in Figure 5.1.
2. Working with undersaturated poor solutions can lead to (partial) dissolution of formed crystals, leading to false measurements.
3. Higher flow rates induce higher dissolution of formed crystals.

The relation between the flow rate Q, the velocity in the channel, Pe and Re can be found in Table 5.1.

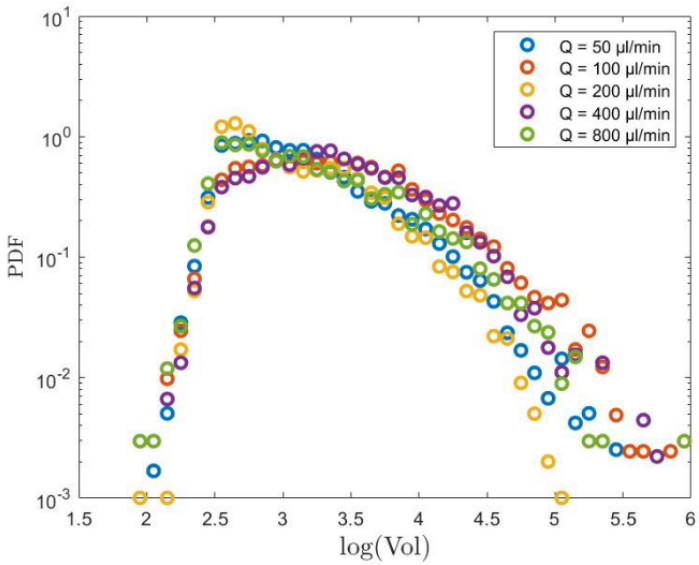

Figure 5.1: Results from experiments performed by Yildiz [7]. All flow rates, and thus all Pe give the same PDF, as all the points overlap. Adopted from Yildiz [7].

5.2. Antisolvent crystallization with saturated poor solution

The experiments performed by Yildiz with both undersaturated good and poor solutions were repeated, with the only difference that the poor solution was now saturated. This mitigates the problems of dissolution into the poor solution, which made proper measurement of final crystal size very challenging. The results of

Table 5.1: Velocity, Péclet and Reynolds in the channel for various flow rates. The low Re indicates laminar flow.

Flowrate $[\mu L/min]$	**Velocity in channel** $[mm/s]$	Pe $[-]$	Re $[-]$
50	0.198	59.5	0.059
100	0.397	119.1	0.119
200	0.794	238.1	0.238
400	1.587	476.2	0.475
800	3.175	952.4	0.951

these experiments can be found in Figure 5.2. These results, albeit they are a bit messier than the ones from Yildiz [7], point in the same direction. There is no correlation between the crystal size and the flow rate, and different flow rates give the same crystal size distribution. This can be seen from the fact that all the PDFs overlap, and are not side by side like in Zhangs research (Figure 1.1b) [5]. The 200 $\mu L/min$ lies out slightly, which is probably due to an air bubble trapped in the channel during that experiment.

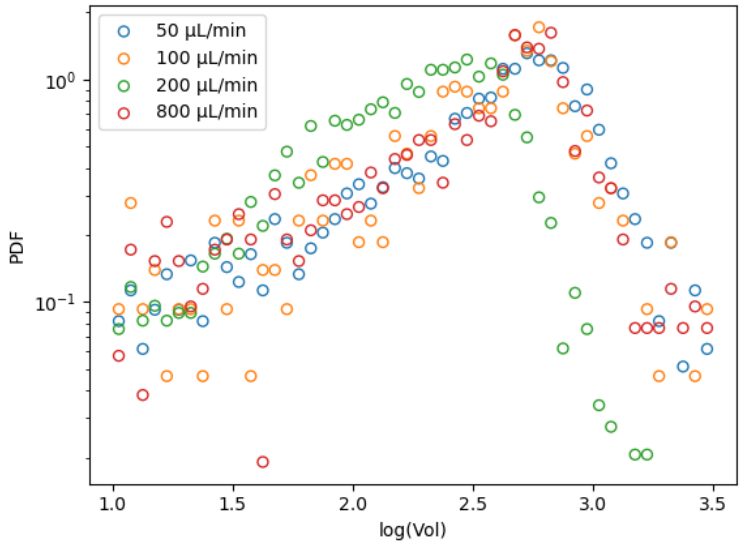

Figure 5.2: Results of experiments with one saturated and one undersaturated solution. On the x-axis, the logarithm of the volume in μm^3. On the y-axis, the PDF. The results show a trend similar to the results from Yildiz [7]. All flow rates give a similar PDF.

5.3. Sedimentation of crystals

The uniformity of the crystal size distributions rises doubts about whether or not the crystals that are observed and measured are actually formed at the solutions interface. Therefore, videos of the channel were made during the experiment to capture the formation of crystals at the interface. Snapshots of a video taken during an experiment with a 50% saturated good solution, 100% saturated poor solution at a flow rate of 200μ L/min (Pe = 238) are shown in Figure 5.3 on page 33. In the video, it is clear that sedimentation of crystals occurs on a very large time scale. This indicates that not all crystals observed on the substrates are crystals formed at the solutions interface.

The sedimentation of crystals can be approached from at theoretical standpoint. To see if a particle stays in suspension, its potential energy E_{pot} $[J]$ (gravity) needs to be matched to its kinetic energy E_{kin} $[J]$ (the random movement its makes and the collisions with its surroundings). The energies are given by

$$E_{pot} = mgh, \tag{5.1}$$

$$E_{kin} = \frac{1}{2} k_B T, \tag{5.2}$$

where m $[kg]$ is the particle mass, g $[m/s^2]$ is the gravitational acceleration, H $[m]$ is the characteristic height,

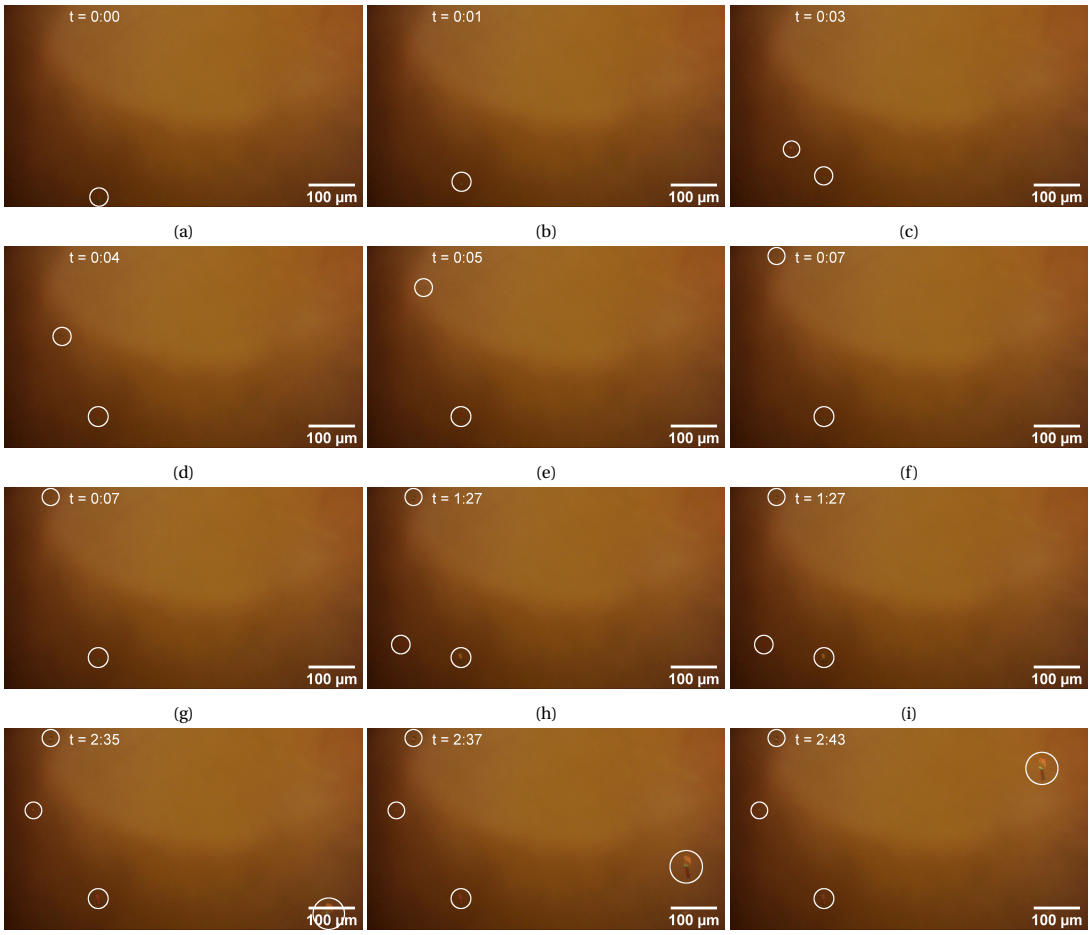

Figure 5.3: Sedimentation of crystals during antisolvent crystallization. Crystals that sediment are highlighted with white circles. Multiple crystals pass and sediment over the course of several minutes, while the supersaturation pulse passes the field of view in a matter of seconds. Experiment performed with 50% saturated good solution, 100% saturated poor solution and at 200 $\mu L/min$ ($Pe = 238$).

$k_B = 1.3806 \cdot 10^{-23}$ $[(m^2 kg)/(s^2 K)]$ is the Boltzmann constant and T $[K]$ is the absolute temperature. As the particle under consideration is submerged, the buoyancy corrected weight needs to be taken into account to compensate for the natural pressure gradient fluids have, such that

$$m = (\rho_c - \rho_w)V, \tag{5.3}$$

where ρ_c $[kg/m^3]$ is the crystal density and ρ_w $[kg/m^3]$ is the solution density (water in this case). This allows for the characteristic height H to be found:

$$H = \frac{k_B T}{2\Delta\rho V}. \tag{5.4}$$

The characteristic height needs to be compared to the relevant height h of the container the process takes place in. In these experiments, that is the channel height. When $H >> h$, the Brownian motion (kinetic energy) is dominant and the particles stay suspended. When $H \sim h$, the particles will sediment diffusively, as the potential and kinetic energy balance each other. When $H << h$, the particles will sediment with gravity. For this work, not H is relevant, but the particle radius R $[m]$ is. We can derive the critical sedimentation radius that is observed by filling out $H << h$ in

$$R \sim V^{1/3} \sim \left(\frac{k_B T}{2\Delta\rho H}\right)^{1/3} \tag{5.5}$$

Doing this for H of one order of magnitude lower than the channel height $h = 3 \cdot 10^{-4}$ m, $\Delta\rho = 0.4$ kg/m^3 and $T = 293$ K, a critical sedimentation radius of $R \sim 5.5 \cdot 10^{-6}$ m (5.5 μm) is found. This in the same order of magnitude as the found sedimented particle size of $\sim 15\mu m$ in Figure 5.1 and Figure 5.2. Note that the critical sedimentation size is theoretically also flow rate independent.

A competition between five forces starts once a crystal has reached its critical sedimentation size. The crystal is pushed in the positive x-direction by the convective flow, but also experiences drag from the fluid in the negative x-direction. It experiences a buoyancy force in the positive y-direction, but also experiences gravity in the negative y-direction. Finally it experience a Stokes drag force in the positive y-direction. As the crystal grows, the gravitational and drag effects increase, leading to sedimentation. This is visualized in Figure 5.4 on page 35. As this sedimentation occurs, the observed crystals are not solely formed and grown at the interface of the good and poor solution. Because of these competing times scales, all previous results (from Korede [6], Yildiz [7] and Van Nes (section 5.2)) are more a representation of the results from a sedimentation antisolvent crystallization experiment rather than from an interface formation and growth antisolvent crystallization experiment. This also explains why all previous experiments showed the same PSD for all Pe: when the observed phenomenon is in the sedimentation time scale, crystal size is the effect that causes the crystal to sediment. That leads to observation of only one size crystal, as visible in Figure 5.1 and Figure 5.2.

5.4. Seeding with glue

As crystals have to grow to reach a certain size, the growth rate is of just as much interest as the final size. After all, the theoretical final crystal size (Equation 2.52) is derived from the linear growth rate $G = \frac{\partial R}{\partial t}$ (Equation 2.51). The growth rate also scales positively with Pe. Furthermore, the growth rate is supersaturation dependent [25, 26], and thus is a good measure of the presence of a supersaturation pulse. To mitigate the effects of sedimentation, the channel was seeded with aspirin crystals to observe growth at the seeds. Crystals that sediment can be ignored in this process.

5.4.1. UV-glue

Large crystals directly from the jar of aspirin were glued into the channel with UV-hardening glue (JML, 5 second fix). Two problems occurred. Firstly, when a normal size droplet of glue was applied, the crystal that needed to be put on top of the droplet had to be very large not to sink in the glue straight away. That caused the crystal to be crushed into a powder when the channel was assembled, as it was larger then the height of the channel. Secondly, applying a reproducible small droplet of glue was experimentally very challenging. The combination of these problems led to the conclusion that gluing with droplets of glue will not work. A snapshot of the experiment can be found in Figure 5.5a.

5.4.2. PDMS

After the failed UV-glue experiment, an attempt was done to glue the crystals in the channel using sticky polydimethylsiloxane (PDMS). Glass slides were coated with PDMS in accordance with the procedure described

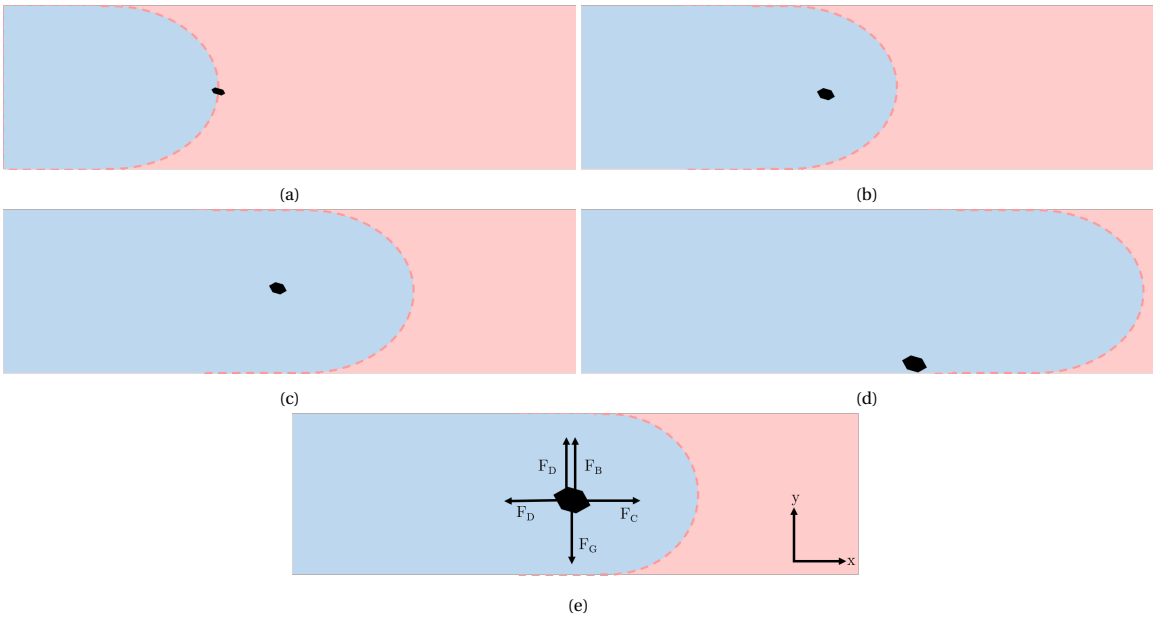

Figure 5.4: Projected trajectory of sedimentation of a crystal. Five forces balance each other: gravity (F_G) in the negative y-direction, buoyancy (F_B) and Stokes' drag (F_D) in the positive y-direction, drag (F_D) in the negative x-direction and the convective flow (F_C) in the positive x-direction. Crystals are formed at the interface. Then, the crystals start growing, and thus gain drag and reduces in velocity compared to the fluid. The interface outruns the crystal. Once the crystal has grown sufficiently, gravitational effects outweigh the buoyancy effects and the crystal starts sedimenting.

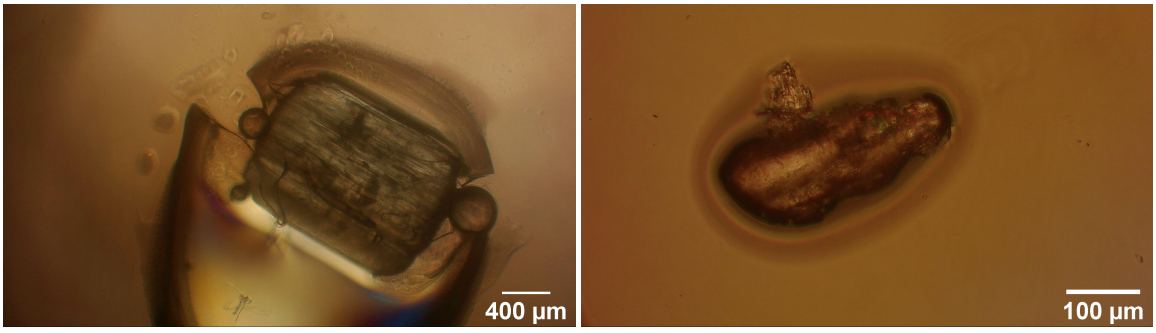

Figure 5.5: Crystals glued into the microfluidic channel. On the left, an aspirin crystal from the jar is glued into the channel with UV-hardening glue. On the right, crystals are sprinkled on PDMS coated glass substrates, which are hardened at 65°C.

section 4.4. Pure aspirin crystals were ground with a pestle and mortar and sieved to two ranges of sizes: $100-150\ \mu m$ and $150-250\ \mu m$. Note that crystals can only be sorted by their second relevant length scale, width in this case. These sorted crystals were sprinkled onto the PDMS coating and the antisolvent crystallization experiment was performed. An example of a crystal glued with PDMS can be found in Figure 5.5b on page 35.

In the experiments where PDMS coated slides were sprinkled, no lateral growth was observed. The 'texture' of the crystals however changed significantly (Figure 5.6), leading to thoughts that there must be some sort of supersaturation causing vertical growth of the crystal. This vertical growth is of less interest, as the dominantly growing face of aspirin crystals is the face in the longest direction [27]. The inhibition of this growth, because the crystal is embedded in the PDMS, causes non-physical behaviour, and thus is of less value.

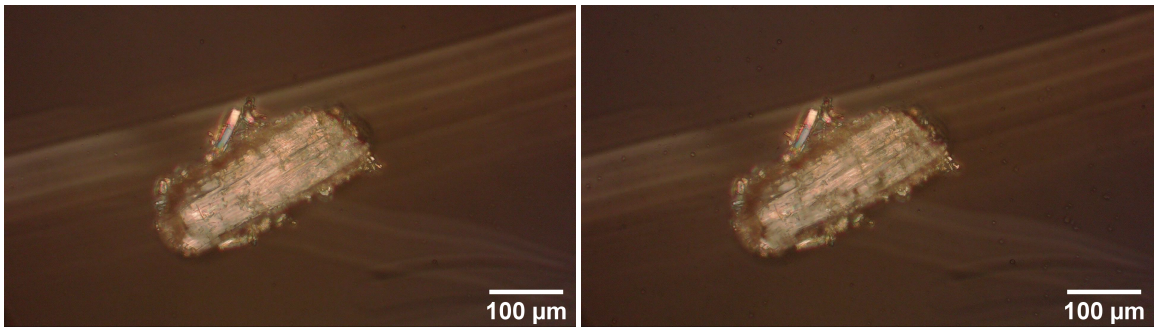

(a) PDMS glued crystal before supersaturation pulse.

(b) PDMS glued crystal after supersaturation pulse.

Figure 5.6: Crystal that has been glued into the channel with PDMS before (left) and after (right) the supersaturation pulse. The texture of the crystal changes over time while its length and width stay constant. This indicates that growth does take place, but not in the lateral direction.

5.5. Seeding with old slides

Another attempt at seeding was performed with slides from previous experiments. These slides contain crystals at their surface from the sedimentation set of experiments. These slides have the benefit of having no lateral growth impairing glues and have relatively uniform crystal size distributions due to the sedimentation effects, with it peak in PDS at $\sim 15\mu m$ in length. An example of such a slide is shown in Figure 5.7a. These experiments, must be performed with both saturated good and poor solutions, as undersaturated solutions dissolve the seeds before the saturation pulse has passed.

For seeded slides, linear growth rate during the supersaturation pulse was measured in experiments with flow rates ranging from 50 $\mu L/min$ to 800 $\mu L/min$ ($Pe = 59-952$). As can be seen in Figure 5.9 on page 38, for all flow rates the amount supersaturation pulse is visible in the height of the linear growth rate. The expected Gaussian supersaturation profile that occurs due to diffusion also is visible in the linear growth rate. The higher the flow rate is, the larger the peak of the linear growth rate is, and the narrower the trend is. This indicates a narrow and intense supersaturation pulse for high flow rates, and a wide and mild supersaturation pulse for lower flow rates. The width of the linear growth rate profile is explained by the fact that the fluid passes over the seed quickly at high flow rates, and slowly at low flow rates. The height of the linear flow rate profiles is explained by realizing that higher flow rates lead to thinner BLs, which have lower diffusive limitations and thus allow for faster crystal growth. The average linear growth rate profile of all trials are plotted in Figure 5.9d on page 38.

The linear growth rate can also be plotted as a function of the Péclet number, as shown in Figure 5.8 on page 37. Growth rate and the Péclet number have a positive correlation, although due to the lack of data no representative fit can be made.

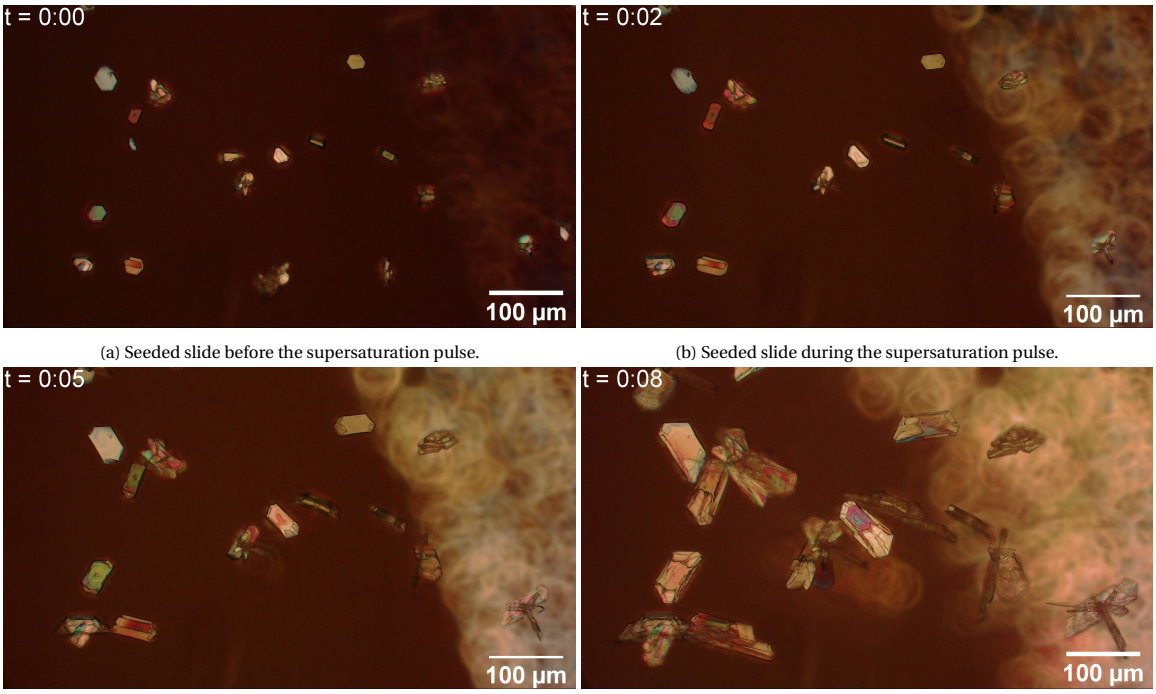

(a) Seeded slide before the supersaturation pulse.

(b) Seeded slide during the supersaturation pulse.

(c) Seeded slide during the supersaturation pulse.

(d) Seeded slide after the supersaturation pulse.

Figure 5.7: Seeded slide before (left) and after (right) the supersaturation pulse. Crystals grow rapidly during the supersaturation pulse, which lasts around 8 seconds. Experiment performed with 100% saturated good solution, 100% saturated poor solution and at a flow rate of 800 $\mu L/min$ ($Pe = 952$).

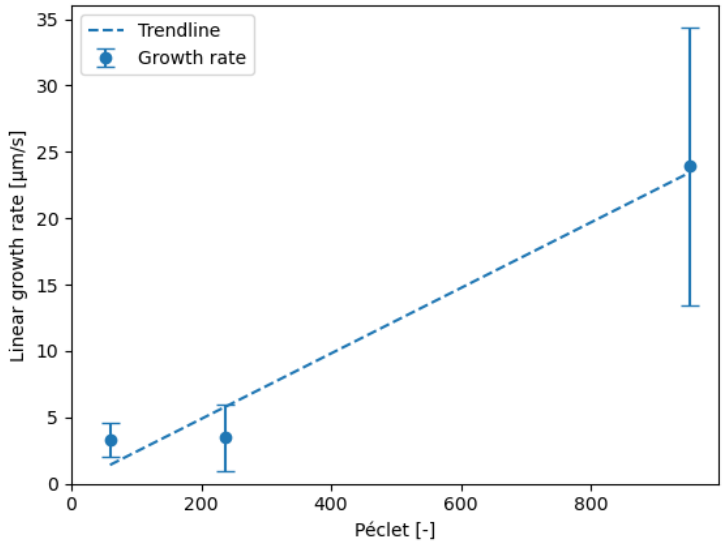

Figure 5.8: Péclet vs. linear growth rate. Theory suggest that $Pe \sim G^{1/3}$, which is plotted in the dotted black line. Too few data points are available to say if the data follow the expected trend. The measurement for $Pe = 238$ is probably off, due to lateral growth inhibition because of too close seeding. Linear growth rate is based on the maximum of the peak of the mean growth rate.

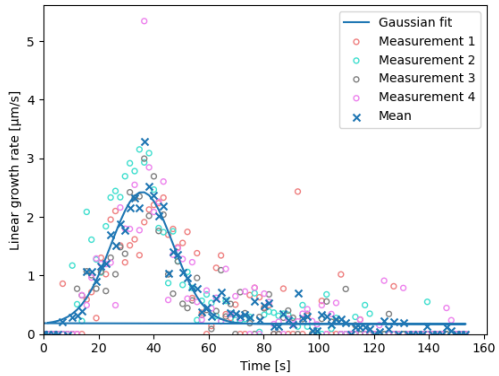

(a) Linear growth rate at 50 $\mu L/min$.

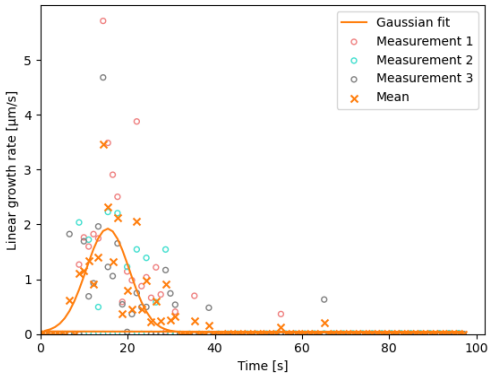

(b) Linear growth rate at 200 $\mu L/min$.

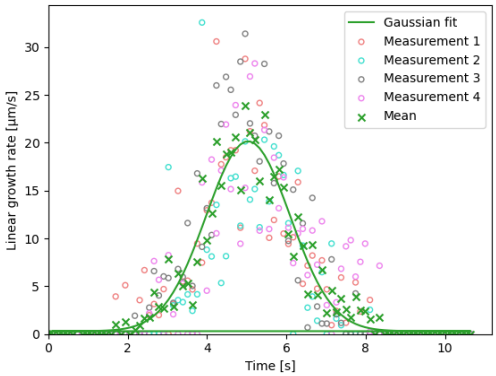

(c) Linear growth rate at 800 $\mu L/min$.

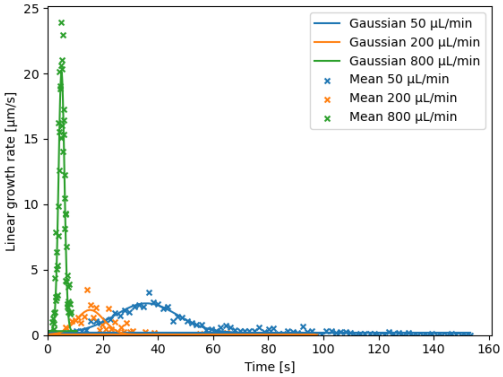

(d) Linear growth rate for the means of the flowrates.

Figure 5.9: Linear growth rate versus time. All flow rates show a Gaussian shape in the linear growth rate. This is in line with what is expected from a passing (Gaussian) supersaturation pulse, as growth rate is supersaturation dependent. The growth rate pulses have a width and a heigth. The width of the growth rate pulse indicated how long it took for the supersaturation pulse to pass. The height of the growth rate pulse indicates how intense the growth was. That is also an indication of how thick the BL was. Higher flow rates give narrower and higher growth rate pulses.

6

Conclusion & Recommendations

6.1. Conclusion

The goal of this research was to find out if the same principles that Zhang found in his microfluidic liquid-liquid-liquid solvent exchange process also apply to a microfluidic liquid-liquid-solid solvent exchange (antisolvent crystallization) system. The main principles are: i) the existence of a supersaturation pulse, ii) the formation of droplets (crystals) of the same size during exposure to the supersaturation pulse at the solvent interface and iii) the relation between the final droplet (crystal) volume and the Péclet number (Pe). Previous research by Korede and Yildiz have proven that antisolvent crystallization in microfluidic systems occurs. However, the Particle Size Distribution (PSD) showed the same crystal size for all Pe. This implicated that the principles of Zhangs research did not match the results of previous authors.

Videos from the experiments show that the uniformity of the PSDs in previous results is due to sedimentation effects, and not necessarily because the solvent interface principles do not hold. The formation and growth of crystals at the interface also induces drag on the crystals. This means the crystals slow down, and the supersaturation pulse outruns the crystal. In the remaining poor solution, the crystal acts as a seed and grows further, until it reaches a critical size. The theoretical critical crystal size is in the order of $R \sim 5.5\ \mu m$, which matches excellently with the observed sedimentation. Then, gravitational effects take over and the crystal sediments. The critical size of the crystal is the same for all flow rates, which explains the uniform PSDs found by Yildiz. This effect automatically means that it is very hard to distinguish between crystals that have formed at the interface and crystals that have sedimented. The occurrence of the sedimentation of crystals makes the antisolvent crystallization process fundamentally different, as it involves two timescales (τ, the temporal pulse width, and the sedimentation time) instead of just one. Drastically reducing saturation of the solutions to reduce the crystal size is unwanted, as lower saturation of the solutions only produce the needle-shape morphology of aspirin, which is difficult to observe.

As crystal growth and the final crystal volume are very closely related, looking at crystal growth is a viable option for validation of the principles. This calls for seeded experiments. Seeding must happen in such a fashion that lateral growth is not impaired. All attempts at gluing crystals into the channel failed, as they impaired lateral crystal growth. Using slides where the crystals from the sedimentation experiments were stuck due to the hydrophobicity of the glass proved to work very well. Slides produced with a 50% saturated good solution, 100% saturated poor solution at a flow rate of 200 $\mu L/min$ proved to have a good balance between initial crystal size and the density of crystals at the slide. Too many crystals in too small an area leads to colliding growing crystals, and thus to lateral growth impairment.

Seeded experiments show that the supersaturation pulse exists, as the (supersaturation dependent) linear growth rate follows the supersaturation pulse shape. The width of the growth rate pulse shows how long it took for the supersaturation pulse to pass. The height of the growth rate pulse shows how intense the crystal growth was. The slower the flow (and thus the lower Pe), the wider the pulse is. This is completely in line with theoretical predictions. The height of the growth rate pulse also shows the expected shape. Fast flow rates cause thin BLs, that induce intense crystal growth, which is shown by a high growth rate pulse. However, at $Q = 200\ \mu L/min$, the growth rate pulse height seems to be too low. This is probably due to experimental errors because of a slide that had seeds too close to each other, but that remains speculative until proven.

The positive correlation between Pe and the linear growth rate exists. A lack of data, due to time con-

straints of this project, makes it impossible to verify if the relation follows the theoretical expectations, that is $\frac{dR}{dt} \sim Pe^{1/3}$. More research should be performed to validate this relation. This research should mainly be seen as a proof of concept: what we thought would happen, did happen. Further validation of the concept can definitely result in publishable results.

6.2. Recommendations

This research shows the potential microfluidic antisolvent crystal growth has. Some more research is needed though. The seeding of the slides before starting the antisolvent crystallization has proven to be very promising, and it is a concept which should be continued upon. A few validations are very straight-forward.

The easiest way to continue this research, is to seed slides with the 'failed' experiment (50% saturated good solution, 100% saturated poor solution, $Q = 200\ \mu L/min$), as this setting gives a nice distribution of evenly sized crystals over the slide. With these seeded slides, a range of Péclet numbers ($Q = 50,\ 100,\ 200,\ 400,\ 800,\ 1600\ \mu L/min$ ($Pe = 59,\ 119,\ 238,\ 476,\ 952,\ 1905$)) for saturated good and poor solution should be tested for the linear growth rate and linear growth rate pulse they produce. The pulse should get narrower and higher for higher Pe.

To validate that the growth is in fact Pe dependent, and not just flow rate dependent, the channel should be halved and doubled (or 1/3 and times 3) in thickness to vary Pe through its characteristic length instead of its characteristic velocity. Doubling the channel thickness also doubles Pe. Thus, a channel that is twice as thick, with half the flow rate should yield the same results. In the same spirit, the concept should be validated with other solutes. A viable option for the solute would be KCl, as within the P&E research group all solubility data (also in aqueous ethanol) are known and the group is very experienced with this solute.

Future researchers should be very careful with experiments at low (roughly ≤ 90%) saturation of the solutions, for two reasons. The first is that the low saturation causes seeds to dissolve, which defeats the purpose of seeding. The second is that low saturation tends to give the needle-shape morphology, which is unwanted.

The current seeding process is laborious and is essentially a big workaround. A seeded slide is a by product of a failed experiment (this is also how we got the idea of using these slides as seeded slides). A proper way of seeding the slides should be developed. All methods that embed crystals in some sort of layer or glue will not work, as they impair lateral growth. The seeds should be spaced evenly and quite far apart, for the same reason. Seeds should have a size of $\sim 15\mu m$ to properly observe the growth. Grinding down large crystals and sieving them is not an optimal solution of obtaining these crystals, for three reasons: i) crystals can only be sorted through sieving by their second largest length scale (width in this case), ii) grinding crystals round of their edges, which at least gives a delay in the physically accurate growth rate (as the edges need to be restored first) and in the worst case show only non-physical behaviour, and iii) the heat generated by grinding might cause morphology switches and/or instability.

Mitgation of the sedimentation process can also be achieved by growing crystals that are below the sedimentation size. This is probably achieved the easiest by switching solvents. The current good solvent dissolves aspirin very well (up to 71 g/L [7]). The very high concentrations also tend to give large crystals. Switching solvent can allow for working at low concentrations while still having a saturated solution. This should help in getting small crystals, without dissolving them.

The videos taken of the growth rate experiments do not only show information on the growth rate, but also give secondary findings, which can be interesting for further research. The crystals on the slide seem to grow, but not on the glass slide. They grow slightly above the glass slide. This could have various reasons. The hydrophobicity of the slide could be too weak, making the interaction between crystal and slide too weak. It could also be that the increased supersaturation causes a morphology switch in the growth behaviour (aspirin is known to be very supersaturation dependent in its morphology [26]). Furthermore, in the videos, it seems like crystals adjust their shape to crystals close by. It is like they feel other crystals are near and then they start growing in another direction. This also could have multiple reasons. One of them is that crystals nearby spend all supersaturation present, and no supersaturation is left for the initial crystal. Another one could be that the crystals nearby impair normal flow behavior, causing a depletion zone in between the crystals. A final suggested research topic is to find out if the total deposition of material is flow rate dependent (is the area under the Gaussians in Figure 5.9 equal?). Researching this can give more information on the growth dynamics of the system.

Bibliography

[1] Alfons Mersmann. *Crystallization technology handbook*. CRC press, 2001.

[2] André B de Haan and Hans Bosch. "8 Crystallization and precipitation". In: *Industrial Separation Processes*. De Gruyter, 2013, pp. 207–240.

[3] John William Mullin. *Crystalization*. Butterworths., 1972.

[4] Allan Myerson. *Handbook of industrial crystallization*. Butterworth-Heinemann, 2002.

[5] Xuehua Zhang et al. "Formation of surface nanodroplets under controlled flow conditions". In: 112.30 (2015), pp. 9253–9257. DOI: 10.1073/pnas.1506071112.

[6] Vikram Korede. "Controlling crystal size in solvent exchange process". In: (2019).

[7] Lale Nur Yıldız. "Controlling Crystal Size in Antisolvent Crystallization Lale Nur Yıldız". In: (2020).

[8] R Boistelle and JP Astier. "Crystallization mechanisms in solution". In: *Journal of Crystal Growth* 90.1-3 (1988), pp. 14–30.

[9] *Crystal Lattice: afbeeldingen, stockfoto's en vectoren | Shutterstock*. https://www.shutterstock.com/search/crystal+lattice. (Accessed on 04/16/2021).

[10] Jan Dalmolen. "Synthesis and Application of New Chiral Amines in Dutch Resolution". PhD thesis. PhD Thesis, University of Groningen, 2005.

[11] Hsü Huai Ting and Warren L McCabe. "Supersaturation and crystal formation in seeded solutions". In: *Industrial & Engineering Chemistry* 26.11 (1934), pp. 1201–1207.

[12] RF Strickland-Constable and REA Mason. "Breeding of nuclei". In: *Nature* 197.4870 (1963), pp. 897–898.

[13] Alfons Mersmann et al. "Attrition and secondary nucleation in crystallizers". In: *Chemical engineering & technology* 11.1 (1988), pp. 80–88.

[14] M Ohara and RC Reid. "Modelling crystal growth rates from solution (Prentice-Hall, Inc., New Jersey, 1973) p. 64." In: ().

[15] FC Frank. "The influence of dislocations on crystal growth". In: *Discussions of the Faraday Society* 5 (1949), pp. 48–54.

[16] W-K_ Burton, N Cabrera, and FC Frank. "The growth of crystals and the equilibrium structure of their surfaces". In: *Philosophical Transactions of the Royal Society of London. Series A, Mathematical and Physical Sciences* 243.866 (1951), pp. 299–358.

[17] AA Chernov. "The spiral growth of crystals". In: *Soviet Physics Uspekhi* 4.1 (1961), p. 116.

[18] William M Deen. "Analysis of transport phenomena". In: (1998).

[19] Diya Chudasama et al. "Image segmentation using morphological operations". In: *International Journal of Computer Applications* 117.18 (2015).

[20] *Morphological Image Processing*. https://www.cs.auckland.ac.nz/courses/compsci773s1c/lectures/ImageProcessing-html/topic4.htm. (Accessed on 04/22/2021).

[21] Kumar Abhinav, Jaideep Singh Chauhan, and Debasis Sarkar. "Image segmentation of multi-shaped overlapping objects". In: *arXiv preprint arXiv:1711.02217* (2017).

[22] Satoshi Suzuki and KeiichiA be. "Topological structural analysis of digitized binary images by border following". In: *Computer Vision, Graphics, and Image Processing* 30.1 (1985), pp. 32–46. ISSN: 0734-189X. DOI: https://doi.org/10.1016/0734-189X(85)90016-7. URL: https://www.sciencedirect.com/science/article/pii/0734189X85900167.

[23] David H Douglas and Thomas K Peucker. "Algorithms for the reduction of the number of points required to represent a digitized line or its caricature". In: *Cartographica: the international journal for geographic information and geovisualization* 10.2 (1973), pp. 112–122.

[24] MI Shamos. “Computational geometry[Ph. D. Thesis]”. In: (1978).

[25] Noriaki Kubota, Masaaki Yokota, and J.W. Mullin. “Supersaturation dependence of crystal growth in solutions in the presence of impurity”. In: *Journal of Crystal Growth* 182.1 (1997), pp. 86–94. ISSN: 0022-0248. DOI: https://doi.org/10.1016/S0022-0248(97)00328-X. URL: https://www.sciencedirect.com/science/article/pii/S002202489700328X.

[26] RB Hammond et al. “Application of grid-based molecular methods for modeling solvent-dependent crystal growth morphology: Aspirin crystallized from aqueous ethanolic solution”. In: *Crystal growth & design* 7.9 (2007), pp. 1571–1574.

[27] Clare Aubrey-Medendorp, Sean Parkin, and Tonglei Li. “The confusion of indexing aspirin crystals”. In: *Journal of pharmaceutical sciences* 97.4 (2008), pp. 1361–1367.

A

Derivations

A.1. Derivation stream function

The stream function for a bidirectional flow in spherical coordinates is defined as

$$v_r \equiv \frac{1}{r^2 \sin(\vartheta)} \frac{\partial \psi}{\partial \vartheta}, \; v_\vartheta \equiv -\frac{1}{r \sin(\vartheta)} \frac{\partial \psi}{\partial r}, \tag{A.1}$$

where v_r and v_ϑ are the fluid velocity in the respective directions. These stream functions have a corresponding Stokes' equation [18], being

$$E^4 \psi = 0, \tag{A.2}$$

where E^2 is an operator that is comparable with the Laplacian operator $\nabla^2 = \frac{1}{r^2}\frac{\partial}{\partial r}\left(\frac{1}{r^2}\frac{\partial}{\partial r}\right) + \frac{1}{r^2 \sin\vartheta}\frac{\partial}{\partial \vartheta}\left(\sin\vartheta \frac{\partial}{\partial \vartheta}\right)$, but is not exactly the same, as

$$E^4 = E^2(E^2), \; E^2 = \frac{\partial^2}{\partial r^2} + \frac{\sin\vartheta}{r^2}\frac{\partial}{\partial \vartheta}\left(\frac{1}{\sin\vartheta}\frac{\partial}{\partial \vartheta}\right). \tag{A.3}$$

This problem needs four boundary conditions to be solved. The first two are a no penetration and a no slip boundary condition at the sphere surface, such that

$$v_r(R, \vartheta) = 0, \; v_\vartheta(R, \vartheta) = 0, \tag{A.4}$$

and the third and fourth represent uniform flow far away from the particle, being

$$v_r(\infty, \vartheta) \to U \cos\vartheta, \; v_\vartheta(\infty, \vartheta) \to -U \sin\vartheta. \tag{A.5}$$

Rewriting the boundary conditions in terms of the stream function instead of velocities using Equation A.1 yields

$$\frac{\partial \psi}{\partial \vartheta}(R, \vartheta) = 0, \; \frac{\partial \psi}{\partial r}(R, \vartheta) = 0 \tag{A.6}$$

and

$$\frac{\partial \psi}{\partial \vartheta}(\infty, \vartheta) \to r^2 U \sin\vartheta \cos\vartheta, \; \frac{\partial \psi}{\partial r}(\infty, \vartheta) \to r U \sin^2\vartheta. \tag{A.7}$$

Integration of the uniform flow boundary conditions, in both situations using the substitution $x = \sin\vartheta$, $dx = \cos\vartheta \partial\vartheta$ for example, yields (for both boundary conditions)

$$\psi(\infty, \vartheta) \to \frac{r^2 U \sin^2\vartheta}{2}. \tag{A.8}$$

Note that as the stream functions value are arbitrary integration constants are set to zero. This outcome suggests to look for a solution for $\psi(r, \vartheta)$ of the form

$$\psi(r,\vartheta) = f(r)\sin^2\vartheta, \tag{A.9}$$

where $f(r)$ is some function of r. Substitution of this suggested solution into the Stokes equation (Equation A.2) gives

$$\begin{aligned} E^4\psi(r,\vartheta) &= 0 \\ E^2\left[E^2\left(f(r)\sin^2\vartheta\right)\right] &= 0 \\ E^2\left[\frac{\partial^2}{\partial r^2}\left(f(r)\sin^2\vartheta\right) + \frac{\sin\vartheta}{r^2}\frac{\partial}{\partial\vartheta}\left(\frac{1}{\sin\vartheta}\frac{\partial}{\partial\vartheta}\left(f(r)\sin^2\vartheta\right)\right)\right] &= 0. \end{aligned} \tag{A.10}$$

Realizing that $\frac{\partial\sin^2\vartheta}{\partial\vartheta} = 2\cos\vartheta\sin\vartheta$, remembering the product rule and omitting the explicit mentioning r-dependency of f for conciseness, this yields

$$\begin{aligned} E^2\left[\sin^2\vartheta\frac{\partial f^2}{\partial r^2} + \frac{\sin\vartheta}{r^2}\frac{\partial}{\partial\vartheta}\left(2\frac{f}{\sin\vartheta}\sin\vartheta\cos\vartheta\right)\right] &= 0 \\ E^2\left[\sin^2\vartheta\frac{\partial f^2}{\partial r^2} + \frac{\sin\vartheta}{r^2}\frac{\partial}{\partial\vartheta}\left(2f\cos\vartheta\right)\right] &= 0 \\ E^2\left[\sin^2\vartheta\frac{\partial f^2}{\partial r^2} - 2\frac{\sin\vartheta}{r^2}f\sin\vartheta\right] &= 0 \\ E^2\left[\sin^2\vartheta\frac{\partial f^2}{\partial r^2} - 2\sin^2\vartheta\frac{f}{r^2}\right] &= 0. \end{aligned} \tag{A.11}$$

Now applying the operator $E^2 = \frac{\partial^2}{\partial r^2} + \frac{\sin\vartheta}{r^2}\frac{\partial}{\partial\vartheta}\left(\frac{1}{\sin\vartheta}\frac{\partial}{\partial\vartheta}\right)$ again gives

$$\frac{\partial^2}{\partial r^2}\left(\sin^2\vartheta\frac{\partial^2 f}{\partial r^2} - 2\sin^2\vartheta\frac{f}{r^2}\right) + \frac{\sin\vartheta}{r^2}\frac{\partial}{\partial\vartheta}\left(\frac{1}{\sin\vartheta}\frac{\partial}{\partial\vartheta}\left(\sin^2\vartheta\frac{\partial^2 f}{\partial r^2} - 2\sin^2\vartheta\frac{f}{r^2}\right)\right) = 0 \tag{A.12}$$

$$\begin{aligned} &\frac{\partial}{\partial r}\left(\sin^2\vartheta\frac{\partial^3 f}{\partial r^3} - 2\sin^2\vartheta\left(\frac{-2}{r^3}f + \frac{1}{r^2}\frac{\partial f}{\partial r}\right)\right) \\ &\qquad + \frac{\sin\vartheta}{r^2}\frac{\partial}{\partial\vartheta}\left(\frac{1}{\sin\vartheta}\left(2\cos\vartheta\sin\vartheta\frac{\partial^2 f}{\partial r^2} - 4\cos\vartheta\sin\vartheta\frac{f}{r^2}\right)\right) = 0 \end{aligned} \tag{A.13}$$

$$\sin^2\vartheta\left(\frac{\partial^4 f}{\partial r^4} - 2\left(\frac{6}{r^4}f + \frac{-2}{r^3}\frac{\partial f}{\partial r} + \frac{-2}{r^3}\frac{\partial f}{\partial r} + \frac{1}{r^2}\frac{\partial^2 f}{\partial r^2}\right)\right) + \frac{\sin\vartheta}{r^2}\frac{\partial}{\partial\vartheta}\left(2\cos\vartheta\frac{\partial^2 f}{\partial r^2} - 4\cos\vartheta\frac{f}{r^2}\right) = 0 \tag{A.14}$$

$$\sin^2\vartheta\left(\frac{\partial^4 f}{\partial r^4} - \frac{12}{r^4}f + \frac{8}{r^3}\frac{\partial f}{\partial r} - \frac{2}{r^2}\frac{\partial^2 f}{\partial r^2}\right) + \frac{\sin\vartheta}{r^2}\left(-2\sin\vartheta\frac{\partial^2 f}{\partial r^2} + 4\sin\vartheta\frac{f}{r^2}\right) = 0 \tag{A.15}$$

$$\sin^2\vartheta\left(\frac{\partial^4 f}{\partial r^4} - \frac{12}{r^4}f + \frac{8}{r^3}\frac{\partial f}{\partial r} - \frac{2}{r^2}\frac{\partial^2 f}{\partial r^2}\right) + \sin^2\vartheta\left(-\frac{2}{r^2}\frac{\partial^2 f}{\partial r^2} + \frac{4f}{r^4}\right) = 0 \tag{A.16}$$

$$\frac{\partial^4 f}{\partial r^4} - \frac{12}{r^4}f + \frac{8}{r^3}\frac{\partial f}{\partial r} - \frac{2}{r^2}\frac{\partial^2 f}{\partial r^2} - \frac{2}{r^2}\frac{\partial^2 f}{\partial r^2} + \frac{4f}{r^4} = 0 \tag{A.17}$$

$$\frac{\partial^4 f}{\partial r^4} - \frac{4}{r^2}\frac{\partial^2 f}{\partial r^2} + \frac{8}{r^3}\frac{\partial f}{\partial r} - \frac{8}{r^4}f = 0 \tag{A.18}$$

$$\frac{\partial^4 f}{\partial r^4} - \frac{4}{r^2}\frac{\partial^2 f}{\partial r^2} + \frac{8}{r^3}\frac{\partial^2 f}{\partial r^2} - \frac{8}{r^4}f = 0 \tag{A.19}$$

This reduces to

$$\left(\frac{\partial^2}{\partial r^2} - \frac{2}{r^2}\right)^2 f = 0, \tag{A.20}$$

which is most easily seen the other way around - when working out $\left(\frac{\partial^2}{\partial r^2}-\frac{2}{r^2}\right)\left(\frac{\partial^2 f}{\partial r^2}-\frac{2f}{r^2}\right)$ which can be found in subsection A.1.1.

Now that the stream function differential equation has been rewritten in terms of $f(r)$, this should happen to the BCs (Equation A.6 and Equation A.8) as well. Remembering that $\psi(r,\vartheta)=f(r)\sin^2\vartheta$,

$$\frac{\partial\psi}{\partial\vartheta}(R,\vartheta)=\frac{\partial\left(f(R)\sin^2\vartheta\right)}{\partial\vartheta}(R,\vartheta)=\frac{\partial f(R)}{\partial\vartheta}\sin^2\vartheta+f(R)\sin\vartheta\cos\vartheta=0\implies f(R)=0, \tag{A.21}$$

$$\frac{\partial\psi}{\partial r}(R,\vartheta)=\frac{\partial\left(f(R)\sin^2\vartheta\right)}{\partial r}(R,\vartheta)=\frac{\partial f(R)}{\partial r}\sin^2\vartheta+\frac{\partial\sin^2\vartheta}{\partial r}f(R)=0\implies\frac{\partial f(r)}{\partial r}\Big|_R=0, \tag{A.22}$$

and

$$\psi(\infty,\vartheta)=f(\infty)\sin^2\vartheta\to\frac{r^2U\sin^2\vartheta}{2}\implies f(\infty)\to\frac{r^2U}{2} \tag{A.23}$$

As Equation A.20 is and equidimensional equation, it can be solved and has solutions of the form $f(r)=r^n$ where n is an arbitrary constant. Filling this out yields

$$\left(\frac{\partial^2}{\partial r^2}-\frac{2}{r^2}\right)^2 r^n=0, \tag{A.24}$$

$$\left(\frac{\partial^2}{\partial r^2}-\frac{2}{r^2}\right)\left(\frac{\partial^2 r^n}{\partial r^2}-\frac{2r^n}{r^2}\right) \tag{A.25}$$

$$\left(\frac{\partial^2}{\partial r^2}-\frac{2}{r^2}\right)\left(n(n-1)r^{n-2}-2r^{n-2}\right) \tag{A.26}$$

$$\left(\frac{\partial^2}{\partial r^2}-\frac{2}{r^2}\right)\left([n(n-1)-2]\,r^{n-2}\right) \tag{A.27}$$

$$[n(n-1)-2]\frac{\partial^2}{\partial r^2}\left(r^{n-2}\right)-\frac{2}{r^2}[n(n-1)-2]\,r^{n-2} \tag{A.28}$$

$$[n(n-1)-2](n-2)(n-3)r^{n-4}-2[n(n-1)-2]\,r^{n-4} \tag{A.29}$$

which results in the fourth order polynomial in n that factors out into

$$(n-2)(n+1)(n-1)(n-4)=0. \tag{A.30}$$

This gives solutions for $n=-1,1,2,4$, which in turn implies to look for solutions of $f(r)$ of the form

$$f(r)=Ar^4+Br^2+Cr+\frac{D}{r}, \tag{A.31}$$

where A, B, C and D are arbitrary contants. The BCs as defined for $f(r)$ must also hold for this equation. As r tends to infinity, the solution should take the form of $\frac{r^2U}{2}$ (Equation A.23). This means that the fourth order term must vanish, and the second order term must take the form $\frac{r^2U}{2}$. This is only possible when $A=0$ and $B=\frac{U}{2}$, leaving

$$f(r)=\frac{U}{2}r^2+Cr+\frac{D}{r}. \tag{A.32}$$

From Equation A.21,

$$\frac{U}{2}R^2+CR+\frac{D}{R}=0, \tag{A.33}$$

and from Equation A.22

$$UR+C-\frac{D}{R^2}=0 \tag{A.34}$$

This leaves a system of two equations and two unknowns, which can be solved for the solutions $C=-\frac{3}{4}UR$ and $D=\frac{1}{4}UR^3$, which means

$$f(r)=\frac{U}{2}r^2-\frac{3}{4}URr+\frac{1}{4}UR\frac{1}{r}. \tag{A.35}$$

From $\psi(r,\vartheta) = f(r)\sin^2\vartheta$, this results in

$$\psi(r,\vartheta) = \sin^2\vartheta\left[\frac{U}{2}r^2 - \frac{3}{4}URr + \frac{1}{4}UR\frac{1}{r}\right] \tag{A.36}$$

which is the same as

$$\psi(r,\vartheta) = UR^2\sin^2\vartheta\left[\frac{1}{2}\left(\frac{r}{R}\right)^2 - \frac{3}{4}\left(\frac{r}{R}\right) + \frac{1}{4}\left(\frac{R}{r}\right)\right] \tag{A.37}$$

This value for the stream function can be plugged into the definition of the stream function as in Equation A.1, giving

$$\begin{aligned} v_r &= \frac{1}{r^2\sin\vartheta}\frac{\partial}{\partial\vartheta}\left(UR^2\sin^2\vartheta\left[\frac{1}{2}\left(\frac{r}{R}\right)^2 - \frac{3}{4}\left(\frac{r}{R}\right) + \frac{1}{4}\left(\frac{R}{r}\right)\right]\right) \\ &= U\cos\vartheta\left[1 - \frac{3}{2}\left(\frac{R}{r}\right) + \frac{1}{2}\left(\frac{R}{r}\right)^3\right] \end{aligned} \tag{A.38}$$

and

$$\begin{aligned} v_\vartheta &= \frac{1}{r\sin\vartheta}\frac{\partial}{\partial r}\left(UR^2\sin^2\vartheta\left[\frac{1}{2}\left(\frac{r}{R}\right)^2 - \frac{3}{4}\left(\frac{r}{R}\right) + \frac{1}{4}\left(\frac{R}{r}\right)\right]\right) \\ &= -U\sin\vartheta\left[1 - \frac{3}{4}\left(\frac{R}{r}\right) - \frac{1}{4}\left(\frac{R}{r}\right)^3\right] \end{aligned} \tag{A.39}$$

When these are nondimensionalized using $\xi = \frac{r}{R}$, the result are the dimensionless velocity components

$$\tilde{v_r}(\xi,\vartheta) = \frac{v_r}{U} = \cos\vartheta\left[1 - \frac{3}{2\xi} + \frac{1}{2\xi^3}\right], \tag{A.40}$$

$$\tilde{v_\vartheta}(\xi,\vartheta) = \frac{v_\vartheta}{U} = -\sin\vartheta\left[1 - \frac{3}{4\xi} - \frac{1}{4\xi^3}\right]. \tag{A.41}$$

A.1.1. Reversed derivation of quadratic differential operators

$$\left(\frac{\partial^2}{\partial r^2} - \frac{2}{r^2}\right)\left(\frac{\partial^2 f}{\partial r^2} - \frac{2f}{r^2}\right) = 0 \tag{A.42}$$

$$\frac{\partial^2}{\partial r^2}\left(\frac{\partial^2 f}{\partial r^2}\right) + \frac{\partial^2}{\partial r^2}\left(\frac{2f}{r^2}\right) - \frac{2}{r^2}\left(\frac{\partial^2 f}{\partial r^2}\right) + \frac{4f}{r^4} = 0 \tag{A.43}$$

$$\frac{\partial^4 f}{\partial r^4} + \frac{\partial}{\partial r}\left(-\frac{2}{r^2}\frac{\partial f}{\partial r} + f\frac{\partial}{\partial r}\left(\frac{-2}{r^2}\right)\right) - \frac{2}{r^2}\frac{\partial^2 f}{\partial r^2} + \frac{4f}{r^4} = 0 \tag{A.44}$$

$$\frac{\partial^4 f}{\partial r^4} + \frac{\partial}{\partial r}\left(-\frac{2}{r^2}\frac{\partial f}{\partial r}\right) + \frac{\partial}{\partial r}\left(\frac{4}{r^3}f\right) - \frac{2}{r^2}\frac{\partial^2 f}{\partial r^2} + \frac{4f}{r^4} = 0 \tag{A.45}$$

$$\frac{\partial^4 f}{\partial r^4} + \frac{4}{r^3}\frac{\partial f}{\partial r} - \frac{2}{r^2}\frac{\partial^2 f}{\partial r^2} + \frac{4}{r^3}\frac{\partial f}{\partial r} - \frac{12}{r^4}f - \frac{2}{r^2}\frac{\partial^2 f}{\partial r^2} + \frac{4f}{r^4} = 0 \tag{A.46}$$

$$\frac{\partial^4 f}{\partial r^4} - \frac{4}{r^2}\frac{\partial^2 f}{\partial r^2} + \frac{8}{r^3}\frac{\partial^2 f}{\partial r^2} - \frac{8}{r^4}f = 0 \tag{A.47}$$

A.2. Derivation of convection-diffusion behaviour

First, we introduce the general convection-diffusion equation

$$\frac{\partial c}{\partial t} + v_r\frac{\partial c}{\partial r} + \frac{v_\vartheta}{r}\frac{\partial c}{\partial\vartheta} + \frac{v_\phi}{r\sin\phi}\frac{\partial c}{\partial\phi} = \frac{D}{r^2}\frac{\partial}{\partial r}\left(r^2\frac{\partial c}{\partial r}\right) + \frac{D}{r^2\sin\vartheta}\frac{\partial}{\partial\vartheta}\left(\sin\vartheta\frac{\partial c}{\partial\vartheta}\right) + \frac{D}{r^2\sin\phi}\frac{\partial^2 c}{\partial\phi^2}. \tag{A.48}$$

Upon realisation that this is an axisymmetric problem and thus $\Theta = \Theta(\xi,\vartheta)$ only ($\Theta \neq \Theta(\phi)$), and the assumption of steady state, this leads to the simplified convection-diffusion equation

$$v_r \frac{\partial c}{\partial r} + \frac{v_\vartheta}{r}\frac{\partial c}{\partial \vartheta} = \frac{D}{r^2}\frac{\partial}{\partial r}\left(r^2 \frac{\partial c}{\partial r}\right) + \frac{D}{r^2 \sin\vartheta}\frac{\partial}{\partial \vartheta}\left(\sin\vartheta \frac{\partial c}{\partial \vartheta}\right) \tag{A.49}$$

which, using

$$\xi = \frac{r}{h},\ \Theta = \frac{c - c_\infty}{c_0 - c_\infty},\ Pe = \frac{\overline{U} h}{D}\ \ (r = h\xi,\ c = \Theta(c_0 - c_\infty) + c_\infty) \tag{A.50}$$

where ξ is the dimensionless length, Θ is the dimensionless concentration and Pe is defined using the relevant scales, being the fluid mean velocity $\overline{U}$, the channel height h and the diffusion coefficient D, and the dimensionless velocity components $\tilde{v}_r = v_r/\overline{U}$ and $\tilde{v}_\vartheta = v_\vartheta/\overline{U}$ as derived in Equation A.40 and Equation A.41, nondimensionalizes to

$$\begin{aligned}\tilde{v}_r \overline{U}\frac{\partial(\Theta(c_0 - c_\infty) + c_\infty)}{\partial(\xi h)} + \frac{\tilde{v}_\vartheta \overline{U}}{\xi h}\frac{\partial(\Theta(c_0 - c_\infty) + c_\infty)}{\partial \vartheta} \\ = \frac{D}{(\xi h)^2}\frac{\partial}{\partial(\xi h)}\left((\xi h)^2 \frac{\partial(\Theta(c_0 - c_\infty) + c_\infty)}{\partial(\xi h)}\right) + \frac{D}{(\xi h)^2 \sin\vartheta}\frac{\partial}{\partial \vartheta}\left(\sin\vartheta \frac{\partial(\Theta(c_0 - c_\infty) + c_\infty)}{\partial \vartheta}\right).\end{aligned} \tag{A.51}$$

As $\frac{\partial(\Theta(c_0 - c_\infty) + c_\infty)}{\partial(\xi h)} = \frac{(c_0 - c_\infty)}{h}\frac{\partial \Theta}{\partial \xi}$ and $\frac{\partial(\Theta(c_0 - c_\infty) + c_\infty)}{\partial \vartheta} = (c_0 - c_\infty)\frac{\partial \Theta}{\partial \vartheta}$, this becomes

$$\begin{aligned}\frac{\tilde{v}_r \overline{U}}{h}(c_0 - c_\infty)\frac{\partial \Theta}{\partial \xi} + \frac{\tilde{v}_\vartheta \overline{U}}{\xi h}(c_0 - c_\infty)\frac{\partial \Theta}{\partial \vartheta} \\ = \frac{D}{\xi^2 h^4}(c_0 - c_\infty)h^2 \frac{\partial}{\partial \xi}\left(\xi^2 \frac{\partial \Theta}{\partial \xi}\right) + \frac{D}{\xi^2 h^2 \sin\vartheta}(c_0 - c_\infty)\frac{\partial}{\partial \vartheta}\left(\sin\vartheta \frac{\partial \Theta}{\partial \vartheta}\right),\end{aligned} \tag{A.52}$$

which can be reordered to

$$\tilde{v}_r \frac{\overline{U} h}{D}\frac{\partial \Theta}{\partial \xi} + \frac{\tilde{v}_\vartheta}{\xi}\frac{\overline{U} h}{D}\frac{\partial \Theta}{\partial \vartheta} = \frac{1}{\xi^2}\frac{\partial}{\partial \xi}\left(\xi^2 \frac{\partial \Theta}{\partial \xi}\right) + \frac{1}{\xi^2 \sin\vartheta}\frac{\partial}{\partial \vartheta}\left(\sin\vartheta \frac{\partial \Theta}{\partial \vartheta}\right), \tag{A.53}$$

which is simply

$$Pe\ \tilde{v} \cdot \tilde{\nabla}\Theta = \tilde{\nabla}^2 \Theta. \tag{A.54}$$

This problem has the boundary conditions

$$\Theta(1, \vartheta) = 1,\ \Theta(\infty, \vartheta) = 0 \tag{A.55}$$

representing c_0 at the sphere surface and c_∞ far away from the sphere. In Equation A.54 $\tilde{\nabla}$ and $\tilde{\nabla}^2$ are dimensionless operators including only ξ and ϑ. Now, for $Pe \gg 1$ (which is the case in this study), we consider the limiting behavior of $Pe \to \infty$. Physically, this means that the convective scale is a lot larger than the diffusive scale. The convection-diffusion equation (Equation A.54) reduces to

$$\tilde{v} \cdot \tilde{\nabla}\Theta = 0 \tag{A.56}$$

when all diffusive terms are negligibly small. This reduces the order of the differential equation. As $v \cdot \nabla\Theta$ is the rate of change of Θ (concentration) along a stream line, this simplification leads to not being able to pass mass from the sphere (crystal) to the fluid and vice versa, and thus the fluid concentration is constant everywhere. As in the BL species transport and thus a concentration gradient must be present, this raises the need for separate solutions for the BL and the bulk fluid (and the matching of these solutions through for example matching asymptotes). The original convection-diffusion equation (Equation A.54) leads to $\nabla^2\Theta = O(Pe)$ for $Pe \to \infty$. In the outer region, the bulk of the fluid, a good initial guess is $\Theta = 0$ as to keep the fluid at a constant concentration c_∞. In the inner region, the BL, the behavior is described by

$$\tilde{v}_r \frac{\partial \Theta}{\partial \xi} + \frac{\tilde{v}_\vartheta}{\xi}\frac{\partial \Theta}{\partial \vartheta} = \frac{1}{Pe}\left[\frac{\partial^2 \Theta}{\partial \xi^2} + \frac{2}{\xi}\frac{\partial \Theta}{\partial \xi} + \frac{1}{\xi^2 \sin\vartheta}\frac{\partial}{\partial \vartheta}\left(\sin\vartheta \frac{\partial \Theta}{\partial \vartheta}\right)\right] \tag{A.57}$$

which is almost the same as Equation A.53, as $\frac{1}{\xi^2}\frac{\partial}{\partial\xi}\left(\xi^2\frac{\partial\Theta}{\partial\xi}\right)=\frac{1}{\xi^2}\left[\xi^2\frac{\partial^2\Theta}{\partial\xi^2}+2\xi\frac{\partial\Theta}{\partial\xi}\right]=\frac{\partial^2\Theta}{\partial\xi^2}+\frac{2}{\xi}\frac{\partial\Theta}{\partial\xi}$. If we now define a new spherical coordinate $\eta=\cos\vartheta$ where $-1\leqslant\eta\leqslant 1$ and introduce the velocity components $\tilde{v_r}$ and $\tilde{v_\vartheta}$ as defined in Equation A.40 and Equation A.41, we get

$$\eta\left(1-\frac{3}{2\xi}+\frac{1}{2\xi^3}\right)\frac{\partial\Theta}{\partial\xi}+\frac{\left(1-\eta^2\right)}{\xi}\left(1-\frac{3}{4\xi}-\frac{1}{4\xi^3}\right)\frac{\partial\Theta}{\partial\eta}=\frac{1}{Pe}\left[\frac{\partial^2\Theta}{\partial\xi^2}+\frac{2}{\xi}\frac{\partial\Theta}{\partial\xi}+\frac{1}{\xi^2}\frac{\partial}{\partial\eta}\left(\left(1-\eta^2\right)\frac{\partial\Theta}{\partial\eta}\right)\right]. \tag{A.58}$$

As $Pe\gg 1$, the BL is thin. This calls for rescaling of the length scale according to

$$Y=(\xi-1)\,Pe^b \;or\; \xi=YPe^{-b}+1, \tag{A.59}$$

where b is an arbitrary, to be determined constant. This rescaling is justified as the length of the BL has to be stretched (as it is thin). This also implies that $b>0$ as Pe is large (leading to $Pe^b>1$). Pe^b is called the stretching factor. Now, defining another variable $x=(\xi-1)$, we can generically say that

$$\xi^{-n}=(1+(\xi-1))^{-n}=(1+x)^{-n}, \tag{A.60}$$

which can expanded as a binomial series as

$$(1+x)^{-n}=1-nx+\frac{n(n+1)}{2}x^2+O(x^3). \tag{A.61}$$

As in the BL $x\ll 1$, high order terms will vanish very quickly and are not needed. Applying the aforementioned transformations to the radial and angular velocity respectively yields

$$\begin{aligned}1-\frac{3}{2\xi}+\frac{1}{2\xi^3}&=1-\frac{3}{2}\left[1-x+x^2\right]+\frac{1}{2}\left[1-3x+6x^2\right]+O\left(x^3\right)=\frac{3}{2}x^2+O\left(x^3\right)\\ 1-\frac{3}{4\xi}-\frac{1}{4\xi^3}&=1-\frac{3}{4}\left[1-x+x^2\right]-\frac{1}{4}\left[1-3x+6x^2\right]+O\left(x^3\right)=\frac{3}{2}x-\frac{9}{4}x^2+O\left(x^3\right)\end{aligned} \tag{A.62}$$

Applying the expansions as in Equation A.62, and the rescaling for ξ as in Equation A.59, to the nondimensional equation with the new radial coordinate η, Equation A.58, we get

$$\begin{aligned}&\eta\left(\frac{3}{2}x^2+O\left(x^3\right)\right)\frac{\partial\Theta}{\partial\left(YPe^{-b}+1\right)}+\frac{\left(1-\eta^2\right)}{\left(YPe^{-b}+1\right)}\left(\frac{3}{2}x-\frac{9}{4}x^2+O\left(x^3\right)\right)\frac{\partial\Theta}{\partial\eta}\\ &\qquad=\frac{1}{Pe}\left[\frac{\partial^2\Theta}{\partial\left(YPe^{-b}+1\right)^2}+\frac{2}{\left(YPe^{-b}+1\right)}\frac{\partial\Theta}{\partial\left(YPe^{-b}+1\right)}+\frac{1}{\left(YPe^{-b}+1\right)^2}\frac{\partial}{\partial\eta}\left(\left(1-\eta^2\right)\frac{\partial\Theta}{\partial\eta}\right)\right].\end{aligned} \tag{A.63}$$

Upon realisation that $\frac{\partial\Theta}{\partial\left(YPe^{-b}+1\right)}=Pe^b\frac{\partial\Theta}{\partial Y}$, $\frac{\partial\Theta^2}{\partial\left(YPe^{-b}+1\right)^2}=Pe^{2b}\frac{\partial\Theta^2}{\partial Y^2}$ and $x=(\xi-1)=YPe^{-b}=O(Pe^{-b})$, this simplifies to

$$\begin{aligned}&\eta\left(\frac{3}{2}Y^2Pe^{-2b}+O\left(Pe^{-3b}\right)\right)Pe^b\frac{\partial\Theta}{\partial Y}+\frac{\left(1-\eta^2\right)}{\left(YPe^{-b}+1\right)}\left(\frac{3}{2}YPe^{-b}-\frac{9}{4}Y^2Pe^{-2b}+O\left(Pe^{-3b}\right)\right)\frac{\partial\Theta}{\partial\eta}\\ &\qquad=\frac{1}{Pe}\left[Pe^{2b}\frac{\partial^2\Theta}{\partial Y^2}+\frac{2}{\left(YPe^{-b}+1\right)}Pe^b\frac{\partial\Theta}{\partial Y}+\frac{1}{\left(YPe^{-b}+1\right)^2}\frac{\partial}{\partial\eta}\left(\left(1-\eta^2\right)\frac{\partial\Theta}{\partial\eta}\right)\right].\end{aligned} \tag{A.64}$$

We now asses the order of magnitude of all five terms in this equation.
As $Pe\gg 1$, the dominant convective and diffusive term must balance each other. That is, $Pe^{-b}\sim Pe^{2b-1}$ or $-b=2b-1$ and thus $b=\frac{1}{3}$. This leads to a dimensionless BL thickness $\xi=YPe^{-1/3}+1$ which scales with $Pe^{-1/3}$.

Term	Type	Order of magnitude
$\eta\left(\frac{3}{2}Y^2Pe^{-2b}+O\left(Pe^{-3b}\right)\right)Pe^b\frac{\partial\Theta}{\partial Y}$	Convective	$O(Pe^{-b})$
$\frac{(1-\eta^2)}{(YPe^{-b}+1)}\left(\frac{3}{2}YPe^{-b}-\frac{9}{4}Y^2Pe^{-2b}+O\left(Pe^{-3b}\right)\right)\frac{\partial\Theta}{\partial\eta}$	Convective	$O(Pe^{-b})$
$\frac{1}{Pe}Pe^{2b}\frac{\partial^2\Theta}{\partial Y^2}$	Diffusive	$O(Pe^{2b-1})$
$\frac{1}{Pe}\frac{2}{(YPe^{-b}+1)}Pe^b\frac{\partial\Theta}{\partial Y}$	Diffusive	$O(Pe^{b-1})$
$\frac{1}{Pe}\frac{1}{(YPe^{-b}+1)^2}\frac{\partial}{\partial\eta}\left(\left(1-\eta^2\right)\frac{\partial\Theta}{\partial\eta}\right)$	Diffusive	$O(Pe^{-1})$

Table A.1: Comparison of the order of magnitude of the various terms in Equation A.64.

A.3. Derivation relation Péclet and crystal volume

Completely analogue to Deens example 11.2-2 [18] and the thesis of Korede [6], we can derive that the thickness of a boundary layer λ of a particle in a creeping flow scales with $\lambda \sim R/Pe^{1/3}$.

The exact same reasoning as for nanodroplets in Zhangs theory [5] applies for crystals. Starting from Equation 2.49 and realising that now c_∞ and $c_{s,wat}$ are the bulk aspirin concentration and the water aspirin saturation concentration respectively, and implementing that $\lambda \sim R/Pe^{1/3}$ and again that $\zeta(t) = \frac{c_\infty(t)}{c_s} - 1 = \frac{c_\infty(t)-c_s}{c_s}$:

$$\left.\frac{\partial c}{\partial r}\right|_R \sim \frac{c_\infty(t)-c_{s,wat}}{\lambda} \sim c_{s,wat}\frac{\zeta(t)}{\lambda} \sim c_{s,wat}\frac{\zeta(t)}{R}Pe^{1/3}. \tag{A.65}$$

Plugging this final term again into Equation 2.48 and taking the aspirin density instead of the oil density:

$$4\pi\rho_{asp}R^2\frac{\partial R}{\partial t} \sim 4\pi DR^2\frac{c_{s,wat}Pe^{1/3}\zeta(t)}{R} \tag{A.66}$$

which simplifies to

$$R\frac{\partial R}{\partial t} \sim \frac{Dc_{s,wat}}{\rho_{asp}}Pe^{1/3}\zeta(t) \tag{A.67}$$

which can be solved, after realising that the final radius R_f is reached at $t=\infty$, that $\int_{-\infty}^{t=\infty}\zeta(t)dt = \zeta_{max}\tau$, and that $t=0$ corresponds to $-\infty$ here as nothing can happen before $t=0$, according to

$$\begin{aligned}
\int_0^{R=R_f} R\partial R &\sim \int_0^{t=\infty}\frac{Dc_{s,wat}}{\rho_{asp}}Pe^{1/3}\zeta(t)\partial t\\
\frac{R^2}{2}\Big|_0^{R_f} &\sim \frac{Dc_{s,wat}}{\rho_{asp}}Pe^{1/3}\zeta_{max}\tau\Big|_0^{\infty}\\
R_f &\sim \left(\frac{Dc_{s,wat}}{\rho_{asp}}Pe^{1/3}\zeta_{max}\tau\right)^{1/2}.
\end{aligned} \tag{A.68}$$

Now, remembering that $V \sim R^3$, $\zeta_{max} = \frac{c_{s,eth}}{c_{s,wat}} - 1$ and $\tau \sim h^2/D$, we get

$$\begin{aligned}
V_f \sim R_f^3 &\sim \left(\left(\frac{Dc_{s,wat}}{\rho_{asp}}Pe^{1/3}\zeta_{max}\tau\right)^{1/2}\right)^3\\
&\sim \left(\left(\frac{Dc_{s,wat}}{\rho_{asp}}Pe^{1/3}\left(\frac{c_{s,eth}}{c_{s,wat}}-1\right)\frac{h^2}{D}\right)^{1/2}\right)^3\\
&\sim h^3\left(\frac{c_{s,wat}}{\rho_{asp}}\right)^{3/2}\left(\frac{c_{s,eth}}{c_{s,wat}}-1\right)^{3/2}Pe^{1/2}.
\end{aligned} \tag{A.69}$$

We can thus conclude that under the assumptions mentioned in subsection 2.2.6 the crystal volume scales with the Péclet number according to $V_f \sim Pe^{1/2}$.

B

Image processing Python script

Full code can be requested and will be provided by the author. Please send an email to R.R.vanNes@student.tudelft.nl.

Listing B.1: Insert code directly in your document

```
# -*- coding: utf-8 -*-
"""
Created on Thu Nov  5 19:27:55 2020

@author: Riemer van Nes

Code for processing folders of images of crystals.
"""

################################################
# This code consists of 8 steps:
# Step 1: Image gathering and preprocessing (rescaling, denoising and thresholding)
# Step 2: Contour retrieval from the image
# Step 3: Separating corner points from contour points
# Step 4: Separating out concave corner points
# Step 5: Defining contour segments
# Step 6: Mapping corresponding contour segments together
# Step 7: Shape fitting of the objects (assigning minimun bounding boxes)
# Step 8: Process data using pandas
################################################

import cv2
import numpy as np
import pandas as pd
from rdp import rdp
import os


####### Tweakable properties #############

# Names of saved documents
image_folder = 'D:\Riemer\Documents\Test\Test' # Location of all images
image_save_folder = 'D:\Riemer\Documents\Test\Test'
excel_loc_name = 'D:\Riemer\Documents\Test\Test\Text.xlsx' # name of excel that contains all data

# Parameters
scale_percent = 100 # Scaling of the image, percent of original size. Try to keep at 100 if not checking
    images live. Adjust pixel_to_um accordingly.
thresh_darkness = 25 # Threshold value
err = 15 # Max allowable ellipse orientation difference to be mapped to the same crystal
eps = 2 # Epsilon for rdp corner point detection. Lower eps gives more corner points. Eps < 1 not
    recommended
pixel_to_um = 1 # Size of a pixel. Depends on the camera, microscope, lens and software. Depends on the
    camera, microscope, lens and software. For Zeiss microscope: 20x magn: 0.4424 micron/pixel. 40x
    magn: 0.3012 micron/pixel

################################################
```

```
44
45  ############ STEP 1: Image gathering and preprocessing ##############
46
47  mytifimages = [imgs for imgs in os.listdir(image_folder) if imgs.endswith('.tif')] # List of all images.
48
49  img = cv2.imread('{}\\{}'.format(image_folder, mytifimages[0])) # Formatting for rescaling of the image.
50
51  # Rescaling dimensions of the image
52  width = int(img.shape[1] * scale_percent / 100)
53  height = int(img.shape[0] * scale_percent / 100)
54  dim = (width, height)
55
56  # Dataframe that will hold all crystal properties
57  df_all_images = pd.DataFrame(columns = ['Image No','Crystal No','Length','Width'])
58
59  for image in mytifimages:
60      img = cv2.imread('{}\\{}'.format(image_folder, image)) # Read the image from the folder.
61
62      print('Processing: {}'.format(image)) # Keep track visually of progress in the console.
63
64      img_resized = cv2.resize(img, dim, interpolation = cv2.INTER_AREA) # Rescalig of the image.
65
66      # Copy of the image (as findContours changes the image), denoising and thresholding
67      contoured = img.copy()
68      denoised=cv2.fastNlMeansDenoisingColored(contoured, None , 35, 35, 7, 21)
69      gray_denoised = cv2.cvtColor(denoised, cv2.COLOR_BGR2GRAY)
70
71      ret, thresh = cv2.threshold(gray_denoised, thresh_darkness, 255, cv2.THRESH_BINARY)
72
73      ################## STEP 2: Contour retrieval ##################
74
75      # Finding contours and drawing them onto the image
76      contours, hierarchy = cv2.findContours(thresh, cv2.RETR_EXTERNAL, cv2.CHAIN_APPROX_NONE)
77      cv2.drawContours(contoured, contours, -1, (0, 255, 0), 3)
78
79      # contours returns a List(array(list(array))) structure such that
80      # contours[m][n][o][p] corresponds to the mth crystal bundle (can also be a single crystal), the nth
            contour point in this crystal bundle,
81      # o can only have value 0 and the p is a 2x1 array which contains the x and y coordinate of the
            contour point
82
83      indices = [] # index all contour points
84      xs = []
85      ys = []
86      border_segments = []
87
88
89      for bundle in range(len(contours)):
90          index = 0
91          for crd in range(len(contours[bundle])):
92              coord = []
93              x = contours[bundle][crd][0][0]
94              y = contours[bundle][crd][0][1]
95              coord.append(x)
96              coord.append(y)
97              coord.append(index)
98              index += 1
99              indices.append(coord)
100             xs.append(x)
101             ys.append(y)
102
103             # Keep track of the crystals that are on the edge of the image
104             if x in [0, img.shape[0] - 1] or y in [0, img.shape[1] - 1]:
105                 if bundle not in border_segments:
106                     border_segments.append(bundle)
107
108     indices = np.array(indices)
109
110     # indices returns a structure such that indices[a][b] corresponds to the ath contour point (for all
            crystal bundles, as every one has a unique x and y combination),
```

```
111     # and b is a 3x1 array with the x coordinate, the y coordinate and the index of this pair within a
            bundle
112
113     ################ STEP 3: Determining corner points from contour points ###########
114
115     corner_points = [] # Stores lists of corner points for all crystal bundles
116
117     for bundle in range(len(contours)): # loop over the number of crystal bundles
118         cp = rdp(contours[bundle][:][:][:], epsilon = eps) # Extract corner points from all contour
                points. Lower epsilon shows too many cornerpoints.
119         corner_points.append(cp)
120
121     # corner_points returns a list(array(list(array))) structure such that
122     # corner_points[m][n][o][p] corresponds to the mth crystal bundle (can also be a single crystal), the
            nth corner point in this crystal bundle,
123     # o can only have value 0 and the p is a 2x1 array which contains the x and y coordinate of the
            corner point
124
125     # # Run these five lines of codes to display the corner points over the image 'Contoured'. Also
            enable cv2.imshow('Contoured', contoured) and cv2.waitKey(0)
126     # for bundle in range(len(corner_points)):
127
128     #     for corn_point in range(len(corner_points[bundle])):
129
130     #         # Show the cornerpoints
131     #         contoured = cv2.circle(contoured, (corner_points[bundle][corn_point][0][0], corner_points[
            bundle][corn_point][0][1]), radius=2, color=(0, 0, 255), thickness=-1)
132     #         # circle drawer works as: cv2.circle(img, (x,y), radius, color, fill)
133
134     ############ STEP 4: Determine concave corner points ##############
135     # Determine the concave corner points with the first Abhinav algorithm
136
137     concave_points = []
138     for bundle in range(len(corner_points)): # Loop over the number of crystal bundles
139         # Loop over the corner points to find the orientation of each corner point
140         # Reset net orientation and the orientation of all corner points for each bundle of crystals
141         net_orientation = 0 # Overall orientation of the contour
142         orientation = [] #Orientation of each cornerpoint
143         for corn_point in range(len(corner_points[bundle])): # Loop over the number of corner points
144
145             # Obtain the corner point, the point prior to the corner point and the point following the
                    corner point
146             point = corner_points[bundle][corn_point][0] # Returns a 2x1 array with [x y]
147
148             if corn_point == 0: # prior corner point for the first corner point is the last corner point
149                 prior = corner_points[bundle][-1][0]
150             else:
151                 prior = corner_points[bundle][corn_point-1][0]
152             if corn_point == len(corner_points[bundle])-1: # Following corner point for the last corner
                    point is the first corner point
153                 following = corner_points[bundle][0][0]
154             else:
155                 following = corner_points[bundle][corn_point+1][0]
156
157             V_1 = point - prior # 2x1 Vector between the prior point and the point of interest
158             V_2 = following - point # 2x1 Vector between the point of interest and the following point
159             cross_product = np.cross(V_1, V_2)
160
161             orientation.append(np.sign(cross_product))
162             net_orientation += orientation[corn_point]
163
164         net_orientation = np.sign(net_orientation)
165         conc_points = []
166
167         # Loop over the corner points again to find the concave corner points
168         for corn_point in range(len(corner_points[bundle])):
169             if orientation[corn_point] != net_orientation:
170                 conc_points.append(corner_points[bundle][corn_point])
171                 contoured = cv2.circle(contoured, (corner_points[bundle][corn_point][0][0], corner_points
                        [bundle][corn_point][0][1]), radius=2, color=(255, 0, 0), thickness=-1)
172                 # print(conc_points)
```

```
173         concave_points.append(conc_points)
174
175     ########### STEP 5: Define contour segments #############
176     # Segment the contours based on the concave points
177
178     L = [] # List which will store the contour segments for all crystals
179     for bundle in range(len(concave_points)): # Loop over the number of crystal bundles
180         L2 = [] # List which will store the contour segments per crystal bundle
181         if len(concave_points[bundle][:]) <= 1: #if there are 0 or 1 concave points
182             L2.append(contours[bundle][:][:][:])
183             if len(L2)>0:
184                 L.append(L2)
185         else:
186             start = 0
187             for corn_point in range(len(concave_points[bundle])):
188                 for cont_point in range(len(contours[bundle])):
189                     if concave_points[bundle][corn_point][0][0] == contours[bundle][cont_point][0][0] and
                            concave_points[bundle][corn_point][0][1] == contours[bundle][cont_point
                        ][0][1]: # Look up in contours where the concave point
190                         if len(contours[bundle][start:cont_point + 1][:][:]) > 0:
191                             L2.append(contours[bundle][start:cont_point + 1]) # +1 because slicing does
                                    not include the final element ([0:10] gives all values from 0 to 9)
192                             start = cont_point + 1
193             if start != len(contours[bundle]): # Add the segment between the last corner point and the
                    end of the contour
194                 L2.append(contours[bundle][start:])
195             L.append(L2) # Append the set of contour segments of each crystal bundle
196
197     # Returns a list L[a][b][c][d][e] where a is the ath crystal bundle, with the bth contour segment of
            crystal a,
198     # c is the cth contour point of contour segment b, d is always 0 and
199     # e is an 2x1 array containing the coordinates of the cth contour point within the contour segment b
200     # L is an extension of contours, such that is separates contours into contour segmenst. Hence, it
            also has one more input (5 vs 4)
201
202     # Note that the number of concave points in a crystal cluster is equal to the number of contour
            segments (and is 1 for 0 concave points)
203
204     ########### STEP 6: Map corresponding contour segments together ###########
205
206     # Determine which contour segments belong together based on their angle using Abhinav's second
            algorithm
207     # Corresponding contour segments will be identified en than sliced from contours to obtain a
            structure that fits as an input for cv2.fitEllipse
208
209     G = [] # List that contains all mapped segments
210
211     small_segments = 0
212     len_small_segments = 0
213     elements = 0
214     used_elements = 0
215     segments = 0
216     unique_segments = 0
217     same_segments = 0
218
219     for bundle in range(len(L)): # Loop over the number of crystal bundles
220         matching_segments = []
221
222         for segment in range(len(L[bundle])): # Loop over the number of contour segments within a crystal
                bundle
223             G2 = []
224             rang = []
225             elements += len(L[bundle][segment])
226             segments += 1
227
228             if len(L[bundle][segment]) >= 5:
229
230                 if segment not in matching_segments:
231                     ellipse = cv2.fitEllipse(L[bundle][segment]) # Fit an ellipse to the contour segment
232                     cv2.ellipse(img, ellipse, (255, 255, 255), 1)
233
```

```
234                     low_idx_loc = np.where((indices[:,0] == L[bundle][segment][0][0][0]) & (indices[:,1]
                            == L[bundle][segment][0][0][1])) #identify location of lower index point
235                     low_idx = indices[low_idx_loc][0][2] # identify lower index
236                     high_idx_loc = np.where((indices[:,0] == L[bundle][segment][-1][0][0]) & (indices
                            [:,1] == L[bundle][segment][-1][0][1])) #identify higher index point
237                     high_idx = indices[high_idx_loc][0][2] # identify higher index
238
239                     part_rang = list(range(low_idx,high_idx+1)) # prepare list of indices that will be
                            sliced from contours
240                     rang.extend(part_rang)
241
242                     unique_segments += 1
243                     used_elements += len(L[bundle][segment])
244
245                     for match in range(len(L[bundle][segment+1:])): # Loop over the remaining contour
                            segments to check whether they match
246
247                         if len(L[bundle][segment+match+1]) >= 5:
248
249                             ellipse_2 = cv2.fitEllipse(L[bundle][segment+match+1])
250
251                             if abs(ellipse[2] - ellipse_2[2]) < err: # Third element in ellipse is the
                                    angle
252
253                                 low_idx_loc = np.where((indices[:,0] == L[bundle][segment+match
                                        +1][0][0][0]) & (indices[:,1] == L[bundle][segment+match
                                        +1][0][0][1])) #identify location of lower index point
254                                 low_idx = indices[low_idx_loc][0][2] # identify lower index
255                                 high_idx_loc = np.where((indices[:,0] == L[bundle][segment+match
                                        +1][-1][0][0]) & (indices[:,1] == L[bundle][segment+match
                                        +1][-1][0][1])) #identify higher index point
256                                 high_idx = indices[high_idx_loc][0][2] # identify higher index
257
258                                 part_rang = list(range(low_idx,high_idx+1)) # prepare list of indices
                                        that will be sliced from contours
259                                 rang.extend(part_rang) # add certain coords to the rang
260
261                                 same_segments += 1
262                                 matching_segments.append(segment+match+1)
263                                 used_elements += len(L[bundle][segment+match+1])
264
265             else:
266                 small_segments += 1
267                 len_small_segments += len(L[bundle][segment]) # keep track of how many data points are
                        lost because ellipse fitting needs at least 5 coordinates
268                 used_elements += len(L[bundle][segment])
269
270             if bundle not in border_segments: # Omit all contours that touch the image border
271                 G2 = contours[bundle][rang]
272                 G.append(G2)
273
274     ############## STEP 7: Shape fitting #################
275
276     crystal_count = 1 # NOTE: count starts on one for easier excel processing later on
277     all_crystals = [] # List that saves the properties of all crystals in the image
278     boxed = img_resized.copy()
279
280     for crystal in range(len(G)):
281
282         if len(G[crystal]) >= 5:
283
284             # Find minimum bounding rectangle for each crystal
285             rectangle = cv2.minAreaRect(G[crystal]) # cv2.minAreaRect output is rectangle = [[x-
                        coordinate, y-coordinate],[width, height], rotation]
286             box = cv2.boxPoints(rectangle) # Generate a box for each minimum bounding rectangle
287             box = np.int0(box)
288             boxed = cv2.drawContours(boxed, [box], 0, (0, 255, 0), 3) # Draw a box for each minimum
                        bounding rectangle in the figure
289
290             # Add number for crystal to the figure
291             x_center = np.mean(box[:,0]) #Location of the text : at the center of x coords .
```

```
292             y_center = np.mean(box[:,1]) #Location of the text : at the center of y coords .
293             cv2.putText(boxed, str(crystal_count) , (int(x_center), int(y_center)), cv2.LINE_AA , 3,
                    (255, 255, 255) , 2)
294
295             # Save crystal properties
296             crystal_properties = []
297             crystal_properties.append(image[6:10]) # image number
298             crystal_properties.append(crystal_count) # crystal number
299             crystal_properties.append(max(rectangle[1])*pixel_to_um) # crystal length
300             crystal_properties.append(min(rectangle[1])*pixel_to_um) # crystal width
301             all_crystals.append(crystal_properties) # Add crystal properties to all crystals
302
303             crystal_count += 1 # Increase crystal count
304
305     ################## STEP 8: Process data with pandas ###########
306
307     df_single_image = pd.DataFrame(all_crystals, columns=['Image No','Crystal No','Length','Width'])
308     # print(df_single_image)
309     df_all_images = df_all_images.append(df_single_image)
310     # print(df_all_images)
311
312     loc_name_prcsd = image_save_folder + '\\' + image[:-4] +'-processed.png' # prepared name of process
            image for saving
313     cv2.imwrite(loc_name_prcsd, boxed)
314
315 # print('The total number of coordinates is ', elements, '. The number of used coordinates is',
        used_elements, ', which is ', used_elements - elements, ' too many.')
316 # print('The total number of contour segments is ', segments, '. The number of primary segments is ',
        unique_segments, ', to which ', same_segments, ' segments are added as they have the same angle.',
        small_segments, 'segments are too short. This are', unique_segments + same_segments +
        small_segments - segments, 'segments too many')
317
318 df_all_images.to_excel(excel_loc_name)
319
320 # cv2.imshow('Img', img)
321 cv2.imshow('Labeled', boxed)
322 # cv2.imshow('Gray', gray_denoised)
323 # cv2.imshow('Threshed', thresh)
324 # cv2.imshow('Contoured', contoured)
325
326 cv2.waitKey(0)
327 cv2.destroyAllWindows
```

C

Experimental design

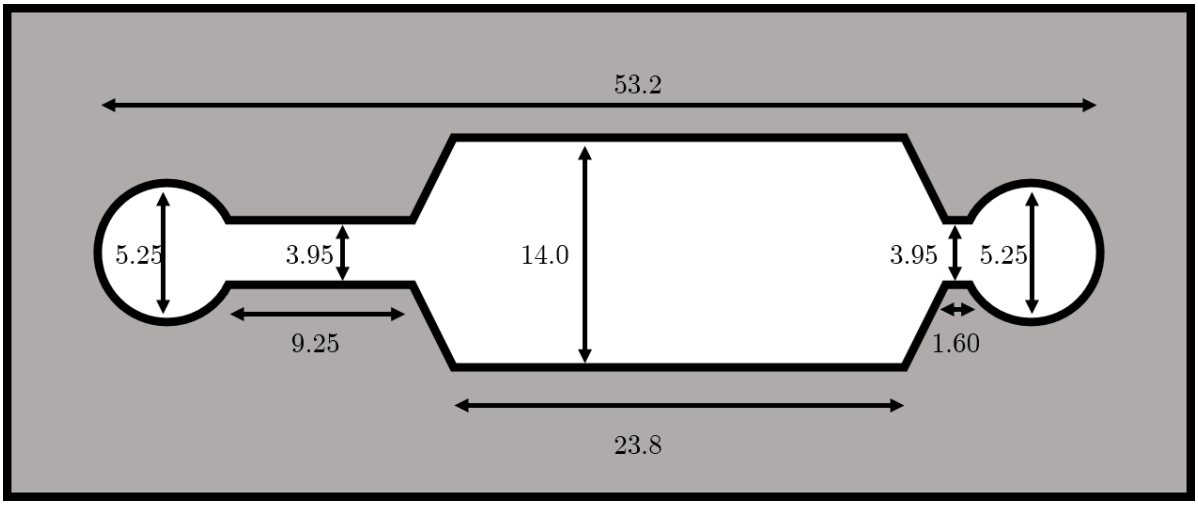

Figure C.1: Design of the channel silicon rubber. All distances are in mm. The channel has a thickness of 0.3 mm.

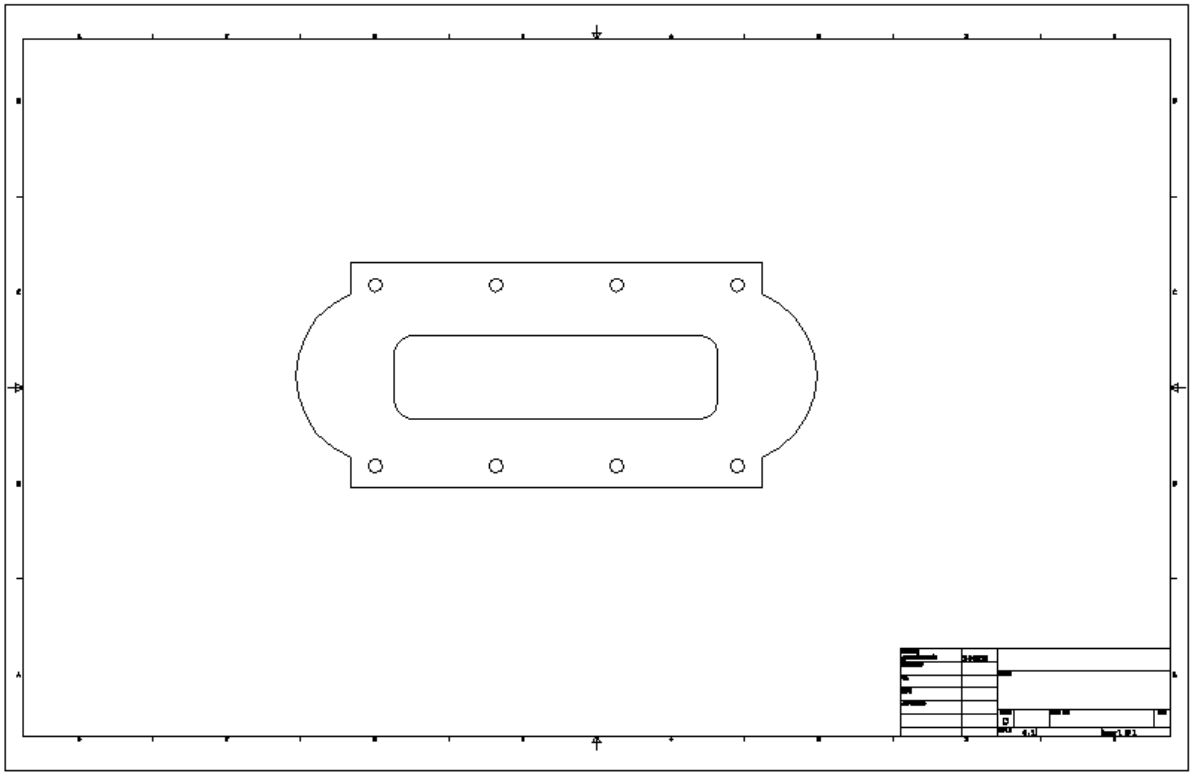

Figure C.2: Design of the channel aluminium support frame.

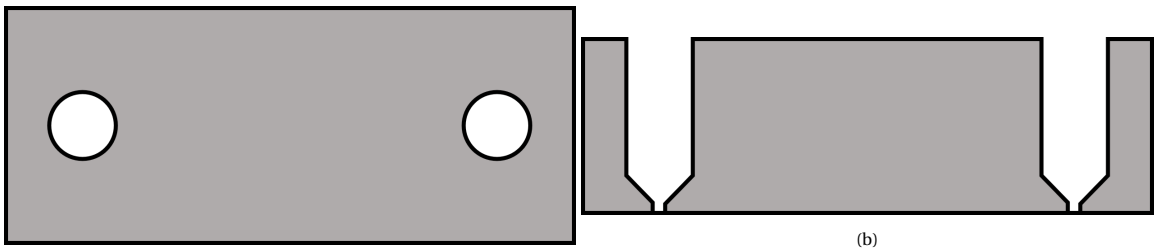

(a) (b)

Figure C.3: Design of the polycarbonate spacer. Top view on the left, sideways intersection on the right. The holes are threaded to fit the microfluidic connectors.

D

Safety - Material Safety Data Sheets

MSDSs of used chemicals can be found in this appendix. Pages that contain the H- and P-rules are shown.

SAFETY DATA SHEET

according to Regulation (EC) No. 1907/2006

Version 6.3
Revision Date 25.06.2020
Print Date 01.09.2020
GENERIC EU MSDS - NO COUNTRY SPECIFIC DATA - NO OEL DATA

SECTION 1: Identification of the substance/mixture and of the company/undertaking

1.1 Product identifiers

Product name : Ethanol

Product Number : V001229
Brand : Vetec
Index-No. : 603-002-00-5
REACH No. : 01-2119457610-43-XXXX
CAS-No. : 64-17-5

1.2 Relevant identified uses of the substance or mixture and uses advised against

Identified uses : Laboratory chemicals, Manufacture of substances

1.3 Details of the supplier of the safety data sheet

Company : Sigma-Aldrich Chemie BV
Stationsplein 4
3331 LL ZWIJNDRECHT
NETHERLANDS

Telephone : +31 078 620-5411
Fax : +31 078 620-5421
E-mail address : technischeservicebenelux@merckgroup.com

1.4 Emergency telephone

Emergency Phone # : +(31)-858880596 (CHEMTREC)
112 (Alarmnummer)

SECTION 2: Hazards identification

2.1 Classification of the substance or mixture

Classification according to Regulation (EC) No 1272/2008
Flammable liquids (Category 2), H225
Eye irritation (Category 2), H319

For the full text of the H-Statements mentioned in this Section, see Section 16.

2.2 Label elements

Labelling according Regulation (EC) No 1272/2008
Pictogram

Signal word Danger

Hazard statement(s)	
H225	Highly flammable liquid and vapor.
H319	Causes serious eye irritation.
Precautionary statement(s)	
P210	Keep away from heat, hot surfaces, sparks, open flames and other ignition sources. No smoking.
P305 + P351 + P338	IF IN EYES: Rinse cautiously with water for several minutes. Remove contact lenses, if present and easy to do. Continue rinsing.
Supplemental Hazard Statements	none

2.3 Other hazards

This substance/mixture contains no components considered to be either persistent, bioaccumulative and toxic (PBT), or very persistent and very bioaccumulative (vPvB) at levels of 0.1% or higher.

SECTION 3: Composition/information on ingredients

3.1 Substances

Formula	:	C_2H_6O
Molecular weight	:	46,07 g/mol
CAS-No.	:	64-17-5
EC-No.	:	200-578-6
Index-No.	:	603-002-00-5

Component	Classification	Concentration
ethanol		
	Flam. Liq. 2; Eye Irrit. 2; H225, H319 Concentration limits: >= 50 %: Eye Irrit. 2A, H319;	<= 100 %

For the full text of the H-Statements mentioned in this Section, see Section 16.

SECTION 4: First aid measures

4.1 Description of first-aid measures

General advice
Consult a physician. Show this material safety data sheet to the doctor in attendance.

If inhaled
If breathed in, move person into fresh air. If not breathing, give artificial respiration. Consult a physician.

In case of skin contact
Wash off with soap and plenty of water. Consult a physician.

In case of eye contact
Rinse thoroughly with plenty of water for at least 15 minutes and consult a physician.

SAFETY DATA SHEET

according to Regulation (EC) No. 1907/2006

Version 6.2
Revision Date 17.09.2019
Print Date 01.09.2020
GENERIC EU MSDS - NO COUNTRY SPECIFIC DATA - NO OEL DATA

SECTION 1: Identification of the substance/mixture and of the company/undertaking

1.1 Product identifiers

Product name	:	Acetylsalicylic acid
Product Number	:	A5376
Brand	:	Sigma
REACH No.	:	A registration number is not available for this substance as the substance or its uses are exempted from registration, the annual tonnage does not require a registration or the registration is envisaged for a later registration deadline.
CAS-No.	:	50-78-2

1.2 Relevant identified uses of the substance or mixture and uses advised against

Identified uses	:	Laboratory chemicals, Manufacture of substances

1.3 Details of the supplier of the safety data sheet

Company	:	Sigma-Aldrich Chemie BV Stationsplein 4 3331 LL ZWIJNDRECHT NETHERLANDS
Telephone	:	+31 078 620-5411
Fax	:	+31 078 620-5421
E-mail address	:	technischeservicebenelux@merckgroup.com

1.4 Emergency telephone number

Emergency Phone #	:	+(31)-858880596 (CHEMTREC) 112 (Alarmnummer)

SECTION 2: Hazards identification

2.1 Classification of the substance or mixture

Classification according to Regulation (EC) No 1272/2008
Acute toxicity, Oral (Category 4), H302

For the full text of the H-Statements mentioned in this Section, see Section 16.

2.2 Label elements

Labelling according Regulation (EC) No 1272/2008
Pictogram

Signal word Warning

Hazard statement(s)
H302 Harmful if swallowed.

Precautionary statement(s)
P301 + P312 + P330 IF SWALLOWED: Call a POISON CENTER/doctor if you feel unwell. Rinse mouth.

Supplemental Hazard Statements: none

2.3 Other hazards

This substance/mixture contains no components considered to be either persistent, bioaccumulative and toxic (PBT), or very persistent and very bioaccumulative (vPvB) at levels of 0.1% or higher.

SECTION 3: Composition/information on ingredients

3.1 Substances

Synonyms : ASA
O-Acetylsalicylic acid
2-Acetoxybenzoic acid
Aspirin

Formula : $C_9H_8O_4$

Molecular weight : 180,16 g/mol

CAS-No. : 50-78-2

EC-No. : 200-064-1

Component	Classification	Concentration
O-Acetylsalicylic acid		
	Acute Tox. 4; H302	<= 100 %

For the full text of the H-Statements mentioned in this Section, see Section 16.

SECTION 4: First aid measures

4.1 Description of first aid measures

General advice
Consult a physician. Show this safety data sheet to the doctor in attendance.

If inhaled
If breathed in, move person into fresh air. If not breathing, give artificial respiration. Consult a physician.

In case of skin contact
Wash off with soap and plenty of water. Consult a physician.

In case of eye contact
Flush eyes with water as a precaution.

If swallowed
Never give anything by mouth to an unconscious person. Rinse mouth with water. Consult a physician.

SAFETY DATA SHEET

according to Regulation (EC) No. 1907/2006

Version 6.5
Revision Date 13.07.2020
Print Date 01.09.2020
GENERIC EU MSDS - NO COUNTRY SPECIFIC DATA - NO OEL DATA

SECTION 1: Identification of the substance/mixture and of the company/undertaking

1.1 Product identifiers

Product name : Sodium hydroxide

Product Number : V000101
Brand : Vetec
Index-No. : 011-002-00-6
REACH No. : 01-2119457892-27-XXXX
CAS-No. : 1310-73-2

1.2 Relevant identified uses of the substance or mixture and uses advised against

Identified uses : Laboratory chemicals, Manufacture of substances

1.3 Details of the supplier of the safety data sheet

Company : Sigma-Aldrich Chemie BV
Stationsplein 4
3331 LL ZWIJNDRECHT
NETHERLANDS

Telephone : +31 078 620-5411
Fax : +31 078 620-5421
E-mail address : technischeservicebenelux@merckgroup.com

1.4 Emergency telephone

Emergency Phone # : +(31)-858880596 (CHEMTREC)
112 (Alarmnummer)

SECTION 2: Hazards identification

2.1 Classification of the substance or mixture

Classification according to Regulation (EC) No 1272/2008
Corrosive to Metals (Category 1), H290
Skin corrosion (Sub-category 1A), H314
Eye irritation (Category 2), H319

For the full text of the H-Statements mentioned in this Section, see Section 16.

2.2 Label elements

Labelling according Regulation (EC) No 1272/2008
Pictogram

Signal word Danger

Hazard statement(s)

H290	May be corrosive to metals.
H314	Causes severe skin burns and eye damage.

Precautionary statement(s)

P260	Do not breathe dusts or mists.
P280	Wear protective gloves/ protective clothing/ eye protection/ face protection.
P301 + P330 + P331	IF SWALLOWED: Rinse mouth. Do NOT induce vomiting.
P303 + P361 + P353	IF ON SKIN (or hair): Take off immediately all contaminated clothing. Rinse skin with water.
P305 + P351 + P338	IF IN EYES: Rinse cautiously with water for several minutes. Remove contact lenses, if present and easy to do. Continue rinsing.
Supplemental Hazard Statements	none

2.3 Other hazards

This substance/mixture contains no components considered to be either persistent, bioaccumulative and toxic (PBT), or very persistent and very bioaccumulative (vPvB) at levels of 0.1% or higher.

SECTION 3: Composition/information on ingredients

3.1 Substances

Formula	:	HNaO
Molecular weight	:	40,00 g/mol
CAS-No.	:	1310-73-2
EC-No.	:	215-185-5
Index-No.	:	011-002-00-6

Component	Classification	Concentration
sodium hydroxide		
	Met. Corr. 1; Skin Corr. 1A; Eye Dam. 1; H290, H314, H318 Concentration limits: >= 5 %: Skin Corr. 1A, H314; 2 - < 5 %: Skin Corr. 1B, H314; 0,5 - < 2 %: Skin Irrit. 2, H315; 0,5 - < 2 %: Eye Irrit. 2, H319; >= 0,4 %: Met. Corr. 1, H290;	<= 100 %

For the full text of the H-Statements mentioned in this Section, see Section 16.

SECTION 4: First aid measures

4.1 Description of first-aid measures

General advice

Consult a physician. Show this material safety data sheet to the doctor in attendance.

SAFETY DATA SHEET

according to Regulation (EC) No. 1907/2006

Version 6.2
Revision Date 05.10.2019
Print Date 01.09.2020
GENERIC EU MSDS - NO COUNTRY SPECIFIC DATA - NO OEL DATA

SECTION 1: Identification of the substance/mixture and of the company/undertaking

1.1 Product identifiers

Product name	:	Trichloro(1*H*,1*H*,2*H*,2*H*-perfluorooctyl)silane
Product Number	:	448931
Brand	:	Aldrich
REACH No.	:	A registration number is not available for this substance as the substance or its uses are exempted from registration, the annual tonnage does not require a registration or the registration is envisaged for a later registration deadline.
CAS-No.	:	78560-45-9

1.2 Relevant identified uses of the substance or mixture and uses advised against

Identified uses	:	Laboratory chemicals, Manufacture of substances

1.3 Details of the supplier of the safety data sheet

Company	:	Sigma-Aldrich Chemie BV Stationsplein 4 3331 LL ZWIJNDRECHT NETHERLANDS
Telephone	:	+31 078 620-5411
Fax	:	+31 078 620-5421
E-mail address	:	technischeservicebenelux@merckgroup.com

1.4 Emergency telephone number

Emergency Phone #	:	+(31)-858880596 (CHEMTREC) 112 (Alarmnummer)

SECTION 2: Hazards identification

2.1 Classification of the substance or mixture

Classification according to Regulation (EC) No 1272/2008
Skin corrosion (Sub-category 1B), H314

For the full text of the H-Statements mentioned in this Section, see Section 16.

2.2 Label elements

Labelling according Regulation (EC) No 1272/2008
Pictogram

Signal word Danger

Hazard statement(s)

H314	Causes severe skin burns and eye damage.

Precautionary statement(s)

P280	Wear protective gloves/ protective clothing/ eye protection/ face protection.
P301 + P330 + P331	IF SWALLOWED: Rinse mouth. Do NOT induce vomiting.
P303 + P361 + P353	IF ON SKIN (or hair): Take off immediately all contaminated clothing. Rinse skin with water.
P305 + P351 + P338	IF IN EYES: Rinse cautiously with water for several minutes. Remove contact lenses, if present and easy to do. Continue rinsing.

Supplemental Hazard information (EU)

EUH014	Reacts violently with water.

2.3 Other hazards

This substance/mixture contains no components considered to be either persistent, bioaccumulative and toxic (PBT), or very persistent and very bioaccumulative (vPvB) at levels of 0.1% or higher.

SECTION 3: Composition/information on ingredients

3.1 Substances

Synonyms	:	Trichloro(3,3,4,4,5,5,6,6,7,7,8,8,8-tridecafluorooctyl)silane 1H,1H,2H,2H-Perfluorooctyl-trichlorosilane
Formula	:	$C_8H_4Cl_3F_{13}Si$
Molecular weight	:	481,54 g/mol
CAS-No.	:	78560-45-9
EC-No.	:	278-947-6

Component	Classification	Concentration
Trichloro(3,3,4,4,5,5,6,6,7,7,8,8,8-tridecafluorooctyl)silane		
	Skin Corr. 1B; H314	<= 100 %

For the full text of the H-Statements mentioned in this Section, see Section 16.

SECTION 4: First aid measures

4.1 Description of first aid measures

General advice
Consult a physician. Show this safety data sheet to the doctor in attendance.

If inhaled
If breathed in, move person into fresh air. If not breathing, give artificial respiration. Consult a physician.

In case of skin contact
Take off contaminated clothing and shoes immediately. Wash off with soap and plenty of water. Consult a physician.

In case of eye contact
Rinse thoroughly with plenty of water for at least 15 minutes and consult a physician.

CMR Safety report P&E

When to write a safety report?

CMR compounds: H340-341-350-350i-351-360-360D-360Df-360f-360FD-360Fd-361-361d-361f-361fd-362
Extremely poisonous: H300-301-302-304-310-311-314-330-331

Chemical name + CAS-number:
Ethanol. CAS: 64-17-5

Hazard- and precautionary statement(s) (H- and P-statements):
H225 Highly flammable liquid and vapor.
H319 Causes serious eye irritation.

P210 Keep away from heat, hot surfaces, sparks, open flames and other ignition sources. No smoking.
P305 + P351 + P338 IF IN EYES: Rinse cautiously with water for several minutes. Remove contact lenses, if present and easy to do. Continue rinsing.

Carcinogenic / ~~Mutagenic~~ / ~~Reprotoxic~~ / ~~extremely poisonous~~

Explain clearly why this compound can't be replaced with a non CMR compound:
All previous experiments have been done with ethanol, and would have to be redone to continue this project. Furthermore, ethanol is a very suitable solve for acetyl salicylic acis.

Purpose use chemical:
As solvent for acetyl salicylic acid, in an antisolvent crystallization setup.

Amount ordered / amount used per experiment
2 Liters. / 100 mL per batch of antisolvent (batches of 200 mL total). Roughly 30 mL antisolvent per experiment.

How to work with the chemical?

Personal protective equipment (e.g. fume hood, safety weighing cabinet):
Only use ethanol in the fume hood and immediately transfer back to the chemicals cabinet once finished.

Personal protective clothing (e.g. safety glasses, lab coat, gloves + type):
Lab coat, goggles, gloves.

What to do with waste?
Inorganic halogenfree.

How to clean spills?
Paper towels and gloves. Rinse with water or acetone.

Author name: Riemer van Nes (4388364)

Signature Area supervisor: